Interactions between Surfactants and Biodegradable Thermo-Responsive Polymeric Nanostructures in Bulk and at Interfaces

by

Baoliang Peng

A thesis
presented to the University of Waterloo
in fulfillment of the
thesis requirement for the degree of
Doctor of Philosophy
in
Chemical Engineering - Nanotechnology

Waterloo, Ontario, Canada, 2013

AUTHOR'S DECLARATION

I hereby declare that I am the sole author of this thesis. This is a true copy of the thesis, including any required final revisions, as accepted by my examiners. I understand that my thesis may be made electronically available to the public.

Abstract

Interactions between surfactants and polymeric nanostructures have gained increasing attention due to their potential application in many disciplines. In this study, a well-defined random copolymer containing 2-(2-methoxyethoxy) ethyl methacrylate (MEO_2MA) and poly(ethylene glycol) methyl ether methacrylate ($PEGMA_{2080}$) (poly(MEO_2MA-*co*-$PEGMA_{2080}$)) was synthesized using the atom transfer radical polymerization (ATRP) process, and its thermo-responsive behaviors in aqueous solution were investigated. In comparison to other thermo-sensitive random copolymers based on oligo(ethylene glycol) methacrylates (OEGMA), this copolymer exhibited an unusual thermal induced two-stage aggregation process. The copolymer chains associated at the first thermal transition followed by a rearrangement process at the second thermal transition to produce a stable core-shell micellar structure.

Furthermore, the binding interactions between cationic surfactants and this copolymer were examined below and above its cloud point. In general, the binding interactions between cationic surfactants and neutral polymers are weak and cationic surfactants are very selective and only bind to those polymers with specific hydrophobic groups. Significant hydrophobic interactions were observed between surfactant monomers and the polymer backbone. The binding occurred uncooperatively at low surfactant concentration, which was confirmed by electromotive force (EMF) measurements. Moreover, the binding affinity of three cationic surfactants follows the sequence: CTAB > TTAB > DoTAB.

Cellulose Nanocrystals (CNC) with diameter of 10-20 nm and length of 200-400 nm, derived from native cellulose, is a promising new class of nanomaterials due to its high specific strength, high surface area, and unique optical properties. Currently, most of researches focused on the improvement of its steric stability, dispersability and compatibility in different solvents or

matrices. A thermo-responsive polymer, namely Jeffamine M600 (a 600 Da polypropylene glycol) was grafted on the surface of cellulose nanocrystals (CNC) via a peptide coupling reaction. The better dispersion of the modified CNC in water was demonstrated, and the interactions between surfactants and M600-grafted CNC were investigated via isothermal titration calorimetry (ITC). Three types of surfactants with dodecyl alkyl chain and different head groups, namely cationic dodecyltrimethylammonium bromine (DoTAB), anionic sodium dodecyl sulfate (SDS), and nonionic poly(ethylene glycol) dodecyl ether (Brij 30) were studied. Physical mechanisms describing the interactions of cationic, anionic and nonionic surfactants and M600-grafted CNC were proposed.

Chitosan molecules are water-soluble in acidic media due to the protonation of amino groups. However, some applications of chitosan are restricted by its poor solubility in basic media. A biocompatible derivative of chitosan, *N*-carboxyethylchitosan (CECh) was synthesized by Michael addition reactions, which possessed high solubility in both acidic and basic media due to the modification by carboxyl groups. The aggregation behavior of CECh in aqueous solution under the effects of pH, polymer concentration, as well as a gemini surfactant, was investigated by turbidity, zeta potential, fluorescence spectroscopy, viscosity, and surface tension measurements.

This research demonstrates that nanostructures comprising of thermo-responsive copolymers can be controlled and manipulated by temperature and surfactants, and they play an important role in the physical properties of surfactants-polymeric complexes. The results from this research provide the fundamental knowledge on the self-assembly behavior and the binding mechanism of various novel polymeric systems and surfactants, which can be utilized to design and develop systems for personal care formulations and drug delivery systems.

Acknowledgments

I would like to express my sincerest gratitude to my supervisors, Dr. Honglai Liu (ECUST) and Dr. Michael K.C. Tam (UW) for their constant guidance, patience, support and encouragement during my Ph.D. studies. I deeply appreciate the opportunity to study and work under their supervision.

I would also like to extend my gratitude to all my labmates in both Dr. Liu and Dr. Tam labs for their help and useful discussion. I would like to mention Dr. Shang and Dr. Kang at ECUST for their help when I commenced my project. Special thanks to Dr. Han at ECUST, who offered me helpful suggestions and strong support to complete my Ph.D. studies. I would like to acknowledge Dr. Yao and Nathan Grishkewich at UW for their advice and assistance to conduct my experiments.

I would like to thank the China Scholarship Council for supporting my living in Canada, and financial support from the University of Waterloo and East China University of Science and Technology for my Ph.D. studies.

I wish to express my immense gratitude to my parents for their constant love, support and encouragement throughout my life. Lastly, the deepest appreciation goes to my wife, L. Liu for her love, support, sacrifice and inspiration.

Table of Contents

AUTHOR'S DECLARATION ii

Abstract iii

Acknowledgments v

List of Figures x

List of Tables xiv

List of Schemes xv

Nomenclature xvi

Chapter 1 Introduction 1

1.1 Background 1

1.2 Research objectives and methodology 4

1.2.1 Synthesis of TRPs based on oligo(ethylene glycol) methacrylates 4

1.2.2 Binding of cationic surfactants with the copolymer 4

1.2.3 Grafting TRPs on CNC surface 5

1.2.4 Study on the interactions between surfactants and TRP-modified CNC 5

1.2.5 Aggregation behavior of *N*-carboxyethylchitosan in the presence of surfactant 5

Chapter 2 Literature Review 6

2.1 Introduction 6

2.2 Thermo-responsive polymers (TRPs) 7

2.2.1 Overview of thermo-responsive polymers 7

2.2.2 TRPs with tunable thermo-sensitivity 11

2.2.3 TRPs based on oligo(ethylene glycol) methacrylates 13

2.2.4 Applications of thermo-responsive polymeric systems 16

2.3 Grafting TRPs onto cellulose nanocrystals (CNC) surface 19

2.3.1 General aspect of CNC 19

2.3.2 CNC properties 21

2.3.3 Surface modification of cellulose nanocrystals (CNC) 24

2.3.4 Polymer grafting of TRPs on CNC surface 28

2.3.5 Applications of CNC 30

2.4 Interaction between polymeric nanostructures and surfactants 35

2.4.1 Overview of polymer/surfactant systems 35

2.4.2 Interactions between TRPs and surfactants 37

2.4.3 Interactions between biodegradable cellulose derivatives and surfactants 41

2.4.4 Interactions between cellulose nanocrystals and surfactants 46
2.4.5 Interactions between biodegradable chitosan derivative and surfactants 49
2.4.6 Applications of polymers and surfactants complexes 51
2.5 Summary 56
Chapter 3 Self-Assembly Behavior of Thermo-responsive Oligo (ethylene glycol) Methacrylates Random Copolymers 57
3.1 Introduction 57
3.2 Experimental 59
3.2.1 Materials 59
3.2.2 Synthesis of P(MEO_2MA-*co*-$PEGMA_{2080}$) via ATRP 59
3.2.3 Characterizations of P(MEO_2MA-*co*-$PEGMA_{2080}$) 60
3.2.3.1 Nuclear magnetic resonance (NMR) 60
3.2.3.2 Gel permeation chromatography (GPC) 60
3.2.3.3 Ultraviolet-visible spectroscopy (UV-Vis) 61
3.2.3.4 Laser light scattering (LLS) 61
3.2.3.5 Transmission electron microscopy (TEM) 62
3.3 Results and Discussion 63
3.3.1 Synthesis of P(MEO_2MA-*co*-$PEGMA_{2080}$) 63
3.3.2 Thermal responsive behaviors of copolymer in aqueous media 64
3.3.3 Microstructure analysis of the copolymer in aqueous media 68
3.4 Conclusions 72
Chapter 4 Binding of Cationic Surfactants to a Thermo-sensitive Copolymer Below and Above its Cloud Point 73
4.1 Introduction 73
4.2 Experimental 75
4.2.1 Materials 75
4.2.2 Isothermal titration calorimetry (ITC) 76
4.2.3 Surfactant selective electrode (SSE) 77
4.2.4 Dynamic light scattering (DLS) 77
4.3 Results and Discussion 78
4.3.1 ITC results for the binding CTAB to poly(MEO_2MA-*co*-$PEGMA_{2080}$) 78
4.3.2 EMF results of binding CTAB to poly(MEO_2MA-*co*-$PEGMA_{2080}$) 83
4.3.3 DLS results on the binding CTAB monomers to the copolymer 87
4.3.4 Effect of surfactant hydrophobicity on the binding interaction 89

4.4 Conclusions 92
Chapter 5 Interactions between Surfactants and Polymer-grafted Cellulose Nanocrystals 94
5.1 Introduction 94
5.2 Materials and Methods 96
5.2.1 Materials 96
5.2.2 Preparation of Jeffamine M600-grafted CNC 97
5.2.3 Fourier-transform infrared spectroscopy 98
5.2.4 Transmission electron microscopy (TEM) 99
5.2.5 Conductometric titrator 99
5.2.6 Nuclear magnetic resonance (NMR) 99
5.2.7 Isothermal titration calorimetry (ITC) 100
5.3 Results and Discussion 101
5.3.1 Characterization of M600-grafted CNC 101
5.3.2 Interactions between M600-grafted CNC and SDS 103
5.3.3 Interactions between M600-grafted CNC and DoTAB 110
5.3.4 Interactions between M600-grafted CNC and a non-ionic surfactant (Brij 30) 113
5.4 Conclusions 115
Chapter 6 Aggregation behavior of *N*-carboxyethylchitosan in aqueous solution: effects of pH, polymer concentration, and presence of a gemini surfactant 116
6.1 Introduction 116
6.2 Experimental 118
6.2.1 Materials 118
6.2.2 Sample preparation 119
6.2.3 Characterizations 119
6.2.3.1 Fluorescence emission spectroscopy 119
6.2.3.2 Viscosity measurements 120
6.2.3.3 Surface tension measurements 120
6.2.3.4 Turbidity measurements 120
6.2.3.5 Zeta potential 120
6.3 Results and Discussion 120
6.3.1 Influence of pH on the aggregation behavior of CECh 120
6.3.2 Influence of polymer concentration on the aggregation behavior of CECh 124
6.3.3 Influence of a gemini surfactant on the aggregation behavior of CECh 127

6.4 Conclusions 132
Chapter 7 Conclusions and Recommendations 134
7.1 General Contributions 134
7.1.1 Thermo-responsive oligo (ethylene glycol) methacrylates copolymer 134
7.1.2 Binding interactions between cationic surfactants and neutral copolymer 135
7.1.3 Interactions between surfactants and TRP-modified CNC 136
7.1.4 Interactions between gemini surfactant and *N*-carboxyethylchitosan 136
7.2 Recommendations for Future work 137
7.2.1 Effect of solvent conditions and polymer properties on surfactants/polymeric nanostructures 137
7.2.2 Rheological properties of TRPs-modified CNC in the presence of surfactant 138
7.2.3 Effect of small molecules and composition on LCST 139
References 141

List of Figures

Figure 2.1 Phase diagram for a binary polymer/solvent mixture exhibiting (a) LCST behavior and (b) UCST behavior. 7

Figure 2.2 Optical transmittances of aqueous solutions of $PTEGMA_{66}$-*b*-$PTEGSt_{72}$ upon heating (▲) and cooling (▼), PTEGSt (●), PTEGMA (■), and mixture (◆) of PTEGSt and PTEGMA at various temperatures. 12

Figure 2.3 Schematic representations of monomers that have been applied for copolymerization with oligo(ethylene glycol) methacrylates or ethoxytri(ethylene glycol) acrylate. 15

Figure 2.4 TEM micrographs of nanocrystals obtained by sulfuric acid hydrolysis of (a) cotton (b) avicel (c-e) tunicate cellulose. The insets of (a) and (b) provide higher resolution images of some characteristic particles 20

Figure 2.5 Numbering system for carbon atoms in anhydroglucose unit of cellulose. 21

Figure 2.6 Phase separation observed between cross polars for different concentrations of CNC (cotton fibers) suspensions at total concentrations of (a) 19.8 wt% and (b) 25.0 wt%.23

Figure 2.7 Schematic diagram illustrating the various types of chemical modifications on CNC surface 24

Figure 2.8 Transmission electron microscopy (TEM) image, (b) High-resolution transmission electron microscopy (HRTEM) image, (c) selected area electron diffraction (SAED) pattern of TiO_2 nanocubes 34

Figure 2.9 Optical characterization and properties of CNC/silica mesoporous films (a) Transmission spectra; (b) Photograph showing different colours of mesoporous silica films S1 to S4. 35

Figure 2.10 Dependence of reduced viscosity on DoTAB concentrations for NaCMC concentrations of 0.5 wt%, 0.75 wt% and 1 wt% at 25 ^{o}C. 44

Figure 2.11 A schematic illustration of the surfactant-induced strengthening and disruption of the association network 46

Figure 2.12 Polarized optical micrographs of the chiral nematic texture (top row) and fingerprints (bottom row) of the anisotropic phase in Cot54 at 31.0 wt% (a and d), Cot63 at 38.7 wt% (b and e), and Cot72 at 27.0 wt% (c and f) suspensions in cyclohexane 47

Figure 2.13 Optical microscope images for neat PS film (A_0 and B_0) and PS/CN/Surfactant composite films with 3% ($A_{1–4}$) and 6% ($B_{1–4}$) CN weight load. CN:Surfactant ratios are 1, CN:Surfactant = 1:0; 2, CN:Surfactant = 1:1; 3, CN:Surfactant = 1:2; 4, CN:Surfactant = 1:4. 49

Figure 2.14 Confocal micrographs of KU-7 cells incubated for 2 hours with CNC/CTAB/fluorescein nanocomplexes with a CNC/CTAB/fluorescein concentration of 0.25 mg/mL. A) White light image of KU-7 cells. B) Staining of the nuclei with DAPI (4', 6-diamidino-2-phenylindole). C) Fluorescein in the cytoplasm. D) An overlay of images B and C. 53

Figure 2.15 The in vitro release of etoposide (▽), docetaxel (□), and paclitaxel (Δ) from CNC/CTAB nanocomplexes with 12.9 mM CTAB in 10 mM phosphate buffered saline at 37 °C 54

Figure 2.16 Schematic illustration of the effect of SDS addition to a semi-dilute HM-HEC solution. 55

Figure 3.1 ^{1}H NMR spectra of P(MEO_2MA-*co*-$PEGMA_{2080}$) in $CDCl_3$ at 25 ^oC. 63

Figure 3.2 GPC profile of P(MEO_2MA-*co*-$PEGMA_{2080}$) at 25 ^oC. 64

Figure 3.3 (A) Transmittance versus temperature for 1 wt% P(MEO_2MA-*co*-$PEGMA_{2080}$) aqueous solution at the wavelength of 500 nm. (B) Optical photographs of 1 wt% P(MEO_2MA-*co*-$PEGMA_{2080}$) aqueous solution at different temperatures. 66

Figure 3.4 Transmittance versus temperature of 0.3, 0.5, 1 wt% P(MEO_2MA-*co*-$PEGMA_{2080}$) aqueous solutions at the wavelength of 500 nm. 67

Figure 3.5 R_h, R_g/R_h and the scattering intensity (inset) of 0.02 wt% P(MEO_2MA-*co*-$PEGMA_{2080}$) solution at different temperatures..... 68

Figure 3.6 (A) TEM images and (B) relaxation time distribution curves of 0.02 wt% P(MEO_2MA-*co*-$PEGMA_{2080}$) solution at different temperatures. 69

Figure 3.7 KC/R(q) versus the square of the scattering vector (q^2) for 0.02 wt% P(MEO_2MA-*co*-$PEGMA_{2080}$) solution at different temperatures. 70

Figure 3.8 Schematic illustration of two-stage thermal induced aggregation process for random copolymer P(MEO_2MA-*co*-$PEGMA_{2080}$) in water. 71

Figure 4.1 ITC curves for titrating 20 mM CTAB into different concentrations of poly(MEO_2MA-*co*-$PEGMA_{2080}$) aqueous solutions at 25.0 °C (a) and 30.0 °C (b).... 79

Figure 4.2 ITC curves for titrating 20 mM CTAB into 0.1 wt% monomer MEO_2MA and $PEGMA_{2080}$ aqueous solutions at 25.0 °C (a) and 30.0 °C (b)..... 82

Figure 4.3 EMF curves for titrating 20 mM CTAB into water (—○—), 0.05 (—●—), 0.1 (—△—) and 0.2 (—▲—) wt% of poly(MEO_2MA-*co*-$PEGMA_{2080}$) aqueous solutions at 25.0 °C (a) and 30.0 °C (b). The insets of (b) are the optical pictures of 0.1 wt% polymer aqueous solution before and after adding CTAB at 30.0 °C..... 85

Figure 4.4 Binding isotherms of $C_b/C_{polymer}$ as a function of free CTAB concentration (C_f) for poly(MEO_2MA-*co*-$PEGMA_{2080}$) aqueous solutions at 25 and 30 °C. (Polymer concentrations: circle 0.05 wt%; triangle 0.1 wt%; square 0.2 wt%). 87

Figure 4.5 The apparent hydrodynamic radius (R_h) of polymer/surfactant complexes as a function of CTAB concentration at 25.0 and 30.0 °C, respectively..... 88

Figure 4.6 ITC curves for titrating 100 mM TTAB and 200 mM DoTAB into different concentrations of poly(MEO_2MA-*co*-$PEGMA_{2080}$) aqueous solutions at 25.0 °C (a, c) and 30.0 °C (b, d), respectively..... 91

Figure 4.7 Schematic illustration of binding cationic surfactant to thermo-sensitive copolymer below (a) and above (b) its cloud point..... 92

Figure 5.1 Calorimetric titration curves of 100 mM SDS into water (left) and 0.1 wt% M600-grafted CNC (right) at 25 ^oC. (a, c) thermogram of raw heats, and (b, d) ITC enthalpy profiles versus real SDS concentration in the sample cell. 100

Figure 5.2 FT-IR spectra of (a) cellulose nanocrystals, (b) carboxylated CNC, and (c) M600-grafted CNC. 101

Figure 5.3 Conductometric titration curves of 0.1 wt% of CNC, carboxylated CNC and M600-CNC against 0.05 M NaOH solution. 102

Figure 5.4 TEM images of (a) cellulose nanocrystals, and (b) M600-grafted CNC. 103

Figure 5.5 (a) Calorimetric titration curves of 100 mM SDS into water, 0.1 wt% CNC suspension, and 0.1 wt% M600-grafted CNC suspensions at 25 ^oC. (b) Calorimetric titration curves for titration of 100mM SDS into water and M600-grafted CNC suspensions of various concentrations: 0.1, 0.25, and 0.5 wt% at 25 ^oC..... 105

Figure 5.6 ^1H NMR spectra of 0.2 wt% M600-CNC (a), 5mM SDS (b), and their mixtures of 0.2 wt% M600-CNC with 5(c), 10(d), and 20 (e) mM SDS in D_2O solvent. The inset

shows the ^{1}H NMR spectra of 0.2 wt% M600-grafted CNC with 5 mM SDS in D_2O solvent at 25, 45, and 60 ^{o}C. 108
Figure 5.7 Transmittance versus temperature for 0.1, 0.7, and 1.0 wt% M600-CNC aqueous solution at the wavelength of 500 nm. 110
Figure 5.8 (a) Calorimetric titration curves of 200 mM DoTAB into water, 0.1 wt% CNC suspension, and 0.1 wt% M600-grafted CNC suspensions at 25 ^{o}C. (b) Calorimetric titration curves for titration of 100mM DoTAB into water and M600-grafted CNC suspensions of various concentrations: 0.05, 0.1, 0.25, and 0.5 wt% at 25 ^{o}C. 111
Figure 5.9 Calorimetric titration curves for titration of 20 mM Brij 30 into water and M600-grafted CNC suspensions of various concentrations: 0.25, and 0.5 wt% at 25 ^{o}C..... 113
Figure 5.10 Schematic diagrams describing the binding interactions for SDS/M600-grafted CNC and DoTAB/ M600-grafted CNC systems in aqueous media. 114
Figure 6.1 The optical transmittance (T%) of CECh aqueous solution at λ = 500 nm under various pHs. 121
Figure 6.2 The zeta potential of CECh aqueous solution under various values of pH. 122
Figure 6.3 Fluorescence spectroscopy of CECh aqueous solution at different values of pH by using pyrene as a fluorescent probe. 123
Figure 6.4 Potentiometric and conductivity titration of 0.05 wt% CECh with 0.1 M NaOH at 25 ^{o}C. Square-filled symbols represent conductivity, and circle-filled symbols represent pH. 124
Figure 6.5 The solution viscosity as a function of CECh concentration at pH 4 and 10. 126
Figure 6.6 The I_1/I_3 values as a function of CECh concentration at pH 4 and 10. 126
Figure 6.7 Surfactant concentration dependence of the micropolarity in 12-*n*-12/CECh solution (C_{CECh} = 0.05 wt%) in basic media. 127
Figure 6.8 The surface tension of CECh/12-*n*-12 aqueous solution as a function of log*C*s in basic media. 129
Figure 6.9 Surfactant concentration log*C*s dependence of viscosity of CECh/12-*n*-12 aqueous solution in basic media. 131
Figure 6.10 The proposed model for CECh aggregation behavior under different conditions. . 132

List of Tables

Table 2.1 Summary of various types of modifications on CNC whiskers..... 27

Table 2.2 Protein binding capacities of magnetized avicel samples..... 33

Table 4.1 A summary of CMC and C_2 for CTAB at different conditions obtained from ITC and EMF measurements..... 80

Table 4.2 A comparison of maximum ΔH at 25.0 °C and minimum ΔH 30.0 °C for titrating CTAB, TTAB and DoTAB into polymer solutions..... 90

Table 5.1 The CAC, C_2, and thermodynamic parameters from calorimetric titration of 100 mM SDS into 0.1, 0.25, and 0.5 wt% M600-grafted CNC suspensions. 106

List of Schemes

Scheme 2.1 Mechanisms describing the (a) ATRP; and (b) RAFT processes 9
Scheme 2.2 Proposed mechanism for the thermal induced phase transition of copolymers P(MEO_2MA-*co*-OEGMA) in aqueous solutions 14
Scheme 2.3 Schematic description of thermo-sensitive nanogels for siRNA delivery 18
Scheme 2.4 Reaction route for surface fluorescently labeled CNC with FITC..... 26
Scheme 2.5 Procedures for steric stabilization of cellulose microcrystals..... 29
Scheme 2.6 Formation of PDMAEMA grafted on rod-like CNC by surface initiated ATRP 30
Scheme 3.1 Synthetic scheme of P(MEO_2MA-*co*-$PEGMA_{2080}$). 60
Scheme 4.1 (a) Chemical structure of statistical copolymer with monomer ratio 99 to 1 (m: n). (b) Chemical structures of cationic surfactants: DoTAB, TTAB and CTAB..... 76
Scheme 5.1 Chemical structures of surfactants: SDS, DoTAB and Brij 30. 97
Scheme 5.2 The reaction route of grafting Jeffamine M600 on the CNC surfaces. 98
Scheme 7.1 Synthesis route for the grafting of PNIPAM from the surface of CNC..... 138

Nomenclature

AIBN: 2, 2’-azobisisobutyronitrile

AFM: Atomic force microscopy

ASA: Alkenyl succinic anhydride

ATRP: Atom transfer radical polymerization

BIBB: 2-bromoisobutyryl bromide

Brij 30: Poly(ethylene glycol) dodecyl ether

CAC: Critical aggregation concentration

CECh: *N*-carboxyethylchitosan

CMC: Critical micellization concentration

CNC: Cellulose Nanocrystals

CRP: Controlled radical polymerization

CTAB: cetyltrimethylammonium bromine

C_b: Concentration of polymer-bound surfactant

C_f: Free surfactant monomer concentration

C_t: Total surfactant concentration

C_2: Saturation concentration

DMF: Dimethyl formamide

DLS: Dynamic light scattering

DODA: Dioctadecyldimethylammonium

DoTAB: dodecyltrimethylammonium bromide

DS: Degree of substitution

EDC: *N*-(3-dimethylaminopropyl)-*N′*-ethylcarbodiimide hydrochloride

EHEC: Ethyl(hydroxyethyl) cellulose

EMF: Electromotive force

EOR: Enhanced Oil Recovery

EPTMAC: Epoxypropyltrimethylammonium chloride

FITC: Fluorescein-5’-isothiocyanate

FT-IR: Fourier-transform infrared spectroscopy

GPC: Gel permeation chromatography

HM-HEC: Hydrophobically modified hydroxyethylcellulose

HRTEM: High-resolution transmission electron microscopy

IEPs: isoelectric points

ITC: Isothermal titration calorimetry

LCSC: Lower critical solution concentration

LCST: Lower critical solution temperature

LLS: Laser light scattering

MBP: Methyl 2-bromopropionate

MEO_2MA: 2-(2-Methoxyethoxy) ethyl methacrylate

M_n: Number average molecular weight

M_w: Weight average molecular weight

NaCMC: Sodium carboxymethyl cellulose

NHS: *N*-hydroxysuccinimide

NMP: Nitroxide mediated polymerization

NMR: Nuclear magnetic resonance

OEGMA: Oligo(ethylene glycol) methacrylates

OTAB: octadecyl trimethylammonium bromides

PDI: Polydispersity index

PDMAEMA:
Poly(dimethylaminoethyl methacrylate)

PEG: Polyethylene glycol

$PEGMA_{2080}$:
Poly(ethylene glycol) methyl ether methacrylate

PEI: Poly(ethylenimine)

PEMA: Poly(*N*-ethylmethylacrylamide)

PNIPAM: Poly(*N*-isopropylacrylamide)

PPG: Polypropylene glycol

PTEGMA: Poly(methoxytri(ethylene glycol) acrylate)

PTEGSt: Poly(4-vinylbenzyl methoxytris-(oxyethylene) ether)

PVCL: Poly(*N*-vinylcaprolactam)

PVP: Poly(vinylpyrrolidone)

RAFT: Reversible addition fragmentation chain-transfer polymerization

R_g: Radius of gyration

R_h: Hydrodynamic radius

SAED: Selected area electron diffraction

SDS: Sodium dodecyl sulfate

SLS: Static light scattering

SSE: Surfactant selective electrode

TEM: Transmission electron microscopy

TEMPO: 2, 2, 6, 6-tetramethylpiperidine-1-oxyl reagent

TGA: Thermal gravimetric analysis

TRPs: Thermo-Responsive Polymers

TTAB: tetradecyltrimethylammonium bromide

UCST: Upper critical solution temperature

UV-Vis: Ultraviolet-visible spectroscopy

XPS: X-ray photoelectron spectroscopy

Chapter 1 Introduction

1.1 Background

Stimuli-responsive polymers are those that undergo conformational and chemical changes in response to an external stimulus arising from changes in environmental conditions. There are many different signals that are capable of modulating the responses of polymeric systems, and they can be broadly classified into either physical or chemical signals. Chemical signals, such as pH, ionic and chemical agents will alter the molecular interactions with polymeric chains and solutes at the molecular level. While physical signals, such as temperature, light, electrical potential, electric or magnetic fields, and mechanical stress alter the energies of chain dynamics and molecular interactions at critical onset points. [Gil and Hudson, 2004; Dai et al., 2009] These smart polymers possess the potential of providing a specific chemical function and tailored molecularly assembled structure, which can be applied in various applications, such as controlled drug delivery, gene therapy, protein separation and purification, textile engineering and membrane science. [Schmaljohann, 2006; Liu and Urban, 2010; Stuart et al., 2010]

Cellulose Nanocrystals (CNC) have garnered a tremendous level of attention in materials science. The CNC particles are rigid rod-like crystals with diameter in the range of 10-20 nm and lengths of a few hundred nanometers. Indeed, CNC particles are excellent polymeric nanomaterials due to their promising physical and chemical properties, such as nano-scale dimension, unique morphology, inherent renewability and sustainability, in addition to their abundance and low cost. They are generated by the removal of amorphous regions of a purified cellulose source via acid hydrolysis, often followed by ultrasonic treatment. Cellulosic sources are diverse, and their degree of crystallinity strongly influences the dimensions of CNC particles. [Klemm et al., 2011] Surface modification is one of the key approaches of modifying the

physical and chemical properties of CNC. This is usually achieved by modifying the CNC particles through the grafting of synthetic polymers onto the CNC surface, without destroying its intrinsic properties. Depending on the polymer that is grafted onto the cellulose, it is possible to attain environmental responsive properties, such as pH, photo, and temperature. [Roy et al., 2009] By grafting polymers onto CNC, the stability of functionalized CNC in various solvents can be enhanced. An alternative to chemical surface modification is the adsorption of surfactants at the colloidal surface to improve nanoparticle stability in organic solvents. As a result of their distinctive properties, CNC particles possess many potential applications, for example as reinforcing fillers in nanocomposite systems. [Favier et al., 1995] Numerous nanocomposite materials were developed by incorporating CNC into a wide range of polymeric matrices, while chemical functionalization of CNC expanded its potential applications in other sectors.

In the last several decades, extensive studies have focused on the interactions between surfactants and water-soluble polymers, which have a wide range of applications. In these studies, both cooperative and non-cooperative bindings were observed, while the binding processes were described by two critical concentrations, i.e. critical aggregation concentration (CAC) and saturation concentration (C_2). A common rule describing the interactions in various polymer concentration regimes was proposed and verified. In the dilute regime, the polymer chains behave as individual entities, and polymer/surfactant interactions may induce intra-chain aggregation. In semi-dilute regime, the polymer/surfactant interactions may induce inter-chain associations. [Nyström et al., 2009] In the thermo-responsive polymers (TRPs) and surfactants systems, surfactants can alter the hydrophobic/hydrophilic balance of polymers, resulting in changes in the phase transition characteristics. Thus, surfactants can play an important role in improving the stability of CNC particles. In this research study, we will focus on the interaction

between surfactants, TRPs and TRP-modified CNC, where the interaction mechanism will be elucidated. Such fundamental knowledge will be necessary to guide formulator in the design and development of personal care products.

The scope of this thesis can be divided into three parts: (1) synthesis of well-defined random copolymer based on OEGMA and investigating its thermo-responsive behavior in aqueous solution, as well as its binding interaction with cationic surfactants; (2) preparation of thermo-responsive polymer grafted CNC and studying its interactions with surfactants at CNC surface; (3) functionalization of chitosan and examining the interactions between its derivative with surfactants. In this thesis, Chapter 1 introduces the general background of the research topics, and the research objectives of this thesis are clearly presented. Chapter 2 reviews the preparation and solution properties of water-soluble thermo-responsive polymers, the characterisctics and modifications of CNC, as well as polymer-surfactant interactions. Chapter 3 reports on the synthesis, characterization and thermo-responsive behavior of P(MEO_2MA-*co*-$PEGMA_{2080}$) The interactions between this neutral copolymer and cationic surfactants are investigated in Chapter 4. In Chapter 5, the preparation of thermo-responsive polymer grafted CNC is introduced, and its interactions with three types of surfactants, i.e. anionic (SDS), cationic (DoTAB) and non-ionic (Brij 30), are also studied. Chapter 6 presents the preparation and properties of one type of chitosan derivative, and its solution behavior in the presence of gemini surfactant was examined. Chapter 7 summarizes the conculsions and original contributions of the doctoral research, and also provides several recommendations for future study.

1.2 Research objectives and methodology

1.2.1 Synthesis of TRPs based on oligo(ethylene glycol) methacrylates

The studies on biocompatible thermo-responsive polymers based on OEGMA have received significant attentions since they exhibited similar thermoresponsive behaviors as PNIPAM. Due to possible concerns on the toxicity of *N*-isopropylacrylamide monomer, a well-defined random copolymer based on oligo(ethylene glycol) methacrylates will be synthesized using the atom transfer radical polymerization (ATRP) process, and its thermo-responsive behaviors in aqueous solution will be investigated. The thermo-responsive behaviors will be monitored by temperature controlled UV-visible spectrophotometer, and laser light scattering (LLS) and transmission electron microscopy (TEM) are employed to explore the morphology.

1.2.2 Binding of cationic surfactants with the copolymer

Binding interactions between cationic surfactants and this copolymer below and above its cloud point will be studied by isothermal titration calorimetry (ITC), surfactant selective electrode (SSE) and dynamic light scattering (DLS). Three types of cationic alkyltrimethylammonium bromide surfactants (RTAB with R equal to C_{12}, C_{14}, and C_{16}), namely DoTAB, TTAB, and CTAB, will be examined, and the binding affinity will be determined. The surfactant-selective electrode (SSE) will be used to monitor the monomeric surfactant concentrations during the surfactant/polymer binding process, in order to complement the ITC measurements, while the possible morphologies of copolymer and surfactant complexes can be elucidated from DLS measurements. These studies can develop fundamental knowledges on the binding mechanism at different temperatures, which is critical for optimizing the formulations of personal care products.

1.2.3 Grafting TRPs on CNC surface

In order to improve the dispersibility and steric stability of CNC, a water-soluble thermo-responsive polymer Jeffamine M600 will be grafted on CNC surface. The M600-grafted CNC will be prepared in a two-step reaction, i.e. TEMPO-mediated oxidation of CNC, followed by grafting of amine-terminated Jeffamine M600 onto oxidized CNC. Carboxylic acid functionalities will be introduced to CNC using the TEMPO-mediated oxidation technique, while the grafting of Jeffamine M600 onto CNC can be achieved via the EDC/NHS reaction. Infrared spectroscopy and transmission electron microscopy (TEM) will be applied to confirm the M600-grafted CNC products.

1.2.4 Study on the interactions between surfactants and TRP-modified CNC

Surface coating is another way to modify CNC particles. In order to obtain a better understanding on the coating mechanism on CNC surface, the interactions between surfactants and M600-grafted CNC on its surface will be investigated by isothermal titration calorimetry (ITC). Three types of surfactants with dodecyl alkyl chain and different head groups, namely cationic dodecyltrimethylammonium bromine (DoTAB), anionic sodium dodecyl sulfate (SDS), and nonionic poly(ethylene glycol) dodecyl ether (Brij 30) will be studied.

1.2.5 Aggregation behavior of *N*-carboxyethylchitosan in the presence of surfactant

N-carboxyethylchitosan (CECh) will be synthesized by Michael addition reaction using chitosan and acrylic acid. The effects of pH, polymer concentration, as well as a gemini surfactant on the aggregation behavior of CECh in aqueous solution will be studied. The solubility of chitosan in basic media is improved by this reaction, and fundamental understanding on interactions between one type of biomacromolecule and gemini surfactant are developed.

Chapter 2 Literature Review

2.1 Introduction

Polymers that respond to temperature changes are often referred as thermo-responsive polymers (TRPs), and are probably the most widely used in environmentally responsive polymeric systems. This is because changes in temperature are not only relatively easy to control, but also easily applicable both *in vitro* and *in vivo*. [Gil and Hudson, 2004] The properties of polymers, such as chain conformation, configuration, and solubility, can be manipulated by controlling the temperature resulting in the formation of aggregates of various sizes and morphologies. Besides this, thermo-responsive microgels, functionalized surfaces, membranes, micelles and various types of robust structures are prepared based on TRPs, and can be widely applied to biomedical systems, separation processes, textile industry etc. [Stuart et al., 2010; Nagase et al., 2009; Crespy and Rossi, 2007] The combination of TRPs and a new promising nanomaterial, namely cellulose nanocrystals (CNC), has gained increasing attention due to their broad potential applications in materials science. CNC particles exhibit exceptional strength and physicochemical properties, and they have been functionalized with various moieties, depending on the desired applications. Surfactants have been used to improve the dispersability of CNC nanoparticles, and complexes of CNC/surfactants were recently reported as drug carriers. [Jackson et al., 2011] Moreover, surfactants/polymer systems have been widely used in many industrial product formulations, such as cosmetics, food additives, pharmaceutical formulations, and additives in enhanced oil recovery. [Kwak, 1998; Holmberg et al., 2002] Therefore, studies on the interactions between surfactant and TRPs in bulk and at interface are extremely important and fundamental insights are critical in guiding future product formulations and development.

The scope of the current review is to provide insights into the preparation and solution properties of water-soluble thermo-responsive polymers (TRPs) both in bulk and at CNC surface. Some common and popular homopolymers are reviewed in details, and various unique multi-responsive copolymers are introduced. Their interactions with surfactants and applications are discussed.

2.2 Thermo-responsive polymers (TRPs)

2.2.1 Overview of thermo-responsive polymers

Thermo-responsive polymers exhibit conformation changes in aqueous solutions at a critical onset temperature, which is commonly referred to as the critical solution temperature. Critical solution temperature corresponds to a temperature where one of its physical properties undergoes a step change. [Gil and Hudson, 2004] Two thermal transitions commonly observed in polymeric systems are the lower critical solution temperature (LCST) and the upper critical solution temperature (UCST). When the dissolved polymeric chains become insoluble with increasing temperature, the phase transition is often referred to as the LCST.

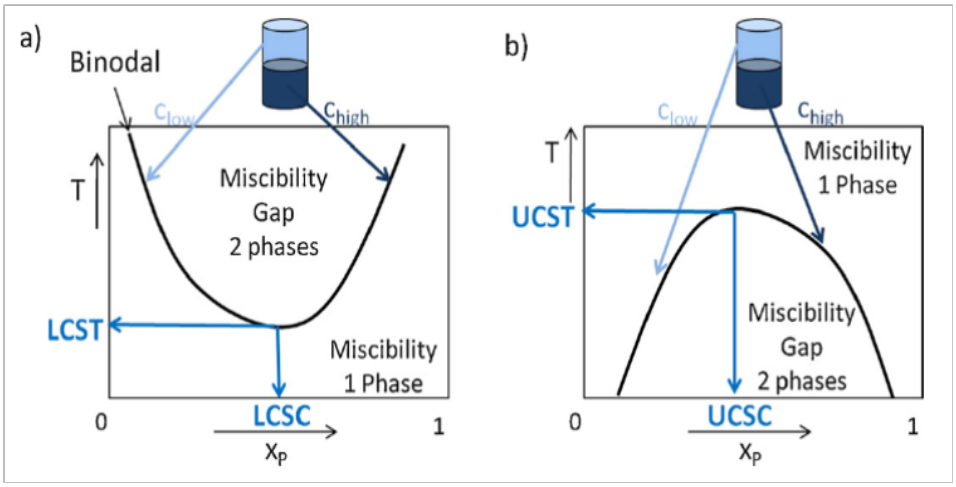

Figure 2.1 Phase diagram for a binary polymer/solvent mixture exhibiting (a) LCST behavior and (b) UCST behavior. [Weber et al., 2011]

As shown in Figure 2.1, the LCST is defined as the minimum temperature of the phase separation curve on concentration-temperature phase diagram, while the corresponding concentration is the lower critical solution concentration (LCSC). On the contrary, in Figure 2.1b, the maximum point on the phase diagram is termed the upper critical solution temperature (UCST), below which the phase separation occurs.

Among the polymers that display a LCST, poly(*N*-isopropylacrylamide) (PNIPAM) is probably the most common and popular thermo-responsive polymer since it exhibits a sharp phase transition (LCST) at around 32 ^{o}C in aqueous media, just below the physiological temperature (37 ^{o}C) As a result, extensive studies have been conducted and reported, and numerous ideas have been offered for their applications as smart materials in biological applications. [Schild, 1992] The fundamental behavior of PNIPAM was extensively studied to gain insights into the mechanism of phase separation. With this understanding, polymers can be designed at the molecular level with controlled LCST, where their response to thermal stimuli can be manipulated for specific applications, e.g. as microvalves in microfluidic devices. [Li et al., 2010] The phase transition of PNIPAM in aqueous media is attributed to a shift in the distribution of hydrophobic and H-bond interactions. Below its LCST, it is hydrated and adopts an extended coil conformation. Beyond the LCST, it undergoes a sharp and reversible coil-to-globule phase transition from a hydrophilic to a more hydrophobic state. [Morris et al., 2010] PNIPAMs with well-defined size and a low polydispersity index (PDI) have been designed and developed using controlled radical polymerizations techniques (CRP), such as atom transfer radical polymerization (ATRP), reversible addition fragmentation chain-transfer polymerization (RAFT), and nitroxide mediated polymerization (NMP). ATRP and NMP control chain growth by a reversible termination process step, while RAFT polymerization controls chain growth

through reversible chain-transfer. The mechanisms of ATRP and RAFT are described in Scheme 2.1. [Wang and Matyjaszewski, 1995; Chiefari et al., 1998; Dai et al., 2009] Controlled radical polymerization is an attractive alternative to anionic polymerization for the preparation of well-defined polymers. It allows the controlled synthesis of a variety of novel well-defined polymer architectures having interesting structure-property-function relationships (such as block and graft copolymers, stars, brushes and bottle-brush structures) starting from a vast array of commercial functional monomers. [Aseyev et al., 2011] Ganachaud et al. [2000] reported on the RAFT polymerization of NIPAM in benzene and 1, 4-dioxane with 2, 2'-azobisisobutyronitrile (AIBN) as radical initiator, while Convertine et al. [2004; 2006] conducted RAFT polymerization of NIPAM in dimethyl formamide (DMF) and water, respectively.

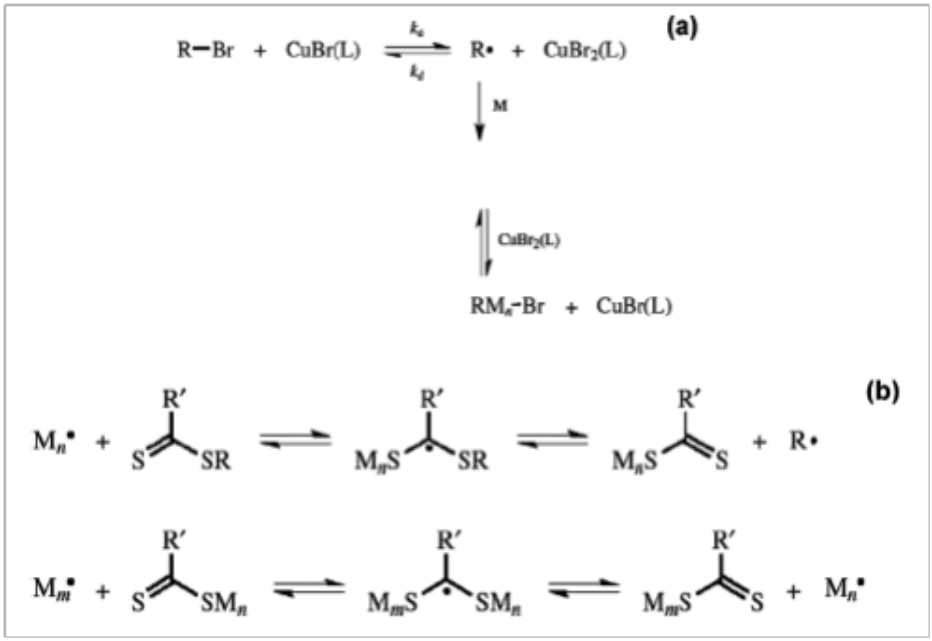

Scheme 2.1 Mechanisms describing the (a) ATRP; and (b) RAFT processes. [Wang and Matyjaszewski, 1995; Chiefari et al., 1998; Dai et al., 2009]

Besides PNIPAM, many other thermo-responsive synthetic polymers with different structures have been prepared and investigated extensively. Xu et al. [2008] reported on the

polymerization of poly(*N*-ethylmethylacrylamide) (PEMA) using both RAFT and ATRP, and investigated the effects of molecular weight, polymer concentration, and end group hydrophilicity/hydrophobicity on the LCST of PEMA. A series of thermo-responsive polymers based on acrylamide monomers, namely *N*-n-propylacrylamide (nPAM), *N*, *N*-diethylacrylamide (DEA), and *N*-ethylmethylacrylamide (EMA), were prepared and studied by Cao and co-workers. [2007] The thermo-responsive behaviors of poly(dimethylaminoethyl methacrylate) (PDMAEMA), poly(*N*-vinylisobutylamide) (PNVIBA), poly(*N*-vinylcaprolactam) (PVCL) were also investigated. [Schacher et al., 2009; Suwa et al., 1998; Hurtgen et al., 2012] Linear polyethers are another class of thermo-responsive polymers. For example, polyethylene glycol (PEG) is one such water-soluble polymer that possesses a LCST greater than 90 ^{o}C, while polypropylene glycol (PPG) normally possesses a much lower LCST since the enhancement on the hydrophobicity of alkyl segments results in the reduction of LCST. Furthermore, block copolymers based on PEG and PPG exhibit thermo-responsive characteristics and the LCSTs are dependent on the ratio of the PPG and PEG segments.

Although most of thermo-responsive polymers are synthetic polymers, the thermo-responsive behavior of some biopolymers such as gelatin, [Gil et al., 2005] agarose, [Ramzi et al., 1998] cellulose derivatives [Hirsch and Spontak, 2002] and elastin-like polypeptides (ELPs) [Mano, 2008] have been reported. Gelatin is a protein derived from the degradation of natural collagen by breaking its triple-helix structure into single-strand molecules. In aqueous solution, their chain conformation transforms from a random coil to triple-helix upon cooling, resulting in the promotion of physical junction and gelation. Gelatin is classified as a thermo-reversible hydrogel and has been used as gelling agent in many applications. Polypeptides based on the fibrous protein elastin were reported to exhibit a natural phase transition. The system based on

the elastin pentapeptide repeat units, Val-Pro-Gly-Xaa-Gly (Xaa = any natural amino acids except proline) was prepared and they exhibited a LCST behavior of around 40 ^{o}C. The transition temperatures of these materials were designed such that particles may be conjugated with drug molecules for temperature mediated medical applications. [Meyer et al., 2001; Dreher et al., 2003]

2.2.2 TRPs with tunable thermo-sensitivity

A novel class of random copolymers with tunable thermo-sensitivity has gained increasing attention since they possess the potential of replacing PNIPAM. A series of copolymers of 2-ethyl-2-oxazoline and 2-n-propyl-2-oxazoline were synthesized by Hoogenboom et al., [2008] and the cloud points of these copolymers could be tuned from 25 ^{o}C to 100 ^{o}C by varying the molecular weight and composition. Soga and co-workers [2004] synthesized a novel class of thermo-sensitive and biodegradable polymers, namely, poly(*N*-(2-hydroxypropyl) methacrylamide mono/di lactate) (poly(HPMAm-mono/di lactate)). The cloud points of poly(HPMAm-monolactate) and poly(HPMAm-dilactate) in water were 65 and 13 °C, respectively. The cloud point of poly(HPMAm-monolactate-*co*-HPMAm-dilactate) copolymers can be tunable by varying the copolymer composition. Lutz et al. [2006] described the synthesis of oligo(ethylene glycol) methacrylates via ATRP, where these polymer systems possess tunable thermo-sensitive characteristics, and this system will be discussed in section 2.2.3. If a block copolymer possesses multiple thermo-sensitive blocks, the aqueous solution might display a single cloud point at an intermediate temperature, or both blocks might collapse independently from one another. [Weber et al., 2011] It was reported that some block copolymers exhibited unique temperature-induced self-assembly behaviors. [Hua et al., 2006; Weiss et al., 2011; Zhang et al., 2011] Hua et al. [2006] prepared block copolymer of poly(methoxytri(ethylene

glycol) acrylate)-*b*-poly(4-vinylbenzyl methoxytris-(oxyethylene) ether) (PTEGMA-*b*-PTEGSt) that exhibited multiple transitions in aqueous solution upon heating (shown in Figure 2.2). It was demonstrated that the two-step thermal induced aggregation process was attributed to the different dehydration temperature of the two blocks, i.e. the first PTEGSt block dehydrated to form micellar structure, followed by the dehydration of PTEGMA block to produce large and polydisperse aggregates, and the solution changed from transparent to cloudy, clear, bluish, and then turbid.

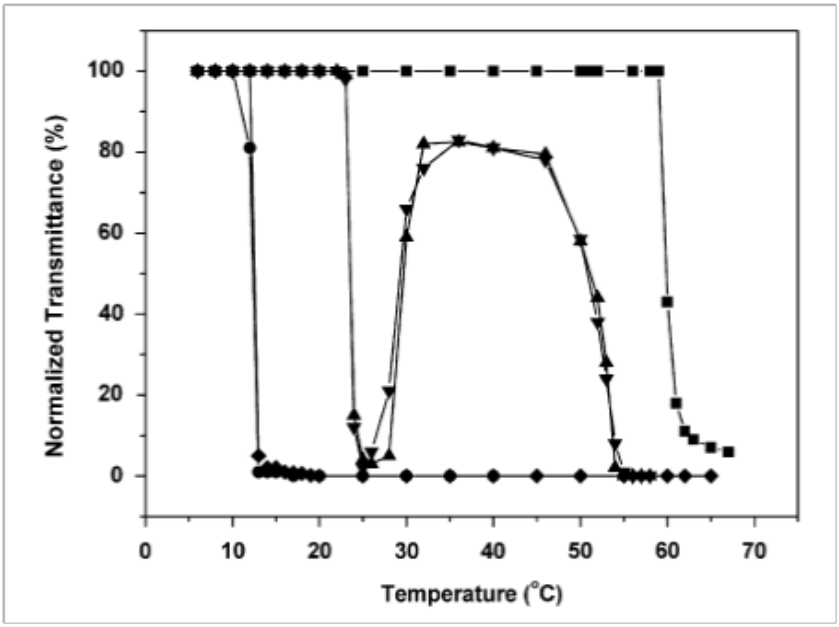

Figure 2.2 Optical transmittances of aqueous solutions of $PTEGMA_{66}$-*b*-$PTEGSt_{72}$ upon heating (▲) and cooling (▼), PTEGSt (●), PTEGMA (■), and mixture (◆) of PTEGSt and PTEGMA at various temperatures. [Hua et al., 2006]

A group of dual thermo-responsive block copolymers containing PPO sequences was prepared and investigated. [Dimitrov et al., 2004; Hasan et al., 2004; Li et al., 2005; Chen et al., 2005] Dimitrov et al. [2004] prepared a number of ABA and BAB triblock copolymers using ethoxyethyl glycidyl ether (EEGE) and propylene oxide (PO) monomers, while Hasan et al. [2004] synthesized PNIPAM-PPO-PNIPAM triblock copolymers with different PNIPAM

segment lengths. These polymers exhibited a two-stage phase transition in aqueous solution, which offers an opportunity to tune the microstructure by changing temperature.

2.2.3 TRPs based on oligo(ethylene glycol) methacrylates

In 2006, Lutz and co-workers published the first report comprising of copolymers of P(MEO_2MA-*co*-$PEGMA_{475}$) that exhibited similar thermo-responsive behaviors as PNIPAM. [Lutz et al., 2006] They randomly polymerized di(ethylene glycol) methyl ether methacrylate (MEO_2MA, M_n = 188 g/mol) and poly(ethylene glycol) methyl ether methacrylate (PEGMA, M_n = 475 g/mol) via atom transfer radical polymerization (ATRP), and they found that the LCSTs of the copolymers could be tuned between 26 and 90 ^oC by varying the monomer composition. For instance, the LCST values for the copolymers increased from 26 ^oC (0% of $PEGMA_{475}$) to a relatively higher temperature as the mole fraction of $PEGMA_{475}$ in the polymer chain was increased. A LCST of 32 ^oC was observed in water for a copolymer possessing 5% of $PEGMA_{475}$ units per chain. The relatively higher LCST was due to the high proportion of longer PEG side chains, which can stabilize the polymeric chains in aqueous solution at a higher temperature. [Lutz and Hoth, 2006] The proposed mechanism (shown in Scheme 2.2) for the temperature-induced phase transition of these copolymers in aqueous solution was illustrated by Lutz and coworkers. [Lutz et al., 2007] The favored formation of H-bonds between the ether oxygens of poly(ethylene glycol) and water surrounding water molecules is the driving force in promoting the aqueous solubilization of P(MEO_2MA-*co*-OEGMA) at room temperature, and this favorable effect is counterbalanced by the hydrophobicity of the non-polar backbone. Above LCST, this balance is disrupted and polymer-polymer interactions are thermodynamically favored compared to polymer-water interactions, resulting in phase separation. In comparison to the traditional PNIPAM system, these polymers have inherent advantages such as: (i) an

excellent bio-repellency below the LCST (i.e., anti-fouling behavior), (ii) reversible phase transitions (i.e., no marked hysteresis), and (iii) bio-inert properties (i.e., no specific interactions with biological materials). [Lutz, 2011] There was some debate on whether the era of PNIPAM is over since this new polymer system might displace PNIPAM as a suitable thermo-responsive polymeric system.

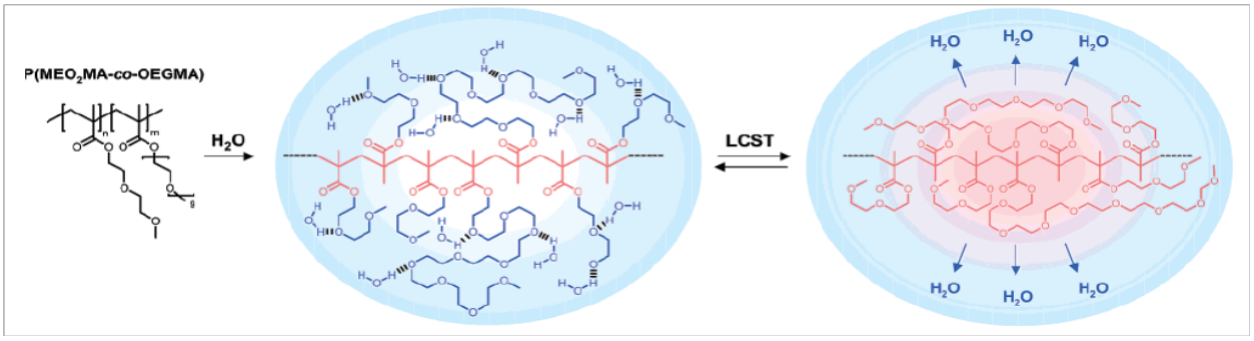

Scheme 2.2 Proposed mechanism for the thermal induced phase transition of copolymers P(MEO_2MA-*co*-OEGMA) in aqueous solutions. [Lutz et al., 2007]

In a report by Ishizone and co-workers, [2008] they polymerized oligo(ethylene glycol) methacrylates with very short side chains of 1 ~ 4 units using anionic polymerization, and they found that polymer with one side unit was insoluble in water, whereas polymers possessing di-, tri-, and tetra(ethylene glycol) units exhibited LCST behavior in aqueous solutions. LCSTs and hydrophilicity of polymers were strongly dependent on the side chain length of oligo(ethylene glycol) units. Armes and co-workers first described the ATRP of an oligo(ethylene glycol) methyl ether methacrylate (OEGMA) with 8 ethylene oxide (EO) units. [Wang et al., 1999; Wang and Armes, 2000] The controlled radical polymerization was performed in aqueous environment at room temperature that led to the formation of POEGMA with a narrow molecular weight distribution. Similarly, well-defined POEGMA was also prepared from ATRP in organic solvents. Lutz [2008] reported that the ATRP of oligo(ethylene glycol)-based monomers is rapid and well-controlled in pure ethanol, which is polar enough to generate fast polymerization

kinetics. While non-polar solvent such as anisole was also successfully applied in the ATRP process of either MEO_2MA, tri(ethylene glycol) methyl ether methacrylate (MEO_3MA), or longer OEGMA oligomers. Besides ATRP, other controlled radical polymerization techniques were also reported for the polymerization of PEG macromonomers. Becer and co-workers [2008] described systematic and parallel polymerizations of various OEGMA monomers using RAFT method. A series of well-defined homopolymers of different side-chain length were prepared and they found that the LCST behavior of polymer solutions strongly depended on the side-chain length, i.e. LCST decreased with decreasing number of ethylene glycol units. Furthermore, they also demonstrated that replacing the methoxy with ethoxy end group could significantly reduce the cloud points due to the greater hydrophobicity. The controlled radical polymerization methods as well as the thermo-responsive properties of oligo(ethylene glycol)-based polymers have been summarized in an excellent review by Lutz. [2008]

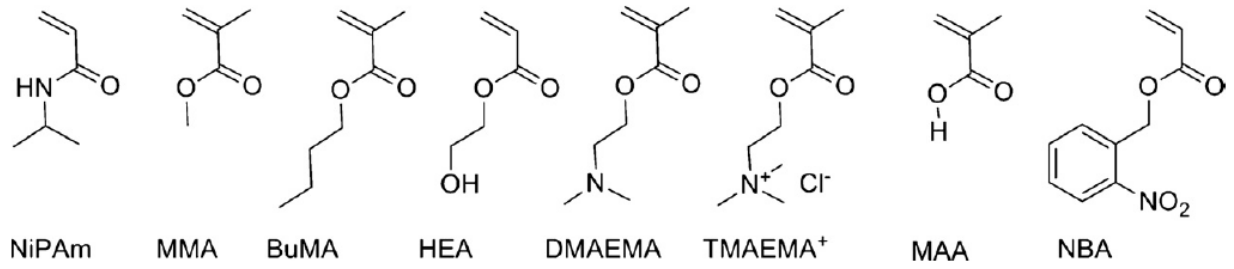

Figure 2.3 Schematic representations of monomers that have been applied for copolymerization with oligo(ethylene glycol) methacrylates or ethoxytri(ethylene glycol) acrylate. [Weber et al., 2011]

A wide range of monomers (shown in Figure 2.3) has been copolymerized with OEGMA to provide additional interesting features to the resulting copolymers and their effect on the phase transition temperatures of POEGMA in aqueous solutions were investigated. Yamamoto et al. [2008] synthesized statistical copolymers of di(ethylene glycol)methyl ether methacrylate

(MEO_2MA) and either methacrylic acid (MAA) or *N*,*N*-dimethylaminoethyl methacrylate (DMAEMA) by ATRP, and they investigated the effect of molar fraction (either MAA or DMAEMA) on the LCST of copolymer solution at different pHs. A similar study on the properties of copolymers based on MAA and two PEO macromonomers with different EO units (PEO_8MA and $PEO_{22}MA$) was conducted by Becer and co-workers. [2008] These copolymers were synthesized by RAFT polymerization. In addition, Jiang and co-workers [2008] developed a thermo- and light-sensitive copolymers containing ethoxytri(ethylene glycol) acrylate (EO_3A) and *o*-nitrobenzyl acrylate (NBA), and they found that the addition of NBA could elevate the LCST compared to PEO_3A due to the hydrophobicity of NBA.

2.2.4 Applications of thermo-responsive polymeric systems

Thermo-sensitivity is one of the most interesting characteristics in stimuli-responsive polymeric nanocarriers and it has been extensively investigated to exploit their applications. For instance, thermo-responsive polymers are very promising materials in biomedical and bioengineering, such as drug and gene delivery, protein chromatography, textile industry, and tissue engineering. [Stuart et al., 2010; Nagase et al., 2009; Crespy and Rossi, 2007] By far, PNIPAM has been the most studied and applied thermo-responsive polymer and therefore can be considered as the gold standard. Functionalized structures based on PNIPAM and other TRPs have been exploited, such as micelles, hydrogels, and functional surface. Some of the major applications of TRPs systems are discussed below.

Drug Delivery Applications of thermo-responsive nanoparticle systems in controlled drug delivery could be the most significant application of such systems. PNIPAM copolymers have been widely studied as drug carriers, especially for oral delivery. Kim and co-workers synthesized poly(*N*-isopropylacrylamide-*co*-butylmethacrylate-*co*-acrylic acid) (poly(NIPAM-

co-BMA-*co*-AA)), and they investigated the intestinal delivery of calcitonin and insulin. They found that the polymeric systems improved the delivery of drugs, and reduced the side effects. [Serres et al., 1996; Ramkisson-Ganorkar et al., 2000] Meyer and co-workers [2001] synthesized two thermo-responsive polymers, elastin-like polypeptide (ELP) and copolymer of *N*-isopropylacrylamide (NIPAM) and acrylamide (AM) that possessed LCSTs slightly above physiological temperature. They developed a new thermal targeting method in which a thermo-responsive drug carrier selectively accumulates in a solid tumor. The delivery of drugs to solid tumors can be achieved by conjugating the drug to the thermo-responsive polymers together with the local heating of tumors. For example, rhodamine-poly(NIPAM-*co*-AM) conjugates were selectively accumulated in a tumor tissue using targeted hyperthermia. Furthermore, hyperthermia can be achieved using an alternating magnetic field with the incorporating of magnetic nanoparticles to these thermo-responsive drug delivery systems, so that the delivery systems can release the active drug compound to the disease tissues. [Brazel, 2008; Du et al., 2010]

Gene Therapy and Delivery Thermo-responsive polymers, as an important family of gene carriers, have been widely studied. Hinrichs and co-workers [1999] polymerized 2-(dimethylamino) ethyl methacrylate (DMAEMA) and *N*-isopropylacryl amide (NIPAM) of various monomer ratios and molecular weights, and they evaluated the copolymers as carrier systems for DNA delivery. They found that the composition and molecular weight of copolymers have significant impact on the stability, cytotoxicity, and transfection efficiency of the polyplexes. Similar polymers were prepared by Kurisawa et al., [2000] that were capable of condensing DNA. Since then, a family of thermo-responsive polymers comprising PNIPAM segment have been reported as gene carriers. [Oupický et al., 2003; Cheng et al., 2006; Mao et

al., 2007] Furthermore, thermo-responsive hydrogel nanoparticles were prepared and studied as gene delivery systems (Scheme 2.3). Choi and co-workers [2006] synthesized Pluronic/poly(ethylenimine) (PEI) hydrogel nanoparticles using a modified emulsification/solvent evaporation method. The prepared Pluronic/PEI nanocapsules exhibited thermal reversible swelling/deswelling behavior. The particle volumes increased drastically as the temperature was decreased, which could induce endosomal disruption. *In vitro* siRNA delivery studies showed that the nanoparticles complexed with siRNA-PEG conjugate enhanced the extent of gene silencing and the RNA activity was significantly increased by cold-shock treatment. [Lee et al., 2008]

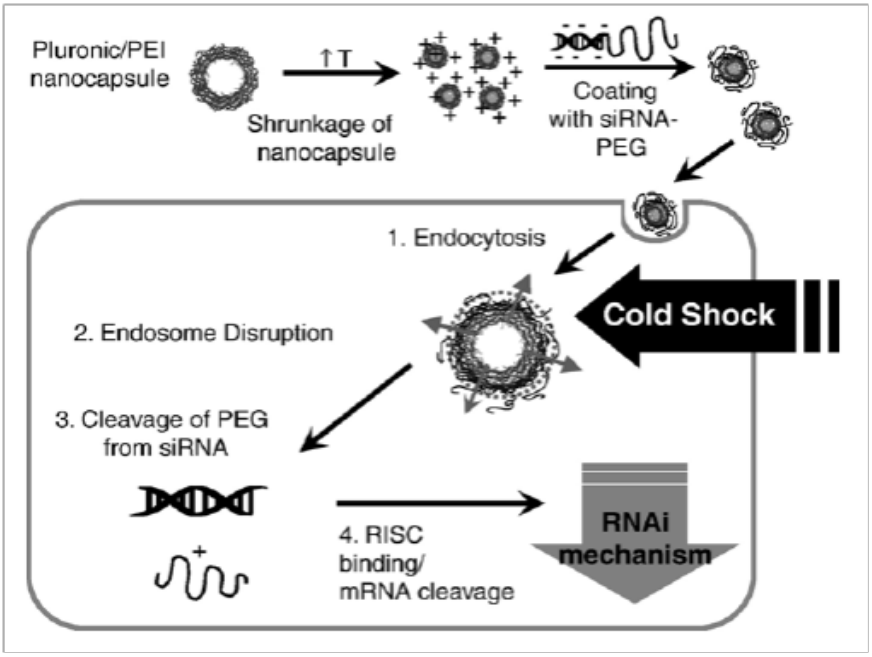

Scheme 2.3 Schematic description of thermo-sensitive nanogels for siRNA delivery. [Lee et al., 2008]

Textile Industry The thermo-responsive polymers were also used in the textile industry to modify and impart new functionality to textiles. The smart textiles with novel functions possess additional permeation properties, which are sensitive to the external climate or the microclimate between the wearer's skin and the fabric. [Crespy and Rossi, 2007] NIPAM was successfully grafted onto a polypropylene non-woven fabric, which was treated by plasma before the reaction. It was reported the modified fabric displayed improved wettability (than the un-modified ones) and unique porous structure after freeze-dry process. [Chen et al., 2002] In contrast with non-woven fabric, Liu and co-workers [1999] conducted the grafting of NIPAM on a cotton cellulose fabric, and they obtained functionalized temperature sensitive fabric surface.

2.3 Grafting TRPs onto cellulose nanocrystals (CNC) surface

2.3.1 General aspect of CNC

Cellulose nanocrystals are rigid rod-like crystals with diameter in the range of 10-20 nm and lengths of a few hundred nanometers (Figure 2.4); e.g. crystallites from tunicates and green algae have lengths in the range of a few micrometers and crystallites from wood and cotton have lengths of the order of a few hundred nanometers. Therefore, the relative degree of crystallinity and the geometrical aspect ratio i.e. the length-*to*-diameter (L/d) are important parameters controlling the properties of CNC-based materials. In this thesis, we use "cellulose nanocrystals" (CNC) to define this material, where have been often referred to as whiskers, microcrystals, nanofibers, microcrystallites. When prepared in sulfuric acid, they possess negative charges on their surface due to the formation of sulphate ester groups during acid treatment, which enhances their stability in aqueous solutions. According to its structure, CNC possesses an abundance of hydroxyl groups on the surface, where chemical reactions can be conducted. Among the three kinds of hydroxyl groups (Figure 2.5), the OH group on the 6 position acts as a primary alcohol,

where most of the modification predominantly occurs. [Roy et al., 2009] Various chemical modifications of CNC, such as esterification, cationization, carboxylation, silylation, and polymer grafting have been reported. [Braun and Dorgan, 2009; Hasani et al., 2008; Habibi et al., 2006; Goussé et al., 2002; Morandi et al., 2009] There is increasing research focus on modification of CNC because of the increasing potential applications of modified CNC in various industrial sectors, such as personal care, nanocomposites, biomedical.

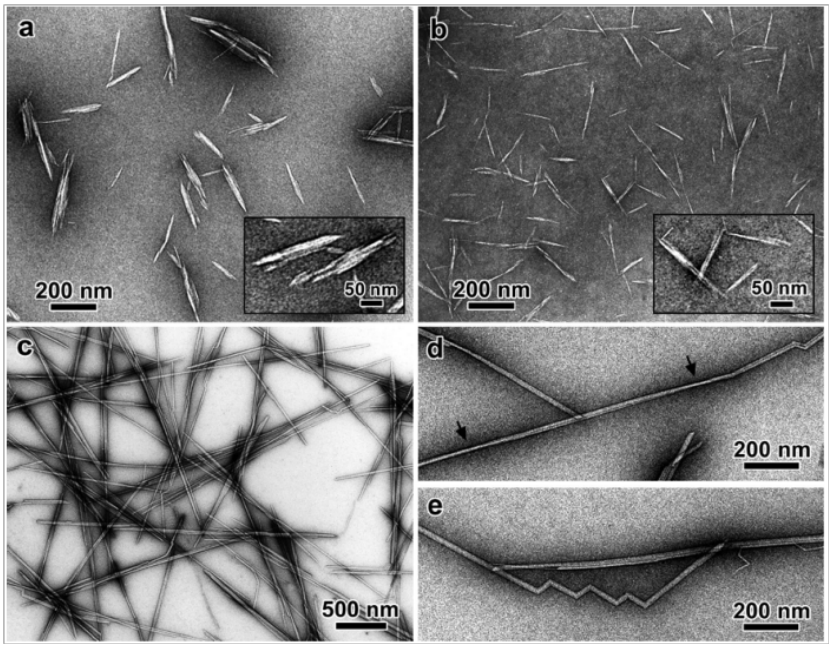

Figure 2.4 TEM micrographs of nanocrystals obtained by sulfuric acid hydrolysis of (a) cotton (b) avicel (c-e) tunicate cellulose. The insets of (a) and (b) provide higher resolution images of some characteristic particles. [Elazzouzi-Hafraoui et al., 2008]

Many polymers were applied to graft on CNC surface, focusing on the improvement of its dispersability and compatibility in different solvents or matrices that are suitable in the production of nanocomposites. [Habibi et al., 2010; Klemm et al., 2011] Among these polymers, water-soluble thermo-responsive polymers exhibit great ability to stabilize CNC particles, and offer an opportunity to produce CNC-based stimuli-responsive structures. As mentioned in

section 2.2.3, oligoPEG-based copolymers exhibit very fast and reversible thermal responsive transition. These copolymers have been grafted onto silicon, gold, and glass substrates and the products have found many potential applications in biomedical and bio-engineering fields. [Jonas et al., 2007; Gao et al., 2009; Ma et al., 2006; Chan et al., 2003] However, to our knowledge, the grafting of oligo(ethylene glycol)-based onto CNC surface has not yet been studied, and thus to investigate the properties of CNC with grafted copolymeric chains must be very interesting.

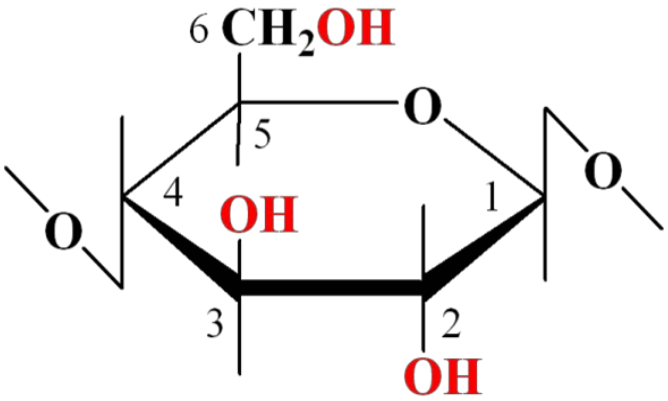

Figure 2.5 Numbering system for carbon atoms in anhydroglucose unit of cellulose.

2.3.2 CNC properties

Cellulose nanocrystals derived from acid hydrolysis using various forest product sources can disperse in water due to their negative charged surfaces. At low concentrations, CNC particles are randomly oriented in aqueous suspension as an isotropic phase, and when the concentration reaches a critical value, they form a chiral nematic ordering, where CNC suspensions transform from an isotropic to an anisotropic chiral nematic liquid crystalline phase. [Revol et al., 1992] As the concentration increased further, aqueous CNC suspensions show a shear birefringence phenomenon. The critical concentration for sulfated CNC typically ranges between 1 and 10% (w/w), which is a function of aspect ratio of CNC, charge density, and

osmolarity. Theories based on different parameters have been studied to explain the phenomena. [Stroobants et al., 1986]

The phase behavior of CNC is sensitive to the presence of electrolytes and their counter ions, as well as macromolecules. The effect of added electrolyte on the phase separation of CNC was studied by Dong et al., [1996] and they found that the addition of electrolytes, e.g. HCl, NaCl and KCl significantly reduced the volume fraction of the anisotropic phase, indicating that addition of electrolytes reduces the anisotropic phase. Dong and Gray [1997] also studied the effect of counter ions on the phase separation behavior and stability of CNC suspensions by adding inorganic counterions, weakly basic organic counterions and highly basic organic tetraalkylammonium salts. It was observed that the types of counter ions had a significant effect on phase separation behavior of CNC suspensions. Similar to electrolytes, the phase separation of CNC suspensions is strongly affected by the addition of macromolecules. Gray and co-workers [Edgar and Gray, 2002; Beck-Candanedo et al., 2006, 2007] conducted a detailed study on the effect of dextran and ionic dyes on the phase equilibrium of CNC suspensions. Surfactant coating used to disperse CNC whiskers in non-polar solvents was first reported by Heux et al., [2000] where CNC whiskers from cotton and tunicate were mixed with Beycostat NA (BNA) surfactant. The authors demonstrated that the chiral nematic phases were formed in spite of a layer of surfactants around the CNC whiskers. Detailed examination of the chiral nematic structure (Figure 2.6) was recently reported. [Elazzouzi-Hafraoui et al., 2009]

The assembling behaviors of CNC under external field, such as an AC electric and a magnetic field were investigated. [Sugiyama et al., 1992; Fleming et al., 2000; Bordel et al., 2006] The effect of AC electric field on the alignment and orientation of CNC was investigated by Habibi et al., [2008], they observed that the application of an AC electric field to CNC

suspensions deposited between two metallic electrodes resulted in the homogeneous alignment of CNC molecules. Moreover, the alignment of cellulose nanocrystals generated films is greatly influenced by the frequency and strength of the applied electric field, while the orientation of cellulose nanocrystals becomes more homogeneous with increasing electric field greater than 2000 V/cm with a frequency ranging between 10^4 and 10^6 Hz. Previous studies [Revol et al., 1994] have shown that CNC suspensions exhibited negative diamagnetic anisotropic susceptibility as they dry under the influence of a magnetic field. The authors also demonstrated that for CNC films, the presence of magnetic field did not facilitate the formation of a chiral nematic phase but it only increased the chiral nematic pitch of the suspensions. A similar study was recently conducted by Pan et al., [2010] where they examined various factors controlling the chiral nematic properties of CNC films.

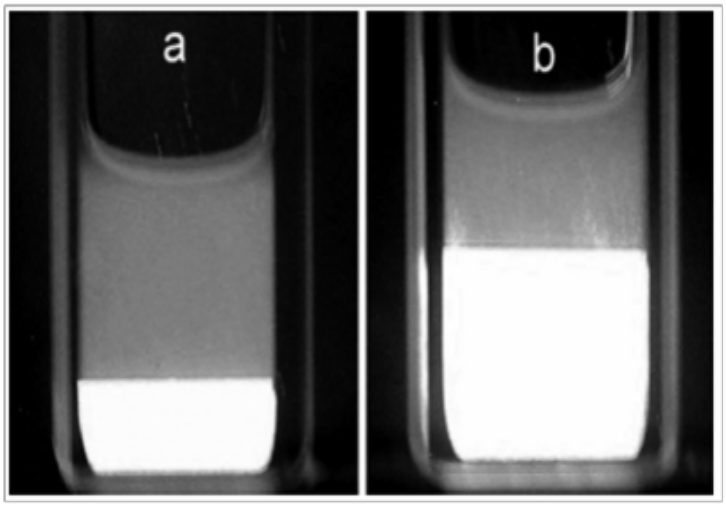

Figure 2.6 Phase separation observed between cross polars for different concentrations of CNC (cotton fibers) suspensions at total concentrations of (a) 19.8 wt% and (b) 25.0 wt%. [Elazzouzi-Hafraoui et al., 2009]

2.3.3 Surface modification of cellulose nanocrystals (CNC)

According to its structure, CNC possesses an abundance of hydroxyl groups on the surface, where chemical reactions can be performed. Various chemical modifications of CNC, such as esterification, cationization, carboxylation, silylation, and polymer grafting (shown in Figure 2.7) have been reported to improve its dispersability and compatibility in different solvents or matrices.

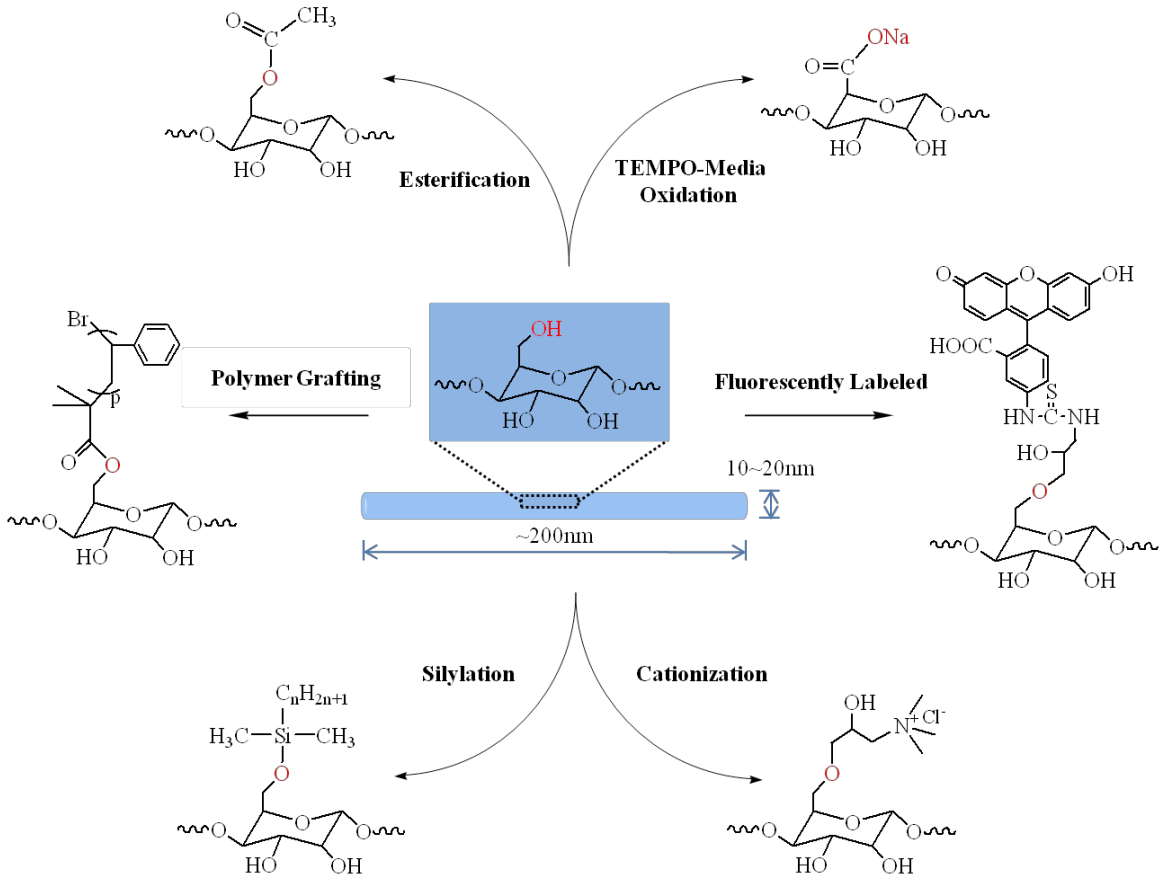

Figure 2.7 Schematic diagram illustrating the various types of chemical modifications on CNC surface. [Braun and Dorgan, 2009; Hasani et al., 2008; Dong and Roman, 2007; Goussé et al., 2002; Habibi et al., 2006; Morandi et al., 2009]

Acetylation and Esterification Sassi and Chanzy [1995] employed acetic anhydride and acetic acid to modify the fibrous and homogenous cellulose, while Yuan et al. [2006] used

straightforward freeze drying and heating of mixtures of alkenyl succinic anhydride (ASA) aqueous emulsions and CNC suspensions to obtain acetylated CNC, which imparted hydrophobicity to the CNC and rendered it soluble in solvent with low polarity. Surface acetylation of CNC whiskers (obtained from MCC) was undertaken by reacting it with vinyl acetate in the presence of potassium carbonate as catalyst. [Çetin et al., 2009] In an attempt to avoid complex surface functionalization routes, Braun and Dorgan [2009] recently combined the synthesis and functionalization of CNC in a single step. By utilizing a mixture of acetic acid, HCl and organic acids, CNC whiskers were synthesized and functionalized using the Fischer esterification process. Apart from the solution process, Berlioz et al. [2009] demonstrated a gas phase process that makes use of evaporation of large excess of palmitoyl chloride to achieve a surface to core esterification. Similar concept was applied to esterification by refluxing hydrolysed CNC in organic acid chloride. [Junior de Menezes et al., 2009]

Cationization Hasani and co-workers [2008] described a one-step method to introduce positive charges on the surface of CNC through the grafting of epoxypropyltrimethylammonium chloride (EPTMAC) onto CNC surfaces. Such surface cationization procedure was conducted via a nucleophilic addition of alkali-activated cellulose hydroxyl groups to the epoxy moiety of EPTMAC. This modification process reversed the surface charge and led to stable aqueous suspensions of CNC with unexpected thixotropic gelling properties.

Fluorescently Labeled CNC Dong and Roman [2007] described a method to label CNC with fluorescein-5'-isothiocyanate (FITC) for fluorescence bioassay and bioimaging applications. To covalently attach FITC moieties to the surface of CNC, they developed a simple method involving a three-step reaction pathway described by the reaction route shown in Scheme 2.4. First, the surface of CNC was decorated with epoxy functional groups via reaction with

epichlorohydrin, and then the epoxy ring was opened with ammonium hydroxide to introduce primary amino groups. Finally, the primary amino group was reacted with isothiocyanate group of FITC to form a thiourea.

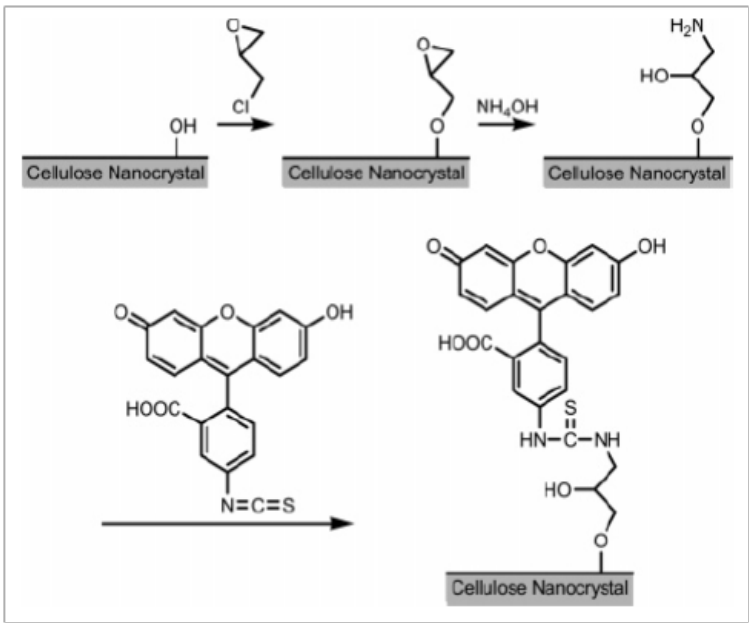

Scheme 2.4 Reaction route for surface fluorescently labeled CNC with FITC. [Dong and Roman, 2007]

Silylation Cellulose whiskers resulting from the acid hydrolysis of tunicate were partially silylated by a series of alkyldimethylchlorosilanes, with alkyl moieties ranging from isopropyl to *n*-butyl, *n*-octyl and *n*-dodecyl. [Goussé et al., 2002] The partially silylated whiskers with degree of substitution (DS) of between 0.6 and 1 can readily redispersed in medium polarity organic solvents, such as acetone and THF. At DS of less than 0.6, the morphological integrity of the whiskers was preserved, however it was disrupted when the DS was greater than 1. Moreover, the partially silylated whiskers were found to be more swollen compared to the needle-like images of unmodified whiskers, indicating the occurrence of slight silylation of the CNC core. In addition, Grunert and Winter [2002] also studied the surface trimethyl silylation of CNC from bacterial cellulose, and investigated their reinforcement characteristics in nanocomposites.

Table 2.1 Summary of various types of modifications on CNC whiskers.

Type of Modification	Modification agent/approach	References
Acetylation	Alkenyl succinic anhydride (ASA)	Yuan et al., 2006
Surface Acetylation	Vinyl acetate in the presence of potassium carbonate as catalyst	Çetin et al., 2009
Fischer esterification process	Mixture of acetic acid, HCl and organic acids	Braun and Dorgan 2009
Surface to core esterification	Gas phase evaporation of large excess of palmitoyl chloride	Berlioz et al., 2009
Cationization	Grafting epoxypropyltrimethylammonium chloride (EPTMAC)	Hasani et al., 2008
FluorescentlyLabelled CNC	Fluorescein-5'- isothiocyanate (FITC)	Dong and Roman 2007
Silylation	Series of alkyldimethylchlorosilanes	Goussé et al., 2002
TEMPO-Media Oxidation	Oxidation of -OH groups to -COOH using 2,2,6,6-tetramethylpiperidine-1-oxyl (TEMPO)	Habibi et al., 2006
Grafting of PEG-NH_2	Reaction of PEG-NH_2 and TEMPO oxidized CNC	Araki et al., 2001
Grafting of polycaprolactone (PCL)	*Grafting-to* approach using isocyanate-mediated coupling reaction	Habibi and Dufresne 2008
Grafting of styrene, DMAEMA or azobenzene polymers	*Grafting-from* approach using surface initiated ATRP	Yi et al., 2008; Morandi et al., 2009; Xu et al., 2008

TEMPO-Media Oxidation Conversion of hydroxymethyl groups into carboxylic groups can be conducted using 2, 2, 6, 6-tetramethylpiperidine-1-oxyl (TEMPO) reagent. [Saito and Isogai, 2004; Saito et al., 2010] This is a simple oxidative route that uses TEMPO as nitroxyl free radial to specifically oxidize primary hydroxymethyl in an environment of NaBr and NaOCl; leaving the secondary hydroxyl groups intact. [Habibi et al., 2006] The morphology and crystal axis of the CNC are critical in determining the accessibility of the hydroxymethyl group. It is generally accepted that only 50% of the surface hydroxymethyl groups are accessible for the TEMPO reaction. Importantly, the structural integrity of CNC was retained after hydrolysis and TEMPO-mediated oxidation. However, excessive oxidation did affect the structural integrity of the original CNC; since the amorphous region of the CNC would be degraded. [Montanari et al., 2005] The various types of modifications on CNC whiskers were summarized in Table 2.1.

2.3.4 Polymer grafting of TRPs on CNC surface

The methods for polymer grafting onto CNC surface are based on two approaches, i.e. “grafting-to” and “grafting-from”. Many techniques for surface modification of CNC whiskers involve the “grafting-to” approach, where a polymer chain is grafted to the CNC surface. In an early report by Araki and co-workers, [2001] an end-functional PEG with its reactive end-group $–NH_2$ is coupled with the functional groups -COOH which are located on the CNC surface using peptide coupling reaction. HCl-hydrolyzed CNC was carboxylated by TEMPO-mediated oxidation, and then EDC/NHS carbodiimide chemistry was used to conduct a room temperature reaction between the -COOH groups on carboxylated CNC and $-NH_2$ groups on PEG-NH_2 (shown in Scheme 2.5). The PEG-grafted CNC was also prepared by Kloser and Gray [2010] from the reaction of desulfated CNCs with epoxy-terminated PEG under alkaline conditions, using an alkaline epoxide ring opening strategy. Recently, Azzam et al. [2010] reported the

grafting of thermo-responsive polymers, namely Jeffamine series, onto CNC via a peptidic coupling reaction. The grafting density was confirmed to be sufficiently high that can offer a steric stabilization of the CNCs at high ionic strength and made the CNCs surface-active. They also investigated the thermo-reversible aggregation behavior of polymer grafted CNC, and discussed the possibility to pave the way for the design of stimuli-responsive bio-based nanocomposite materials.

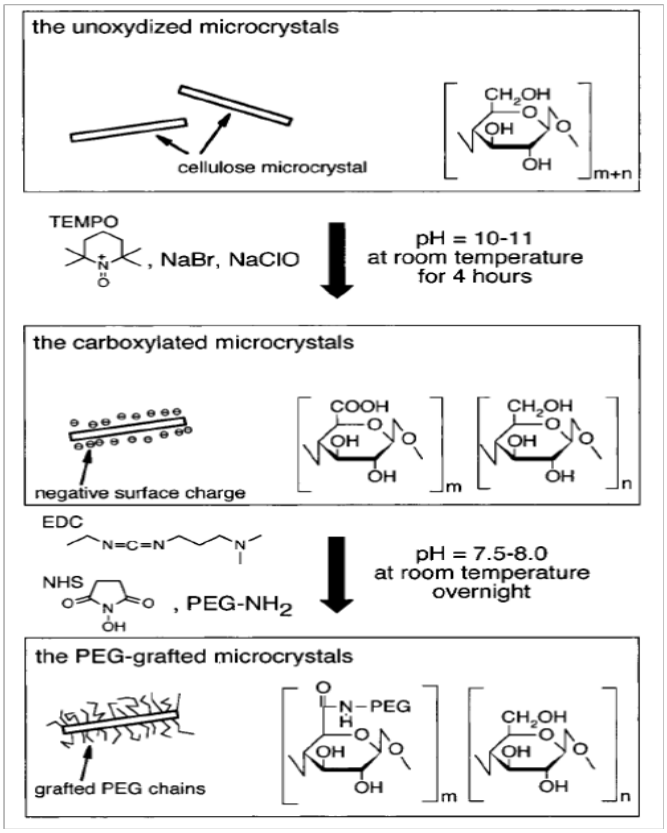

Scheme 2.5 Procedures for steric stabilization of cellulose microcrystals. [Araki et al., 2001]

The “grafting-from” approach has been used to grow polymer chains from the CNC surface via the atom transfer radical polymerization (ATRP). This technique allows for very precise control over the grafting process that produces well-defined monodispersed particles. [Wang and Matyjaszewski, 1995] Surface initiated ATRP is a two-step process: the first step is the esterification of hydroxyl groups on CNC surface with 2-bromoisobutyryl bromide (BIBB),

which is followed by the polymerization of monomers. Thermo-responsive polymer, namely poly(*N*, *N*-dimethylaminoethyl methacrylate) was grafted onto CNC surface via surface-initiated ATRP by Yi et al. [2008] (Scheme 2.6). The PDMAEMA-grafted CNC was found to exhibit chiral nematic structure in lyotropic state, while the fingerprint texture of product suspensions was sensitive to temperature and the thermo-induced changes were reversible. Similar protocol was reported by Zoppe et al. [2010] in their study of grafting poly(*N*-isopropylacrylamide) on CNC surface with various grafting densities and molecular weights. They revealed that poly(NIPAM)-*g*-CNC in aqueous dispersions exhibited a sharp increase in dispersion viscosity as the temperature approached the LCST in contrast with unmodified CNC which showed no thermo-responsive behavior. Furthermore, the surface interaction forces of poly(NIPAM)-*g*-CNC were also investigated.

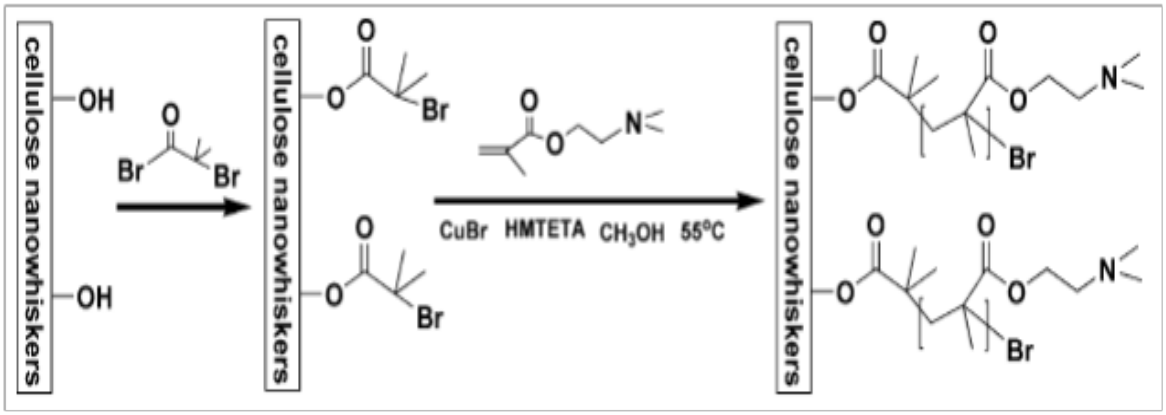

Scheme 2.6 Formation of PDMAEMA grafted on rod-like CNC by surface initiated ATRP. [Yi et al., 2009]

2.3.5 Applications of CNC

As a result of their distinctive properties, cellulose nanocrystals have the potential of becoming an important class of renewable nanomaterials, which could find many useful applications. The main application of CNC is as reinforcing fillers in nanocomposite materials.

Chemical functionalization of CNC improves its dispersability in organic solvents and this greatly expands its potential applications in various sectors. The following section highlights some recent studies on potential applications of CNC.

Nanocomposite Films The mechanical properties of nanocomposite films mainly depend on the morphology and dimensions of the two constituents, i.e. CNC and polymeric matrix, as well as the processing techniques. Any other factor that interferes or controls the formation of the percolating whiskers network will also change the mechanical performance of the nanocomposite. [Dufresne A., 2008] The geometrical aspect ratio, defined as the length-to-diameter (L/d), is a major factor that controls the mechanical properties of nanocompsites and determines the percolation threshold value. This factor is related to the original cellulose fibers and production conditions, which was previously discussed. Fillers with a high aspect ratio produce the best reinforcing effect. It was reported that the highest modulus increase in the rubbery state of the poly(Styrene-*co*-BuA) matrix and thermal stability were obtained with tunicin whiskers ($L/d \sim 67$) in comparison with bacterial ($L/d \sim 60$) or Avicel whiskers ($L/d \sim 10$). [Samir et al. 2005] Sisal nanowhiskers with high aspect ratio were studied by de Rodriguez and co-workers [2006] as filler in the nanocomposites with polyvinyl acetate (PVAc) as the matrix. They found that the high aspect ratio could ensure percolation, resulting in mechanical improvements and thermal stability at lower fiber loads. Dubief et al. [1999] also reported on the mechanical behavior of composites based on amorphous PHO when reinforced with tunicin microcrystals. They proved that tunicin whiskers with high aspect ratio led to higher mechanical properties through the formation of a rigid filler network. Similar effects on the dependence of mechanical properties of nanocomposites on aspect ratio were also reported using carbon nanotubes as fillers. [Jiang et al., 2007; Wong et al., 2009]

Drug Delivery The materials for drug delivery seem to be one of the most interesting research fields. Abundant researches were conducted to investigate various drug delivery systems, such as liposomes, micelles, microgels. [Ha and Gardella, 2005] Considering the safety and efficacy, cellulose nanocrystals has attracted increasing attention in biomedical applications (such as a drug carrier), due to its attractive properties. The toxicity assessment of CNC in human brain microvascular endothelial cells was conducted and CNC was non-toxic to cells and could be used as carriers in the targeted delivery of therapeutics. [Roman et al. 2010] Recently, a comprehensive assessment involving toxicity tests with rainbow trout hepatocytes and nine aquatic species were conducted by a team of Canadian researchers. [Kovacs et al., 2010] From the initial ecotoxicological characterization of CNC, no serious environmental concerns were observed. However, further testing will be necessary, such as the evaluation on the fate, potential CNC uptake and exposure studies, so that a detailed risk assessment of CNC can be determined.

Protein Immobilization Marchessault and co-workers [2006] provided a description of a "proteins fishing" phenomenon for magnetic MCC. The first step is the ferrite synthesis that yields predominantly magnetite. Two different approaches have been envisaged for preparing magnetic MCC, where the order of magnetization and oxidation of MCC was altered, producing Mag-Oxy-MCC (oxidation first) and Oxy-Mag-MCC (magnetization first). The results of protein binding capacities of magnetic MCC are summarized in Table 2.2, which were determined using Bovine Serum Albumin (BSA) as a model protein ligand. A novel nanocomposite consisting of CNC and gold nanopaticle was recently investigated as a matrix for enzyme/protein immobilization. [Mahmoud et al., 2009] Cyclodextrin glycosyl transferase (CGTase) and alcohol oxidase were used as test models, and they showed a phenomenally high loading rate in

the matrix. The novel matrix also exhibited significant biocatalytic activity, and it is anticipated that the approach could be extended to other enzymes.

Table 2.2 Protein binding capacities of magnetized avicel samples. [Marchessault et al., 2006]

Sample	*% Bound Proteins (w/w)*
Mag-MCC	8.02
Mag -Oxy-MCC	21.53
Oxy-Mag-MCC	17.41

Nanostructures via Templating with CNC Since Mobil researchers reported the first synthesis of mesoporous material in 1992, [Kresge et al.] this approach has attracted significant attention in fundamental and applied fields. Herein, CNC has already been used as a template in the synthesis of mesoporous materials. Porous titania with anatase structure was prepared using CNC as a template and aqueous Tyzor-LA solution as a cheap and stable titania precursor. [Shin et al., 2007] The titania material possesses high specific surface area, and may be applied to many fields, such as catalysis, catalyst support and photovoltaics. A new CNC-inducing route was proposed for the synthesis of shape-controlled nanoparticles. [Zhou et al., 2007] The novel cubic-shaped TiO_2 nanoparticles (Figure 2.8) with high crystallinity and uniform size were prepared using CNC as morphology-inducing and coordinate agent at low temperature. Thermal gravimetric analysis (TGA) suggests that CNC is probably embedded in the TiO_2 nanoparticles to promote the development of regular anatase nanocubes.

Some metal nanoparticles have been synthesized on CNC surface via a reduction method, such as Ni nanoparticles [Shin et al., 2007] and Au-Ag alloy nanoparticles. [Shin et al., 2008] In these processes, CNC serves as a dual role, as a matrix and a stabilizing template, to produce stable dispersions of nanoparticles on CNC surface, and the crystallinity of CNC was maintained

during the alloy formation. [Shin et al., 2008] These reducing processes could be recognized as "green" processes ascribed to the use of CNC and applied to the preparation of transition metal nanoparticles, which have high oxidizing property without additional reducing agents.

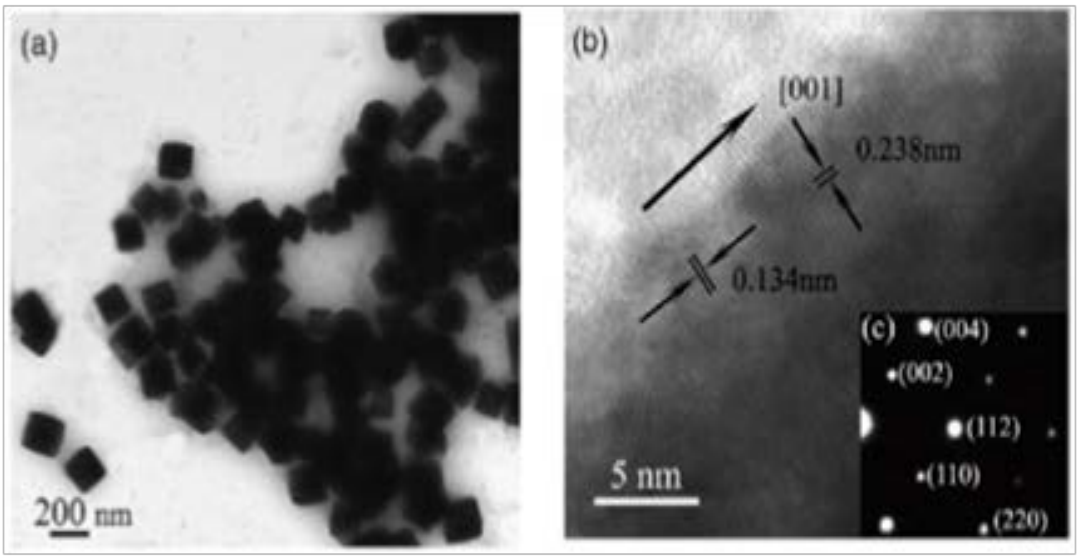

Figure 2.8 Transmission electron microscopy (TEM) image, (b) High-resolution transmission electron microscopy (HRTEM) image, (c) selected area electron diffraction (SAED) pattern of TiO_2 nanocubes. [Zhou et al., 2007]

A recent discovery of free-standing mesoporous silica films with tunable chiral nematic structures was made by the research group of MacLachlan at the University of British Columbia. [Shopsowitz et al., 2010] Various types of mesoporous silica films were produced by calcinating the CNC/silica composite systems and the transmission spectra of the mesoporous silica films are shown in Figure 2.9(a). Photograph of the different colours of mesoporous silica films S1 to S4 are shown in Figure 2.9(b), where the proportion of $Si(OMe)_4$: CNC increased from samples S1 to S4. The colours in these silica films arise only from the chiral nematic pore structure present in the materials. This discovery could lead to the development of novel materials for applications such as tunable reflective filters and sensors. In addition, CNC could be used as a hard template to produce other new materials with chiral nematic structures.

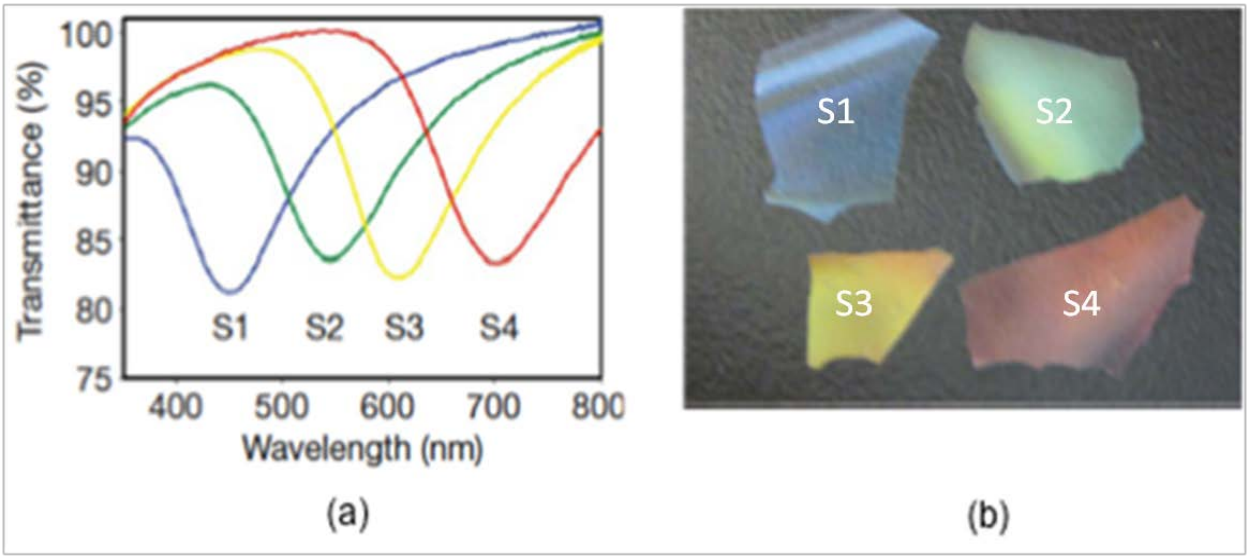

Figure 2.9 Optical characterization and properties of CNC/silica mesoporous films (a) Transmission spectra; (b) Photograph showing different colours of mesoporous silica films S1 to S4. [Shopsowitz et al., 2010]

2.4 Interaction between polymeric nanostructures and surfactants

2.4.1 Overview of polymer/surfactant systems

Mixtures of water-soluble polymer and surfactant have received a great deal of attention and they been systemically studied in the past decades, because of their wide applications in many industrial product formulations, such as cosmetic products, food additives, pharmaceutical formulations, enhanced oil recovery. [Kwak, 1998; Holmberg et al., 2002] The behavior of polymer/surfactant mixtures can be quite different from individual polymer or surfactant solution due to their interactions that can result in significant changes in the phase behaviour, rheological and interfacial properties. [Tam and Wyn-Jones, 2006] Surfactant molecules can self-assemble into aggregates of different morphologies up to a critical concentration, i.e. critical micellization concentration (CMC), while in the presence of polymers, micelles can form at a lower concentration due to polymer/surfactant interactions, which is denoted as polymer-induced

micellization. In polymer/surfactant systems, two critical concentrations are used to describe the interactions between polymer and surfactant molecules. The critical aggregation concentration (CAC) indicates the onset for the formation of polymer/surfactant complex, while the saturation concentration (C_2) implies the polymer chains become saturated with bound surfactant molecules. [Bao et al. 2008] In general, polymer/surfactant interactions can be divided into two broad categories: (1) charged polymers and oppositely charged surfactants and (2) uncharged polymers and all types of surfactants. For charged polymers and oppositely charged surfactants, electrostatic attraction dominates the binding interactions at low surfactant concentration. At higher surfactant concentration, hydrophobic interaction dominates the binding when all the charged groups on polymer chains are neutralized. These interactions will induce the restructuring of polymer chains and the occurrence of precipitation. [Dai and Tam, 2004] For uncharged polymers and ionic surfactants, their behavior is mainly controlled by the hydrophobic interaction. For example, the interactions between uncharged poly(ethylene glycol) (PEG) and anionic surfactant sodium dodecyl sulfate (SDS) have been widely studied, and strong cooperative binding interactions, which are controlled by the equilibrium of polymer-induced micellization at low SDS concentration and ion-dipole association at high SDS concentration. [Dai and Tam, 2001; Wang and Olofsson, 1995] While the cationic surfactant dodecyltrimethylammonium bromide (DoTAB) possesses the same length carbon tail as SDS but with different hydrophilic head groups, it only binds to very hydrophobic polymers, such as hydrophobically modified water-soluble polymers. [Couderc et al. 1999] Therefore, the binding process and resulting mechanisms are dependent on surfactant type, polymer molecular weight, chemical structure, hydrophobic content of polymer and other parameters. The interactions between uncharged polymers and surfactants are simpler in the absence of electrostatic effect.

The CMC of nonionic surfactants are usually orders of magnitude lower than ionic, which is strongly influenced by unfavorable electrostatic interactions. [Hansson and Lindman, 1996] Hence, nonionic surfactants tend to form micelles and possess weak interaction with uncharged polymers compared to charged polymers with oppositely charged surfactants and also uncharged polymers/ionic surfactants. However, their interactions can be significantly altered by temperature, solvent quality, electrolyte, and chemical structure of polymers and surfactants.

In this section, we will focus on the behaviors of thermo-responsive polymers and surfactant systems in bulk solution, while both the synthetic and natural TRPs and their interactions with anionic, cationic and non-ionic surfactants under different conditions are summarized. In addition, the biodegradable CNC, chitosan and their derivatives are introduced, and their interactions with surfactants are also reviewed.

2.4.2 Interactions between TRPs and surfactants

Since PNIPAM is the most widely studied thermo-responsive polymer, its interactions with surfactant molecules have gained increasing attention. Especially, the surfactant effects on the conformational change of PNIPAM in water have been extensively studied using various techniques, such as laser light scattering (LLS), conductometric measurements, small angle neutron scattering, fluorescence spectroscopy, and nuclear magnetic resonance. [Chen et al., 2011] The interaction of PNIPAM with an anionic (SDS) and three cationic (DTAB and CTAB, and dodecylammonium chloride, DAC) surfactants was reported by Loh and co-workers. [2004] They used isothermal titration calorimetry that allows the precise determination of parameters to characterize polymer-surfactant interactions. They found that the interaction of PNIPAM with ionic surfactants is significantly affected by temperature. A temperature increase can strengthen the polymer surfactant interaction, owing to a reduction in the degree of PNIPAM hydration that

becomes more important near the LCST. Different surfactants displayed different binding affinities toward PNIPAM, with the intensity following the sequence: SDS > CTAB > DAC > DTAB. This sequence confirms that anionic surfactants are much more effective in binding to nonionic polymers and also that the surfactant hydrophobicity plays an important role in this interaction. The amount of bound surfactant and overall energy of interaction were found to remain constant for all surfactants within the temperature range examined.

The possible morphologies of PNIPAM and SDS were also studied. Chee and co-workers [2011] reported that SDS interacts with PNIPAM to form micellar structures along the macromolecular backbone upon CAC. Binding of SDS to PNIPAM induces a switch in the chain conformation from a flexible, solvent-saturated coil to a surfactant-swollen structure due to electrostatic repulsion between ionic head groups. At the LCST, addition of a small amount of SDS is sufficient to dissociate the collapsed PNIPAM chain into isolated globular structures. Further addition of SDS induces a switch in the macromolecular chain conformation from a globule to a swollen coil. Walter et al. [1996] thought the surfactants form a surface layer with the polymer globule to prevent phase separation when the temperature increases to the LCST.

The interactions of surfactant with homo- and co-polymers based on ethylene oxide (EO) and propylene oxide (PO) were important field for TRPs and surfactant systems. The temperature-dependent solvation of ethylene oxide (EO) and propylene oxide (PO) blocks especially in aqueous solutions makes block copolymers particularly useful for thermal reversible micellization processes. Li and co-workers [2001] studied a series of Pluronic polymers and their interactions with surfactants. For example, they investigated the interactions between a cationic surfactant (TTAB) and Pluronic triblock copolymer F127, which is a nonionic surfactant with structural formula $EO_{97}PO_{69}EO_{97}$, where EO represents the ethylene oxide block

and PO represents the propylene oxide block. The results showed that TTAB formed a polymer/micellar complex with monomeric F127. Binding TTAB to F127 led to the transformation of aggregated F127 chains into mixed micelles, as more TTAB was added, the aggregates dissociate into smaller mixed F127/TTAB aggregates. They also found that small amounts of TTAB reduced the critical micelle temperature of F127. Similar work was conducted by introducing SDS, and the investigations showed a different binding and aggregation process between SDS and F127 that comprised of induced micellization, growth of mixed micelles, breakdown of mixed micelles, and binding of SDS to monomeric F127. [Li et al., 2001]

Natural biopolymers and their derivatives have received increasing attention due to their biocompatible, biodegradable, non-toxic and other attractive properties. In the last several decades, extensive studies have been made on the interactions between surfactants and water-soluble biopolymers. Ethyl(hydroxyethyl) cellulose (EHEC) is one type of nonionic cellulose derivatives containing hydrophilic ($-CH_2CH_2OH$) and hydrophobic ($-CH_2CH_3$) micro-domains distributed randomly along the polymer backbone. It is water-soluble and exhibits a lower critical solution temperature (LCST) in aqueous solution. [Nyström et al., 2009] In recent decades, more research has been focused on the field of uncharged polymer and surfactant interactions, where the poly(ethylene oxide) (PEO) based uncharged polymers and SDS systems were most extensively studied. Aqueous solution behaviors of nonionic EHEC biopolymer in the presence of a surfactant have received increasing attention and they were examined in the dilute and semi-dilute regime. [Bloor et al., 1996; Walderhaug et al., 1995] Various experimental approaches have been employed to study different physicochemical properties of EHEC in aqueous solution in the presence of surfactants. The picture that emerged from these investigations is that both anionic and cationic surfactants interact strongly with the EHEC

polymer, resulting in a number of changes in the macro- and micro-scale properties, such as cloud point, bulk viscosity, microviscosity, and micropolarity. [Singh and Nilsson, 1999] Hoff et al. [2001] studied the interaction between EHEC and SDS in dilute aqueous solutions at different temperatures using viscometry. They demonstrated that at low polymer concentrations the polymer-surfactant complexes are molecularly dispersed, and with small amounts of surfactant, the viscosity displayed a strong shear-thinning profile while the shear rate dependence of the viscosity was less pronounced at high surfactant concentrations. Combining with other measurements, a sharp collapse of the polymer/surfactant aggregates occurred at surfactant concentration slightly above CAC, while the EHEC/SDS complexes expanded with increasing SDS concentration due to the enhanced electrostatic repulsion. At high surfactant concentration, the complexes structure contracted due to screening of electrostatic interactions.

It is well-established that aqueous solutions of EHEC in the presence of an ionic surfactant exhibit a thermo-reversible sol-gel transition in the semi-dilute regime, where the polymer chains overlap each other. [Walderhaug et al., 1995] These EHEC/surfactant systems can transform from a viscous solution to a clear and stiff gel at elevated temperatures, and the gel point temperature strongly depends on the polymer/surfactant composition, which is similar to the cloud point. This sol-gel transition of EHEC/surfactant aqueous solutions has been studied in details using various techniques. [Walderhaug et al., 1995; Bu et al., 2004; Ostrovskii et al., 1999; Kjøniksen et al., 1998; 2005] A series of samples at different SDS/EHEC ratios (r) were examined by rheometry over a temperature range of 10 to 45 ^{o}C. [Kjøniksen et al., 1998] The results indicated that semi-dilute systems formed gels upon heating at moderate ratios (r) of SDS/EHEC due to the strengthening of the association network of EHEC and SDS molecules. This thermo-induced gelling phenomenon was mainly due to the increased hydrophobicity of

EHEC at higher temperature, resulting in stronger inter-polymer interactions. [Lindman et al., 1990] The surfactant molecules also played an important role in stabilizing and strengthening the associative junctions that connect many different polymer chains. [Kjøniksen et al., 1998] However, at high ratios of SDS/EHEC, the association network was disrupted and no thermo-reversible gelling behavior was observed over similar temperature range and moderate SDS/EHEC ratios.

2.4.3 Interactions between biodegradable cellulose derivatives and surfactants

In the last several decades, extensive studies have been conducted on the interactions between surfactants and water-soluble cellulose derivatives, which have a wide range of applications. In these studies, both cooperative and noncooperative bindings were observed, while the binding processes were investigated in a high concentration regime.

Carboxymethylcellulose (CMC) is one of the most important cellulose ethers derived from cellulose, which can be synthesized by the alkali-catalyzed reaction of cellulose with chloroacetic acid. It behaves as an anionic polyelectrolyte at pH > 4, and is generally used as the sodium salt, i.e. sodium carboxymethyl cellulose (NaCMC). [Chakraborty, Chakraborty and Ghosh, 2006] The interactions between NaCMC and various cationic surfactants have been extensively studied, and they displayed similar behaviors as synthetic anionic polyelectrolyte. For the oppositely charged systems, complexation start to form due to the strong electrostatic attraction above a surfactant concentration called the critical aggregation concentration (CAC). It has been reported that the polymer/surfactant association already occurs below CAC ascribing to the noncooperative binding, which becomes more cooperative above CAC. [Wang and Tam, 2002] Upon increasing surfactant concentration, the binding sites on polyelectrolyte decrease and eventually saturate with surfactant molecules. Then the hydrophobic effects start to take over of

the interactions instead of electrostatic attraction, and phase separation with precipitation of a concentrated phase may occur. [Trabelsi, Raspaud and Langevin, 2007] In general, the polyelectrolyte chains start to partially collapse at low surfactant concentration, while their complexes are quite polydispersed, with increasing surfactant concentration, the multi-chains aggregates formed result in the occurrence of precipitation. In comparison with flexible synthetic polymers, NaCMC is semi-flexible with a more rigid backbone, which could influent the chain collapse resulting in different kinds of aggregate structures. [McLoughlin, Impéror-Clerc and Langevin, 2006] It has been realized that many factors can affect the interaction process, such as NaCMC molecular weight and charge density, surfactant chain length, head group size, counterion, as well as ionic strength, temperature.

The interactions of NaCMC with DoTAB and CTAB were studied by Trabelsi et al. [2007] using light scattering, surfactant-selective electrode, viscosimetry, and zeta-potentiometry. They found that NaCMC and surfactants molecules formed spherical, rigid, and monodisperse aggregates at low polymer concentrations, while larger, polydisperse, and softer ones at high polymer concentrations. In addition, the surfactant tail length by four CH_2 groups drastically changed the aggregate size, as the NaCMC/CTAB aggregates were much larger than NaCMC/DoTAB ones. Similar results were reported by Mata et al. [2006] by comparing the size of aggregates formed by NaCMC with DoTAB, tetradecyltrimethylammonium bromide (TTAB), and CTAB. Furthermore, they also discussed the effect of the head group size of tetradecyl quaternary ammonium surfactant on the mixed aggregates using TTAB, tetradecylpyridinium bromide (TPyB), and tetradecyltriphenylphosphonium bromide (TTPB) and found that increasing the head group size result in a steeper growth of the aggregates. On the other hand, the properties of NaCMC, such as molecular weight (M_w) and degree of substitution (DS), also

played an important role in the complexation studies. Naves and Petri [2005] have investigated the effect of M_w and DS on the interaction between NaCMC and CTAB, where they found the formation of NaCMC/CTAB complex in the bulk solution were significantly affected by DS of NaCMC rather than the molecular weight. The effects of solution environment, such as ionic strength, temperature on complexation of NaCMC/cationic surfactants were studied as well. [Wang et al., 2005; Chakraborty, Chakraborty and Ghosh, 2006] The salt effect on the complex formation between NaCMC and DoTAB was studied by Wang and co-workers [2005] using microcalorimetry, turbidimetric titration, steady-state fluorescence measurements, and fluorescence polarization technique. The salt-enhancing effect on the complex formation was observed. The reason is that the increasing of NaCMC/DoTAB interaction owing to the growth of micelles exceeded the screening of interaction, resulting in the enhanced complex formation.

In dilute aqueous solution of NaCMC and cationic surfactants, some unique structures of the concentrated phases were formed above the precipitation threshold. Trabelsi et al. [2007] used by X-ray diffraction to study the structures formed by NaCMC and DoTAB, TTAB, CTAB and octadecyl trimethylammonium bromides (OTAB). Different cubic structures were observed in the presence of surfactant with a short aliphatic chain (DoTAB), while for larger surfactant chain lengths (TTAB and CTAB) the structure of the precipitates can be either cubic or 2D hexagonal depending on the initial surfactant and polymer concentrations, and for still larger chain length (OTAB), the structure became lamellar. In semi-dilute solution regime, the steady and dynamic rheological behaviors of NaCMC and DoTAB were also investigated. [Wu et al., 2009] They observed three scaling regions of the viscosity profiles over two critical DoTAB concentrations, namely C_1 and C_2 (see Figure 2.10). The three regions may correspond to three

states of NaCMC/DoTAB formation with increasing surfactant concentration, i.e. no network formation, network extent progressive formation and perfect network formation, respectively.

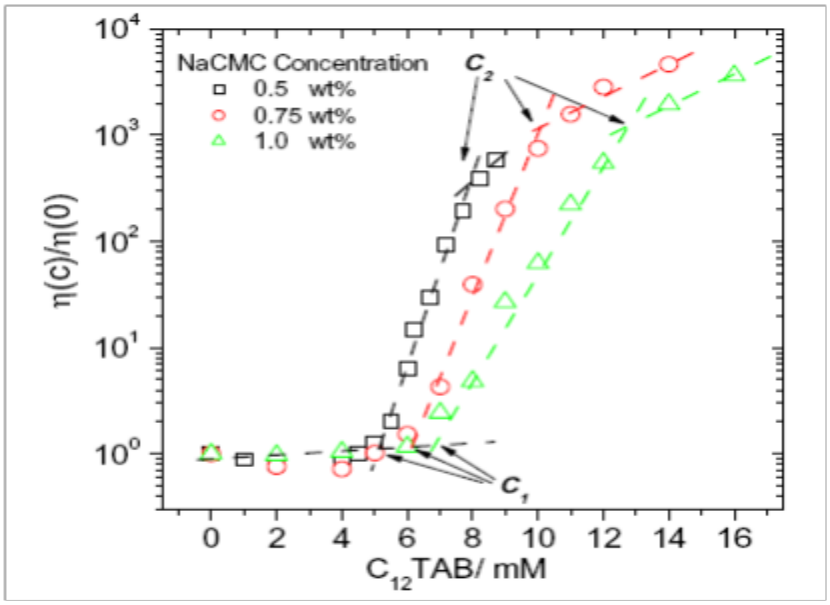

Figure 2.10 Dependence of reduced viscosity on DoTAB concentrations for NaCMC concentrations of 0.5 wt%, 0.75 wt% and 1 wt% at 25 ^{o}C. [Wu et al., 2009]

Ethyl(hydroxyethyl) Cellulose (EHEC) is one type of nonionic cellulose derivatives with hydrophilic (-CH_2CH_2OH) and hydrophobic (-CH_2CH_3) microdomains distributed randomly along the polymer backbone. It is water-soluble and possesses a lower critical solution temperature (LCST) in aqueous solution. Ridell and co-workers [2002] studied the interactions between EHEC and anionic surfactants, and examined the effects of the counterion, which were dodecyl sulfates with potassium, sodium, and lithium as counterions (KDS, NaDS, LiDS). It was found that the counterion influenced the interaction starting concentration in the order of KDS < NaDS < LiDS, and the nature of the complexation. The interaction between EHEC and cationic surfactants were also reported by many groups. [Zana et al., 1992; Bloor, Mwakibete and Wyn-Jones, 1996; Bu, Kjøniksen and Nyström, 2004] A series of cationic surfactants, namely alkyltrimethylammonium halides RTAX with R equal to C_{12}, C_{14}, and C_{16} and **X** either Br or C1,

and dodecylammonium chloride were employed in the interaction studies with EHEC in comparison with SDS. They found that both SDS and cationic surfactants can bind onto EHEC molecules, while the binding sites may be different. From both the calorimetric and viscosity results, it was noted that SDS interacted with EHEC through both the ethyl and the ethylene oxide groups while the RTAX surfactants predominately interact with the alkyl groups. [Wang and Olofsson, 1995]

The hydrophobically modified EHEC, namely HM-EHEC, exhibited higher viscosity values than EHEC due to the intra- and intermolecular interactions of the hydrophobic moieties. In the presence of surfactants, hydrophobic interactions were affected and the association strength could be augmented or weakened by the level of surfactant addition. [Thuresson, Lindman and Nyström, 1997] In aqueous media, the remarkable rheological and structural properties of surfactant and HM-EHEC have also been investigated in comparison to unmodified EHEC. Evertsson and Nilsson [1999] studied the association behavior of HM-EHEC and its interaction with SDS in the dilute concentration regime using fluorescence probe. They discussed the noncooperative and cooperative binding process of SDS to HM-EHEC, and found the surfactant/polymer aggregates were rigid and hydrophobic in the noncooperative binding region at a very low degree of SDS adsorption. Thuresson and co-workers [1997] systematically examined the interactions between various surfactants (anionic, cationic, and nonionic) and two cellulose derivatives, i.e. EHEC and HM-EHEC. They found that in the presence of an ionic surfactant, the rheological measurements revealed strong polymer/surfactant interaction for both EHEC and HM-EHEC, and the interaction was more significant at low surfactant concentration for HM-EHEC. In contrast, the polymer/surfactant interaction was weaker in the presence of a nonionic surfactant. Moreover, they reported that with increasing the surfactant chain length, the

disruption of the association process was delayed. A schematic picture describing the surfactant-induced strengthening and disruption of the association network is presented in Figure 2.11. [Nyström et al., 2009]

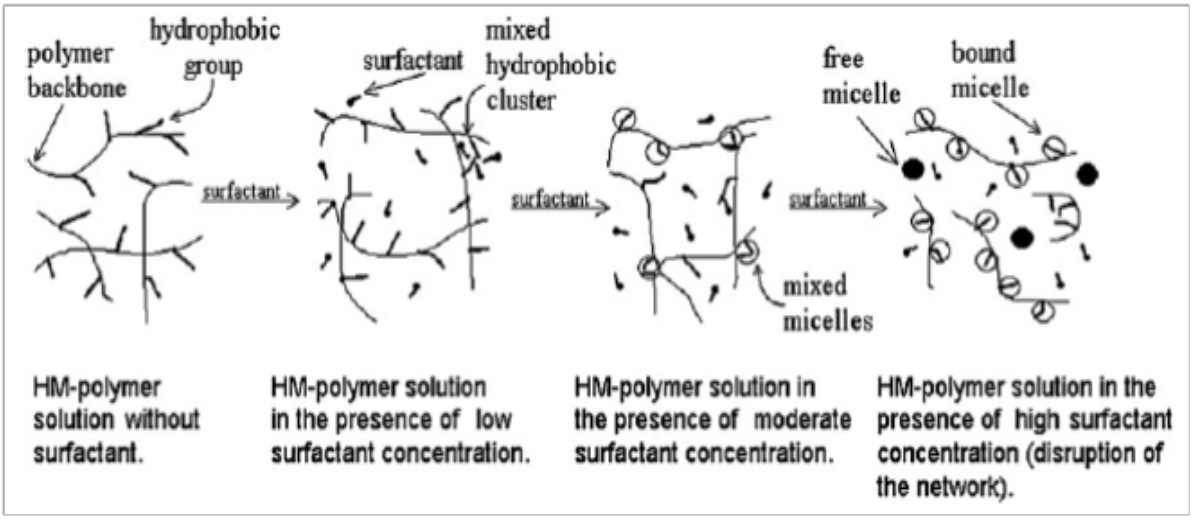

Figure 2.11 A schematic illustration of the surfactant-induced strengthening and disruption of the association network. [Nyström et al., 2009]

2.4.4 Interactions between cellulose nanocrystals and surfactants

Cellulose nanocrystals (CNC) possess negative charges on their surface due to the formation of sulphate ester groups during sulfuric acid treatment, which enhances their stability in aqueous solutions, but restrict its dispersability in most non-polar solvents. One possible route to improve this is to coat the CNC surface with a surfactant, which has been successfully demonstrated by Heux and co-workers. [Heux, Chauve and Bonini, 2000; Ljungberg et al., 2005; Ljungberg, Cavaillé and Heux, 2006; Elazzouzi-Hafraoui, Putaux and Heux, 2009] The surfactant used in their studies was a phosphoric ester of polyoxyethylene(9) nonylphenyl ether, with a commercial name Beycostat NA (BNA). To prepare a CNC suspension in non-polar solvents, the cellulose suspension in water was mixed with the surfactant at a weight ratio of 4:1 of BNA to cellulose. After adjusting the pH to 8 using aqueous sodium hydroxide, the

suspension was freeze-dried and then redispersed in toluene. The final suspensions of the surface coated whiskers in non-polar solvents, such as toluene and cyclohexane, did not precipitate nor flocculate. [Heux, Chauve and Bonini, 2000] Three types of CNC particles, namely Col54, Col63, Col72, were prepared with acid treatment of cotton linters at 54, 63, and 72 ^{o}C, respectively, while their suspensions in cyclohexane were examined using polarized light microscopy. All the suspensions' anisotropic phases displayed the same patterns consisting of alternating dark and illuminated zones, which were referred to chiral nematic textures. [Elazzouzi-Hafraoui, Putaux and Heux, 2009] Polarized optical micrographs of the chiral nematic texture (Figures 2.12 a-c) and fingerprints (Figures 2.12 d-f) of the anisotropic phase in CNC suspensions in cyclohexane were shown in Figure 2.12.

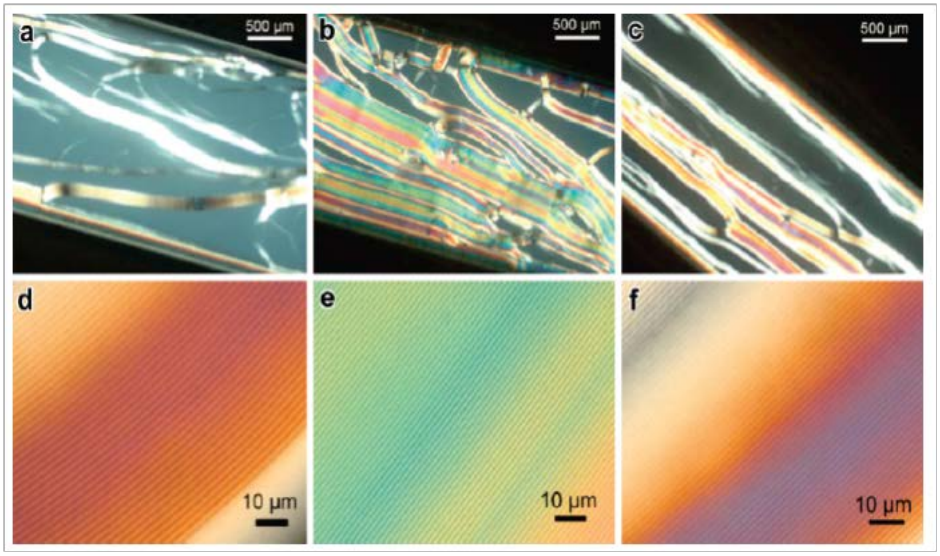

Figure 2.12 Polarized optical micrographs of the chiral nematic texture (top row) and fingerprints (bottom row) of the anisotropic phase in Cot54 at 31.0 wt% (a and d), Cot63 at 38.7 wt% (b and e), and Cot72 at 27.0 wt% (c and f) suspensions in cyclohexane. [Elazzouzi-Hafraoui, Putaux and Heux, 2009]

CNCs have been realized as a promising renewable biomaterial and used as a reinforcing component in high performance nanocomposites. Many new nanocomposite materials with

attractive properties were obtained by the physical incorporation of CNC into a natural or synthetic polymeric matrix. In order to improve the dispersion of CNC in hydrophobic matrix, surfactant was employed by some researchers. [Bondeson and Oksman, 2007; Kim et al., 2009; Rojas, Montero and Habibi, 2009] Kim et al. [2009] utilized a nonionic surfactant sorbitan monostearate (span-60) to improve the dispersion properties of CNC in a hydrophobic polystyrene matrix and to prevent the formation of aggregates. Figure 2.13 shows the optical microscope images of PS/CN/Surfactant composite films at various CN/Surfactant ratios from 1:0, 1:1, 1:2, and 1:4. Compared with neat PS film, adding CNC to a PS matrix resulted in the aggregation of nanoparticles, implying low dispersion of CNC. A better dispersion was observed by adding small amounts surfactant, while agglomeration appeared at CN/Surfactant ratio of 1:4 due to the effect of self-aggregation of the surfactant. [Kim et al., 2009] Therefore, these results showed that the optimum addition of surfactant produced better dispersion of cellulose particles in the polystyrene matrix. Furthermore, they also proved that the mechanical properties of the resulting composite were improved due to an enhanced compatibility.

Smooth monolayer films consisted of CNC and a cationic surfactant dioctadecyldimethylammonium (DODA) were prepared by Langmuir-Blodgett [Habibi et al., 2007] vertical and Langmuir-Schaeffer [Habibi et al., 2010] horizontal deposition. The morphology and chemical composition of these films were characterized using atomic force microscopy (AFM) and X-ray photoelectron spectroscopy (XPS). It was demonstrated that these layers offer an opportunity to investigate the interfacial properties relevant to the chemical and biological transformations of cellulose. Alternatively, these films can be used as a coating technology to modify the surface of other materials to achieve unique properties. [Habibi et al., 2010]

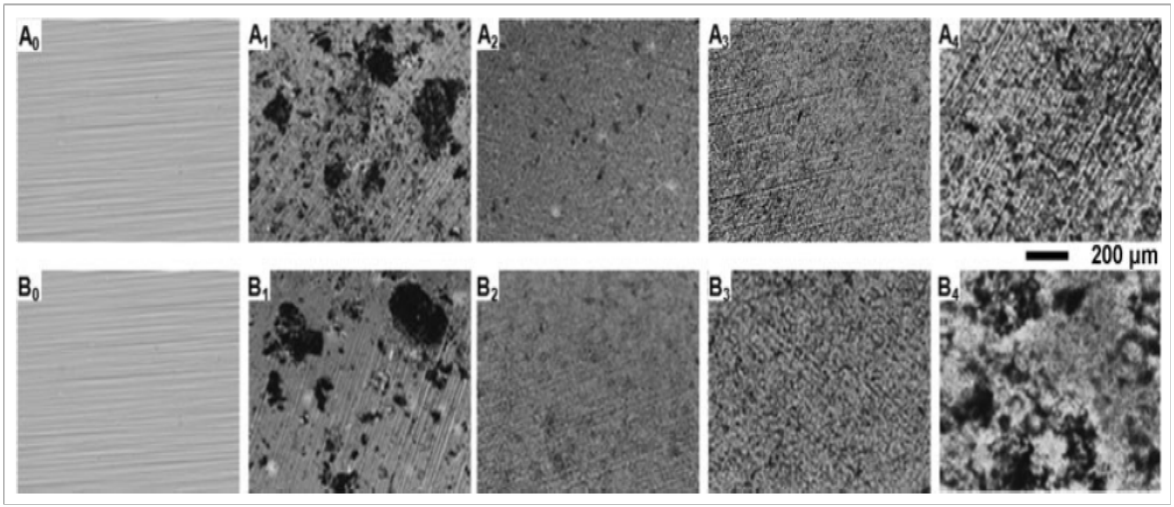

Figure 2.13 Optical microscope images for neat PS film (A_0 and B_0) and PS/CN/Surfactant composite films with 3% ($A_{1–4}$) and 6% ($B_{1–4}$) CN weight load. CN:Surfactant ratios are 1, CN:Surfactant = 1:0; 2, CN:Surfactant = 1:1; 3, CN:Surfactant = 1:2; 4, CN:Surfactant = 1:4. [Kim et al., 2009]

2.4.5 Interactions between biodegradable chitosan derivative and surfactants

Chitosan is a (1→4)-linked 2-amino-2-deoxy-*β*-D-glucan derived from fully or partially deacetylated chitin, which is the most abundant natural biomacromolecule. Chitosan is an important polysaccharide, having unique structures, properties and wide ranging applications in many industrial sectors, such as tissue engineering, transplant and cell regeneration, encapsulation, and wastewater treatment. Recently, chitosan has been developed as drug carriers in the microparticulated and conjugated drug delivery systems due to its biocompatibility and biodegradability. Even though, one drawback in chitosan is that it is only soluble in acidic medium, therefore, improving its water-solubility is important for its further application as biomaterial. Chemical modification of chitosan is an efficient way to alter the properties of chitosan, such as trimethylated, *N*-succinylated, thiolated, azidated, sugar-modified and enzyme-modified chitosans. [Ravi Kumar et al., 2004] Among these methods, introducing anionic and

cationic functional groups to chitosan structure is very important in order to improve its solubility in aqueous medium. For example, the sulfochitosan and carboxyalkylated chitosan are soluble not only in acidic medium but also basic medium, moreover, the solubility of *N*-carboxyalkylated chitosan in water offers higher biodegradability and more biocompatible than chitosan molecules. Park et al., [2003] demonstrated that the gluconic acid modified chitosan can enhance its susceptibility to lysozyme in their biodegradability study. As a consequence, it provided a possible way to control the aqueous solubility and biodegradability of chitosan by simple modification with gluconic acid.

Chitosan has been used to prepare nanoparticles, nanospheres, hydrogels, films, fibres and so on. In preparing these nanostructures, surfactants can play an important role as an emulsifier, dispersant, or foaming agent. Therefore, the study on the interaction between surfactant and chitosan and its derivatives is a very interesting subject that is the focus of many researchers. [Pavinatto, Caseli and Oliveira, 2010; Casettaria et al., 2012] Chitosan/surfactant complexes can be formed in aqueous solutions due to electrostatic attraction, hydrophobic interaction or other forces, while the addition of surfactant has a significant effect on the structural, dynamic and rheological properties of chitosan solutions. For example, it is reported that surfactants can increase chitosan's solubility in water or in organic solvents by forming complexation. [Casettaria et al., 2012] The unique vesicles containing amphiphilic chitosan derivatives and the conventional cationic surfactant was prepared by Fan et al., [2011] while the formation of vesicles was driven by hydrophobic and electrostatic interactions. Pavinatto *et al.* [2010] reviewed the use of chitosan in nanostructured films produced with the Langmuir-Blodgett (LB) or the electrostatic layer-by-layer (LbL) techniques, and they emphasized on the role of surfactants in improving the surface activity of chitosan in diluted solution. A gemini surfactant

consists of two conventional surfactant molecules, which are chemically bonded together by a spacer. Hence, the properties of gemini surfactant should be different from the conventional ones, which may exhibit some novel behavior in the surfactant/chitosan complex. The fundamental knowledge developed from such studies will provide the information necessary for the development of new and novel systems for applications in the biomedical and chemical fields.

2.4.6 Applications of polymers and surfactants complexes

As a result of their distinctive properties, the polymer/surfactant systems have been found in a wide range of useful applications. This section highlights the potential applications of polymer/surfactant systems in the following fields.

Biomedical Applications The polymer/surfactant complexes are commonly found in many biomedical products, where surfactant is used as additive in a drug formulation or as molecules present in an in-vivo environment. [Schmaljohann, 2006] Surfactants can alter the hydrophilic/hydrophobic balance of polymers provided they bind to the polymer chain causing a shift in the transition temperature. While the size of polymer aggregates can also be changed, for example, PNIPAM shows a monotonous increase in the hydrodynamic radius R_h upon the addition of an ionic surfactant (SDS), while the transition temperature increases with increasing surfactant concentration until it levels off at a defined surfactant concentration. [Makhaeva et al., 1998] Thermo-responsive gels have been investigated for biomedical applications, such as drug delivery vehicles and chromatographic or separation technology, [Ramkissoon-Ganorkar et al., 1999; Gan and Lyon, 2002] where the particle size can be controlled by altering the surfactant concentration in the system. [Ito et al., 1999] Isogai et al. [1996] studied the volume collapse behavior on binding of tetraphenylphosphonium chloride (TPPC) to an anionic polyelectrolyte network poly(2-(acrylamido)-2-methylpropanesulfonic acid) (PAMPS) gel. They found that the

amount of TPPC inducing volume collapse decreased with increasing temperature, and the binding process is non-cooperative and insensitive to temperature change in spite of the strong hydrophobic interaction of TPPC.

Drug Delivery Drug delivery systems is highly innovative in terms of materials to assist delivery and release drugs, and the materials for drug delivery have become one of the most interesting research fields. Considering the safety and efficacy, the use of natural polymers matrix is one of the most popular approaches in formulating a drug delivery carrier. Among the natural polymers, water-soluble cellulose derivatives have been widely studied in the applications of drug delivery, and found good performance in combination with surfactants. [Scherlund, Brodin and Malmsten, 2000; Terayama et al., 2001] To enhance the dispersion of hydrophobic drugs in water, a combination of surfactant and cellulose derivatives systems is a good strategy. The aqueous dispersion behavior of a well-know enzymatic inhibitor, i.e. 5-(3-ethoxy-4-pentyloxyphenyl)-2, 4-thiazolidinedione (CT112) was studied in the presence of SDS and cellulose derivatives. It is found that the dispersion of CT112 was enhanced, and more stable dispersion of CT112 particles was prepared. [Terayama et al., 2001] Scherlund et al. [2000] studied the interaction behavior of ionic surfactants and EHEC and HM-EHEC, and investigated the *in vitro* drug release behaviors of anesthetic agents (lidocaine and prilocaine) based on these surfactant/polymer systems. The results showed that small amounts of active ingredients can be incorporated into the systems, while the stability and drug release indicated a possibility of formulating a local anesthetic drug delivery system using the surfactant/polymer systems.

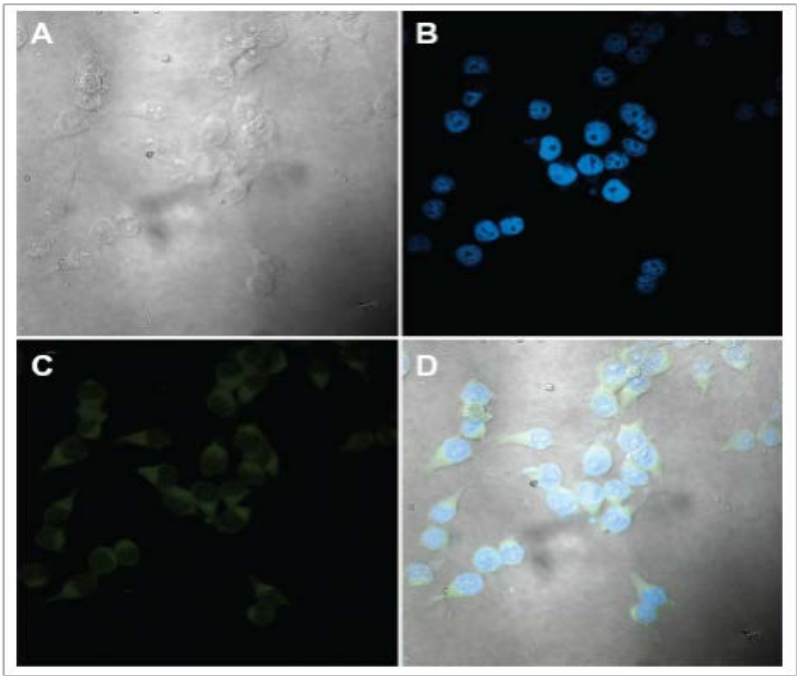

Figure 2.14 Confocal micrographs of KU-7 cells incubated for 2 hours with CNC/CTAB/fluorescein nanocomplexes with a CNC/CTAB/fluorescein concentration of 0.25 mg/mL. A) White light image of KU-7 cells. B) Staining of the nuclei with DAPI (4', 6-diamidino-2-phenylindole). C) Fluorescein in the cytoplasm. D) An overlay of images B and C. [Jackson et al., 2011]

Cellulose nanocrystals (CNC) have attracted increasing attention in biomedical applications due to its attractive properties. As a relatively new material, the applications of materials based on CNC have not been widely studied. Therefore several papers have been published, reporting on the application of drug delivery of surfactant/CNC combinations. [Levis and Deasy, 2001; Podczeck, Maghetti and Newton, 2009; Jackson et al., 2011] Recently, the CNC and CTAB complexes were studied by Jackson and co-workers, [2011] and they found that the complexes could bind to KU-7 cells and evidence of cellular uptake was observed (see Figure 2.14). Furthermore, they found the CTAB-coated CNC was shown to bind significant quantities of the nonionized hydrophobic anticancer agents docetaxel (DTX), paclitaxel (PTX),

and etoposide (ETOP) and release these drugs in a controlled manner over several days (see Figure 2.15). Similar release profiles were observed for these three agents, 59% and 44% of the total bound DTX and PTX were released in 2 days, respectively. While a total of 75% of the ETOP was released over 4 days.

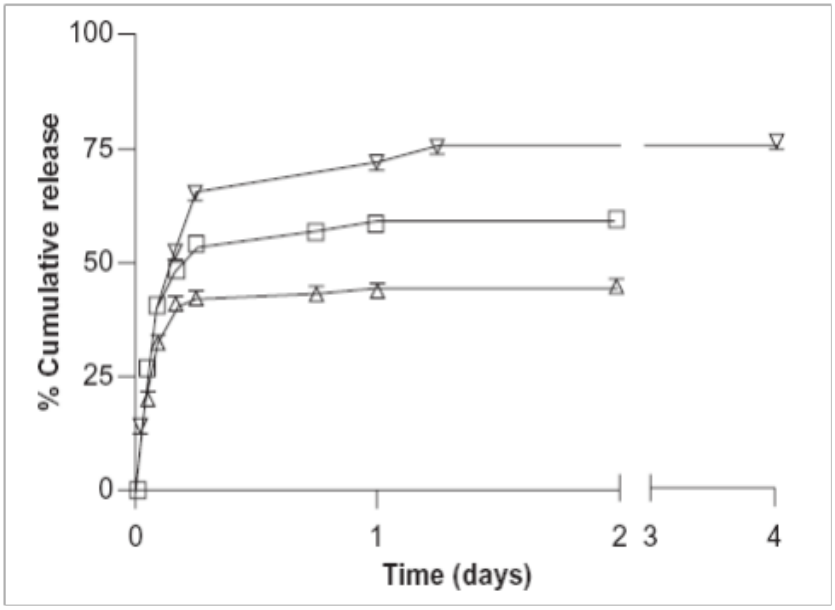

Figure 2.15 The in vitro release of etoposide (▽), docetaxel (□), and paclitaxel (Δ) from CNC/CTAB nanocomplexes with 12.9 mM CTAB in 10 mM phosphate buffered saline at 37 °C. [Jackson et al., 2011]

Enhanced Oil Recovery (EOR) EOR methods have been employed to increase the extraction of crude oil since the efficiency of oil recovery during the primary stage is relatively low. EOR processes include all methods that use external sources of energy and/or materials to recover oil and it can be classified as thermal (steam flooding, hot water drive, in situ combustion), chemical (polymer, surfactant) or miscible methods (hydrocarbon gas, CO_2, nitrogen). [Satter and Thakur, 1994] In chemical EOR processes, water-soluble polysaccharides were commonly employed as viscosifying agents of aqueous solutions used in oil recovery projects due to their environmentally-friendly properties. [Taylor and Nasr-El-Din, 1998; Mothé

et al., 2006] In addition, low interfacial tension with regard to the oil-phase was also necessary. [Hou et al., 2005] Therefore the combination of polysaccharides and surfactants could be good candidates for EOR operations.

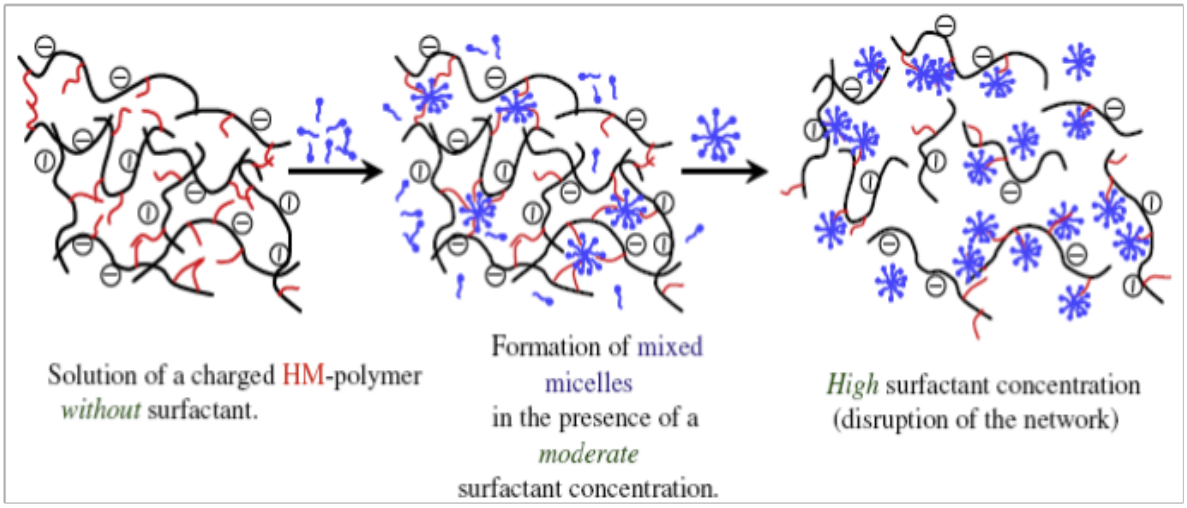

Figure 2.16 Schematic illustration of the effect of SDS addition to a semi-dilute HM-HEC solution. [Kjøniksen et al., 2008]

Kjøniksen et al. [2008] prepared a charged hydrophobically modified hydroxyethylcellulose (HM-HEC) and studied its potential applications in the presence of an anionic surfactant (SDS) in EOR processes. A relatively high viscosity was obtained even at very low concentration (0.2 wt%) in (HM-HEC) aqueous solutions, which was a very important feature in connection to EOR. [Sabhapondit et al., 2003] The viscosity results for the HM-HEC/SDS systems disclosed strong interactions between HM-HEC and SDS molecules at moderate SDS concentration, resulting in a significant viscosification of the HM-HEC/SDS mixture. It was also observed that the viscosity of the mixture was strongly dependent on the temperature, i.e. the viscosity decreased with increasing temperature. However, this phenomenon was not found for mixtures with high SDS concentration due to the disruption of the association complexes comprising HM-HEC and SDS (Figure 2.16). The investigation of HM-HEC/SDS

composition and temperature on the solution rheological properties allow us to develop a viscosifying agent for EOR applications.

2.5 Summary

From the literature review, we concluded that biodegradable TRPs are the most attractive and convenient environmentally responsive polymer systems, while CNC particles exhibited exceptional strength and physicochemical properties, and can be functionalized depending on desired applications. Therefore, the combination of TRPs and CNC can extend their potential applications in many disciplines, and the presence of surfactants may improve their properties. Moreover, as an important category of biocompatible and biodegradable natural material, the properties and applications of chitosan and its derivatives are introduced, and the interactions between *N*-carboxyethylchitosan (CECh) and gemini surfactants exhibit very interesting behaviors. Therefore, studies on the interactions of surfactant and these biodegradable polymers in bulk and at interface could be very useful and important.

In this doctoral research, we conducted fundamental studies on the preparation of well-defined thermo-responsive polymers based on oligo(ethylene glycol) methacrylates, functionalization of CNC and chitosan, as well as the interactions of surfactant with these novel systems. The goal of this fundamental study is an attempt to explore their applications as targeted drug delivery carriers and in personal care products. The curiosity in optimizing the formula motivated our work to design and prepare well-defined systems.

Chapter 3 Self-Assembly Behavior of Thermo-responsive Oligo (ethylene glycol) Methacrylates Random Copolymers

3.1 Introduction

Thermoresponsive polymers have attracted increasing interests due to their promising potential in a wide range of biomedical and nanotechnology applications, such as drug delivery, [He, Kim and Lee, 2008] controlled bioadhesion, [Cunliffe et al., 2003] and tissue engineering. [Okano et al., 1995] These polymers usually display phase transition temperatures that are signified by either the upper critical solution temperature (UCST) or lower critical solution temperature (LCST). Among the polymers that exhibit the LCST, poly (*N*-isopropylacrylamide) (PNIPAM) is the most widely studied system, where it possesses a LCST of ~32 ^{o}C in water. [Schild, 1992] Below the LCST, the polymeric chains hydrate and adopt an extended chain conformation. Beyond the critical temperature, the polymeric chains undergo a sharp and reversible coil-to-globule transition. [Morris et al., 2010]

Due to possible concerns on the toxicity of *N*-isopropylacrylamide monomer, Lutz and coworkers prepared a series of biocompatible polymers that exhibited similar thermoresponsive behaviors as PNIPAM. [Lutz Akdemir and Hoth, 2006; Lutz, 2008, 2011] They randomly copolymerized di(ethylene glycol) methyl ether methacrylate (MEO_2MA, M_n = 188 g/mol) and poly (ethylene glycol) methyl ether methacrylate (PEGMA, M_n = 475 g/mol) P(MEO_2MA-*co*-$PEGMA_{475}$) via atom transfer radical polymerization (ATRP), and observed that the LCSTs of the copolymers could be tuned to between 26 and 90 ^{o}C by varying the monomer compositions. For instance, the LCST values for the copolymers increased from 26 ^{o}C (0% of $PEGMA_{475}$) to a relatively higher temperature as the mole fraction of $PEGMA_{475}$ in the polymer chain was

increased. A LCST of 32 ^{o}C was observed in water for copolymers containing 5% of $PEGMA_{475}$. The relatively higher LCST was attributed to the longer PEG side chains due to their hydrophobic-hydrophilic characteristic. [Lutz and Hoth, 2006] The mechanism describing the temperature-induced phase transition of these copolymers in aqueous was proposed and illustrated by Lutz and co-workers. [Lutz et al., 2007] Kitano et al. [2004] studied the effects of macrocycles on the LCSTs of copolymers, where the LCSTs of 2-(2-methoxyethoxy) ethyl methacrylate and ω-methoxy(oligoethyleneoxy) ethyl methacrylate (MOEMA) increased significantly with increasing content of MOEMA. Similar studies on these copolymer systems were reported by Ishizone and coworker, [2003, 2008] who polymerized very short side chain oligo(ethylene glycol) methacrylates (1 ~ 4 units) using anionic polymerization. They investigated the LCST characteristics of polymers containing di-, tri-, and tetra (ethylene glycol) units in the aqueous solutions. The LCSTs and solubility of the copolymers were strongly dependent on the length of oligo(ethylene glycol) side chain units, and only one thermal induced aggregation process was reported. [Han, Hagiwara and Ishizone, 2003; Kitano et al., 2004; Lutz, Akdemir and Hoth, 2006; Lutz and Hoth, 2006; Lutz et al., 2007; Ishizone et al., 2008] Multiple thermal induced aggregation processes were reported for various block copolymers comprising two or more thermal sensitive blocks, where these systems displayed sharp and rapid temperature-induced self-assembly behaviors. [Hua, Jiang and Zhao, 2006; Yamamoto, Pietrasik and Matyjaszewski, 2007; Dimitrov et al., 2007; Skrabania et al., 2007; Xie et al., 2009; Weiss, Böttcher and Laschewsky, 2011; Zhang, Liu and Li, 2011; Li, Lavigueur and Zhu, 2011] However, to the best of our knowledge, multi-step aggregation processes have not been reported for random copolymer systems.

In this chapter, we report a unique double thermal induced aggregation behavior of a random copolymer containing oligo(ethylene glycol) methacrylates i.e. MEO_2MA (M_n = 188 g/mol) and PEGMA (M_n = 2080 g/mol). The brush-like random copolymer was prepared by ATRP, [Lutz, Akdemir and Hoth, 2006] and the synthesis route is shown in Scheme 3.1. The thermo-responsive behaviors of this copolymer in aqueous solution were investigated by means of UV-Vis spectroscopy, Laser light scattering (LLS) and Transmission electron microscopy (TEM), while an unusual thermal induced two-stage aggregation process was observed.

3.2 Experimental

3.2.1 Materials

2-(2-Methoxyethoxy)ethyl methacrylate (M_n ~ 188, 95%), poly(ethylene glycol) methyl ether methacrylate (M_n ~ 2,080, 50 wt% in water) were purchased from Sigma-Aldrich and purified by passing through a column filled with basic alumina before use. Methyl 2-bromopropionate (MBP), copper (I) bromide, 2, 2’ bipyridyl (Bipy) and ethanol were purchased from Sigma-Aldrich and used as received. Water used in all experiments was obtained from a Millipore-Q water purification system, which has a resistivity of 18.2 MΩ·cm.

3.2.2 Synthesis of P(MEO_2MA-*co*-$PEGMA_{2080}$) via ATRP

The copolymer was synthesized in ethanol via ATRP using MBP as the initiator and CuBr/Bipy as the catalyst. A typical procedure was described as follows: CuBr (35.9 mg, 0.25 mmol) and Bipy (78.1 mg, 0.5 mmol) were added to a 25 mL flask, and then the flask was sealed and purged with argon for 30 min. Then, a degassed mixture of 2-(2-methoxyethoxy) ethyl methacrylate (2.3 g, 12.4 mmol), poly(ethylene glycol) methyl ether methacrylate (2080 g/mol) (0.26 g, 0.0625 mmol), methyl 2-bromopropionate (20.9 mg, 0.125 mmol) and ethanol (3.32 mL)

was transferred using a double tipped needle into the flask charged with CuBr/Bipy equipped with a magnetic stirring bar under argon atmosphere. The mixture was heated at 60 °C for 3h, and the reaction was stopped by opening the flask after several hours. The reacted mixture was dialyzed against Millipore Water for 2 days, and then the final product was collected after freeze drying. The number averaged degree of polymerization (DP_n) was designed as 100, and the statistical composition of MEO_2MA:$PEGMA_{2080}$ was 99:1.

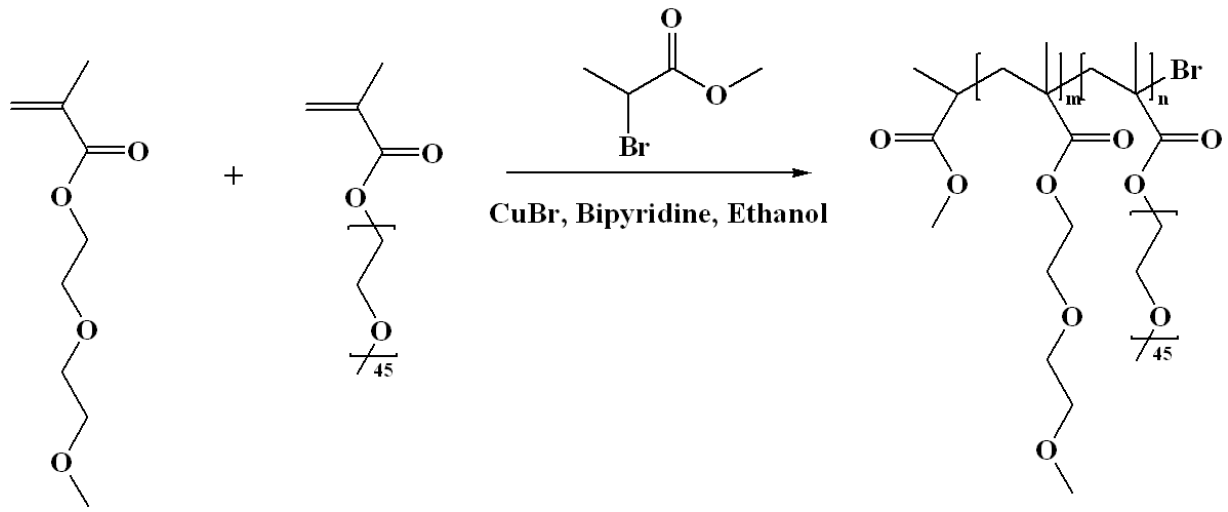

Scheme 3.1 Synthetic scheme of P(MEO_2MA-*co*-$PEGMA_{2080}$).

3.2.3 Characterizations of P(MEO_2MA-*co*-$PEGMA_{2080}$)

3.2.3.1 Nuclear magnetic resonance (NMR)

^1H NMR spectra were recorded in $CDCl_3$ on a Bruker AV300 NMR spectrometer operating in the Fourier transform mode. All analyses were performed at 25 °C.

3.2.3.2 Gel permeation chromatography (GPC)

Molecular weight and molecular weight distribution were determined by OmniSEC GPC system equipped with a ViscoGel Column, a RI and light scattering detectors. Tetrahydrofuran

(THF) was used as eluent at a flow rate of 1.0 mL/min. For calibration, linear polystyrene standards (PSS) were used.

3.2.3.3 Ultraviolet-visible spectroscopy (UV-Vis)

The thermal responsive measurements were performed on a Varian (Carey 100 Bio) UV-visible spectrophotometer equipped with a temperature controller. Transmittance of the copolymer solutions with concentration of 0.3, 0.5, 1.0 wt% were monitored as a function of temperature. All the measurements were performed at a heating rate of 1 °C/min and at a visible wavelength of 500 nm.

3.2.3.4 Laser light scattering (LLS)

Light scattering measurements were performed on a Brookhaven BI-200SM goniometer and BI-9000AT digital correlator equipped with an argon-ion laser. A 0.45 μm filter was used to remove dust prior to all the measurements, and the experimental temperature was controlled by a PolyScience water-bath. For dynamic light scattering (DLS), the time correlation function of the scattering intensity $G_2(t)$ is defined as $G_2(t) = I(t)\, I(t + \Delta t)$, where $I(t)$ is the intensity at time t and Δt is the lag time, and the inverse Laplace transform of REPES in the Gendist software package was used to analyze time correlation functions with the probability of reject set at 0.5. Thus, the apparent hydrodynamic radius R_h can be determined from the Stokes-Einstein equation:

$$R_h = \frac{kTq^2}{6\pi\eta\Gamma} \qquad (1)$$

where k is the Boltzmann constant, q is the scattering vector ($q = 4\pi n \sin(\theta/2)/\lambda$, where n is the refractive index of solvent, θ is the scattering angle, and λ is the wavelength of the incident laser light in vacuum), η is the solvent viscosity, and Γ is the decay rate.

Static light scattering (SLS) was used to measure the average radius of gyration (R_g) and weight-average molar mass (M_w) of the aggregates. In this experiment, the M_w of the micelles can be obtained from SLS measurements based on the Debye equation:

$$\frac{KC}{R(q)} = \frac{1}{M_w}\left(1 + \frac{1}{3}R_g^2 q^2\right) + 2A_2C \qquad (2)$$

where K is an optical parameter ($K = [4\pi^2 n_{tol}^2 (dn/dc)^2]/N_A\lambda^4$ where n_{tol} is the refractive index of toluene (1.494), dn/dc is the refractive index increment of the polymer measured using BI-DNDC, N_A is Avogadro's constant, and λ is the wavelength), C is the concentration of the polymer solution, $R(q)$ is the Rayleigh ratio, q is the scattering vector, and A_2 is the second virial coefficient. The absolute excess time-averaged scattered intensity, i.e., Rayleigh ratio $R(q)$, is expressed by the equation:

$$R(q) = R_{tol,90}\left(\frac{n}{n_{tol}}\right)^2 \frac{I - I_0}{I_{tol}} \sin\theta \qquad (3)$$

where $R_{tol,90}$ is the Rayleigh ratio of toluene at scattering angle 90° with a value of 40×10^{-6} cm^{-1}, n is the refractive index of the solvent, I, I_0, and I_{tol} are the scattered intensities of the solution, solvent, and toluene, respectively, and θ is the scattering angle. In our case, the concentration of the polymer solution is sufficiently low (0.02 wt%), and therefore the $2A_2C$ term in eq. 2 is expected to be negligible. Therefore, the intercept of the plot of $KC/R(q)$ against q^2 yields the inverse of the apparent weight-average molar mass (M_w^{app}); consequently, the aggregation number of the micelle can be evaluated using the equation $Z = M_w^{app}/M_w$, where M_w is the molar mass of the single polymer chain. [Ravi et al., 2003; Wang et al., 2007]

3.2.3.5 Transmission electron microscopy (TEM)

Transmission electron microscopic studies were performed using a Philips CM10 electron microscopy. The TEM samples were prepared by depositing one drop of 0.02 wt% particle

suspensions onto carbon coated TEM copper grid, which was placed on a filter paper. The excess liquid was absorbed by filter paper and the remaining liquid was allowed to air-dry overnight at room temperature.

3.3 Results and Discussion

3.3.1 Synthesis of P(MEO_2MA-*co*-$PEGMA_{2080}$)

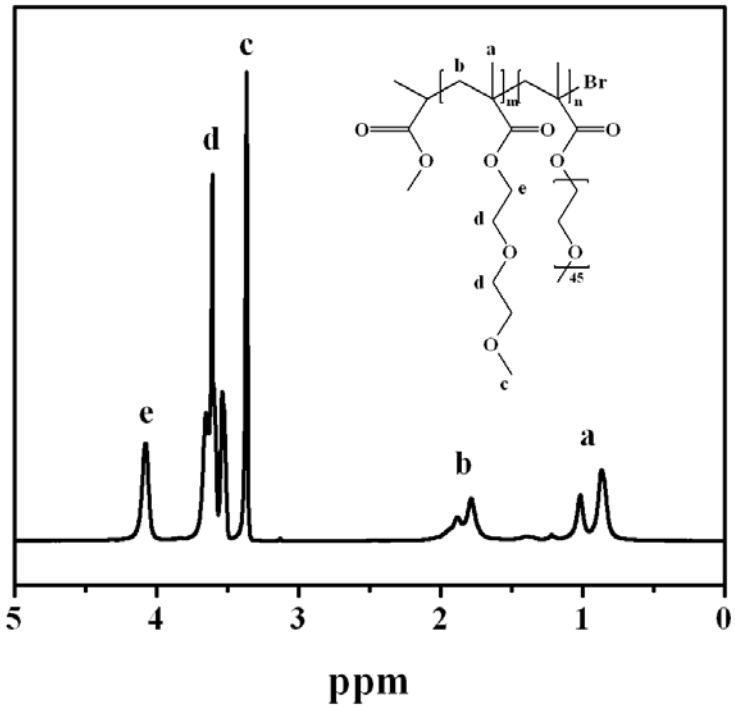

Figure 3.1 ^{1}H NMR spectra of P(MEO_2MA-*co*-$PEGMA_{2080}$) in $CDCl_3$ at 25 ^oC.

The ^{1}H NMR spectra of P(MEO_2MA-*co*-$PEGMA_{2080}$) is shown in Figure 3.1, and all the peaks corresponding to the protons on the copolymer are assigned correctly as reported in literature. [Lutz et al., 2007] The GPC results, shown in Figure 3.2, indicate the number average molecular weight (M_n), weight average molecular weight (M_w), and polydispersity index (PDI) of the copolymer was 17300 g/mol, 27900 g/mol, and 1.61. The number average degree of

polymerization (DP_n) of 84 was calculated from the GPC results based on the statistical composition. The PDI is somewhat larger than normally expected for an ATRP process, however it has been previously reported that the polymerization of OEGMA-based monomer using CuBr catalyst generally yielded a PDI of between 1.5-1.8. [Lutz and Hoth, 2006] However, molecular weight distribution was found to have no significant effect on phase transition for copolymers of comparable composition. [Lutz and Hoth, 2006]

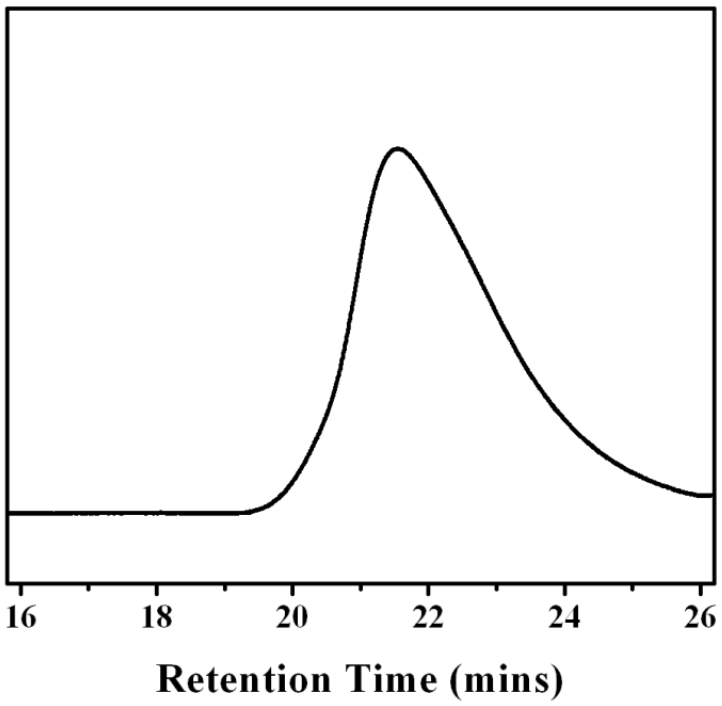

Figure 3.2 GPC profile of P(MEO_2MA-*co*-$PEGMA_{2080}$) at 25 ^oC.

3.3.2 Thermal responsive behaviors of copolymer in aqueous media

The thermo-responsive properties of 1 wt% copolymer aqueous solution were obtained from temperature-dependent UV/Vis transmittance measurements at the wavelength of 500 nm (Figure 3.3A). The solution was transparent at low temperature, and upon heating, it immediately

turned cloudy at 27 ^{o}C (T_1). Then the solution became white at 29 ^{o}C corresponding to a zero transmittance (%T). Such behavior is attributed to the dehydration of the polymer backbone and the short oligo(ethylene glycol) methacrylates side chains, where the polymer chains adopted a more compact globular structure induced by the intra- and inter-molecular aggregation of the polymeric chains. However, the polymer solution became less turbid when the temperature was raised to 33 ^{o}C (T_2), where the transmittance increased from 0 to 48%. Upon further heating, the polymer solution turned bluish and the transmittance decreased to a steady value of 26% when the temperature exceeded 40 ^{o}C. This colloidal dispersion was extremely stable and did not precipitate from solution.

In this study, we performed a detailed microstructural analysis on the phase transition of this copolymer using light scattering and TEM techniques. We hypothesize that the microstructure of the aggregates at higher temperature comprised of a hydrophobic 188 Da oligo(ethylene glycol) methacrylates core stabilized by a small fraction of the longer $PEGMA_{2080}$ shell. Photographs of 1 wt% P(MEO_2MA-*co*-$PEGMA_{2080}$) in aqueous solution at 25, 29, and 39 ^{o}C are shown in Figure 3.3B, and the corresponding transmittance of 0.3, 0.5, 1.0 wt% P(MEO_2MA-*co*-$PEGMA_{2080}$) in aqueous solution are shown in Figure 3.4. The results confirmed the occurrence of multiple thermal transitions, where the critical phase transition temperatures remained the same, implying that the phase transitions of P(MEO_2MA-*co*-$PEGMA_{2080}$) in water were insensitive to polymer concentration. [Lutz et al., 2007] The T% versus temperature curve of this copolymer is markedly different compared with previously reported results on copolymers of oligo(ethylene glycol) methacrylates, [Lutz and Hoth, 2006; Lutz et al., 2006; 2007] where only one sharp transition was reported. It is obvious that the length of the side chain can significantly alter the solution properties. By using poly(ethylene glycol) methyl ether

methacrylate with a molecular weight of 2080 g/mol instead of the 475 g/mol, unusual solution properties were observed. Similar results were only reported for different block copolymers in contrast to the random copolymer reported in this study. [Hua, Jiang and Zhao, 2006; Weiss, Böttcher and Laschewsky, 2011; Zhang Liu and Li, 2011; Li, Lavigueur and Zhu, 2011]

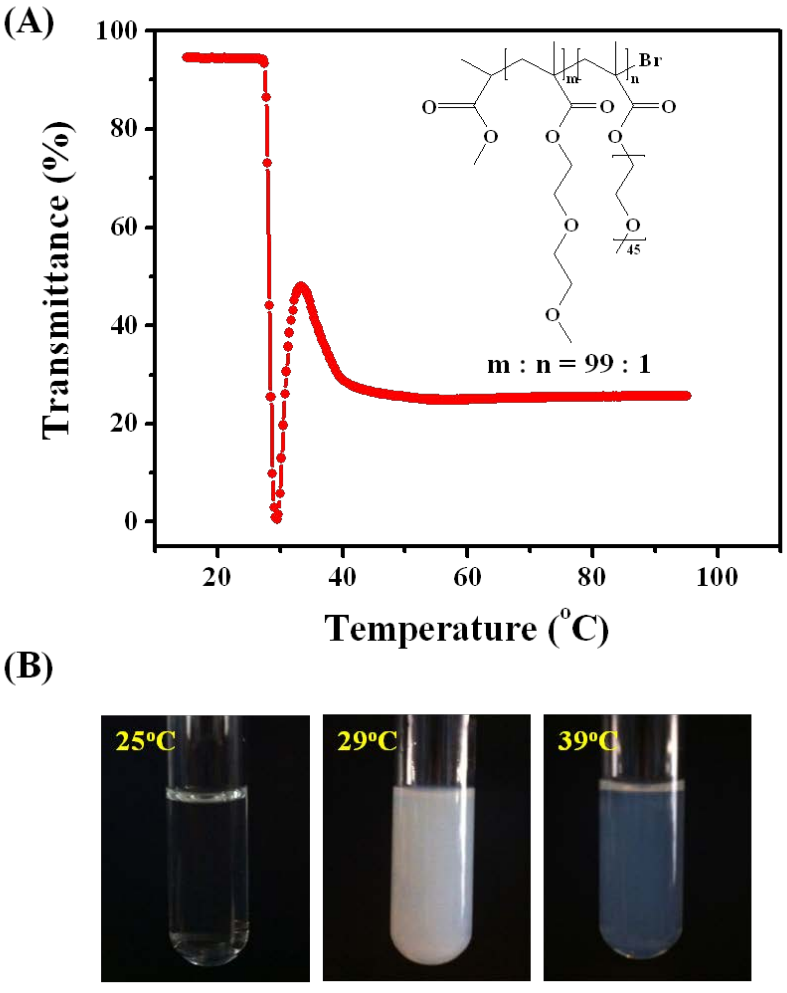

Figure 3.3 (A) Transmittance versus temperature for 1 wt% P(MEO_2MA-*co*-$PEGMA_{2080}$) aqueous solution at the wavelength of 500 nm. (B) Optical photographs of 1 wt% P(MEO_2MA-*co*-$PEGMA_{2080}$) aqueous solution at different temperatures.

Hua et al. [2006] reported that block copolymer of poly(methoxytri(ethylene glycol) acrylate)-*b*-poly(4-vinylbenzyl methoxytris-(oxyethylene) ether) (PTEGMA-*b*-PTEGSt) exhibited multiple transitions in aqueous solution upon heating. It was demonstrated that the two-step thermal induced aggregation process was a result of the different dehydration temperature of the two blocks, i.e. the PTEGSt block forming micellar structure at the first transition, and the dehydration of PTEGMA block induced the formation of aggregates. This is signified by changes in the solution property ranging from being transparent, to cloudy, clear, bluish, and then turbid again. The microstructural transformation of P(MEO_2MA-*co*-$PEGMA_{2080}$) with increasing temperature was elucidated by performing detailed dynamic light scattering (DLS) measurements.

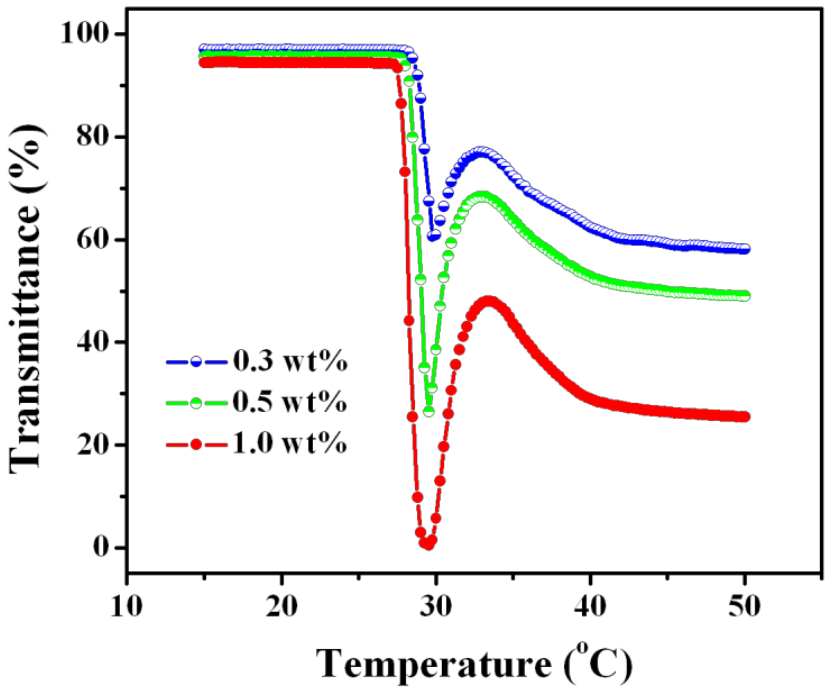

Figure 3.4 Transmittance versus temperature of 0.3, 0.5, 1 wt% P(MEO_2MA-*co*-$PEGMA_{2080}$) aqueous solutions at the wavelength of 500 nm.

3.3.3 Microstructure analysis of the copolymer in aqueous media

The hydrodynamic radius (R_h) as a function of temperature of 0.02 wt% P(MEO_2MA-*co*-$PEGMA_{2080}$) in aqueous solution determined from the DLS measurements at various scattering angles is shown in Figure 3.5. The R_h values were small (~6 nm) below 27 ^oC, indicating that the random copolymers were molecularly dissolved in water. The R_h values then increased to 137 nm at 29 ^oC, suggesting the formation of large aggregates, in good agreement with the minima in the transmittance plot (Figures 3.3 and 3.4). Upon further heating to 33 ^oC, the particle size began to decrease and remained relatively constant at around 55 nm.

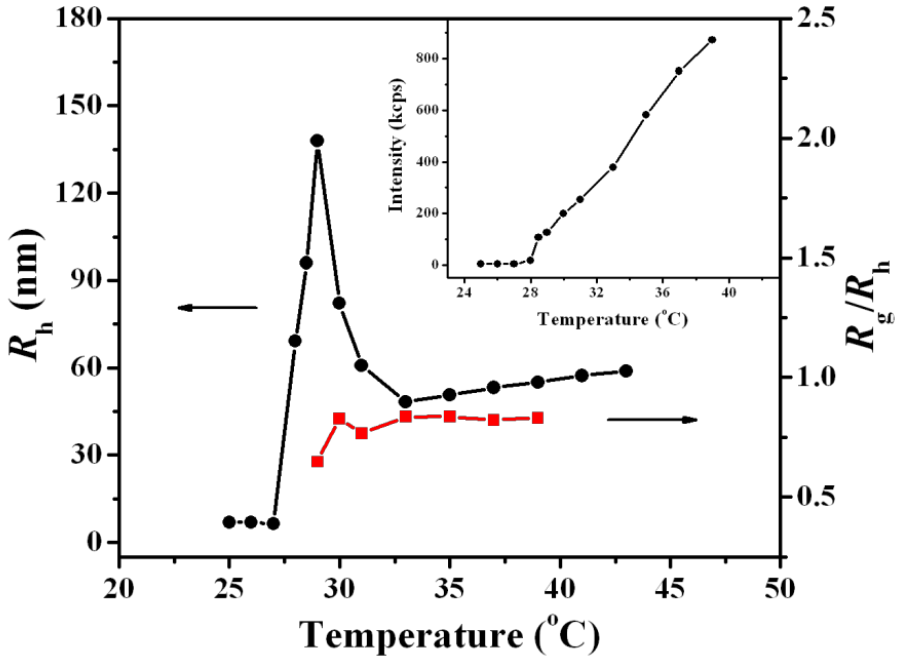

Figure 3.5 R_h, R_g/R_h and the scattering intensity (inset) of 0.02 wt% P(MEO_2MA-*co*-$PEGMA_{2080}$) solution at different temperatures.

In order to investigate the conformational change as a function of temperature, the radius of gyration (R_g) was measured at a temperature range 29 to 40 ^oC, and the R_g/R_h values were used to

examine the morphology of microstructure. Over this temperature range, the ratios of R_g/R_h remained constant at between 0.6 ~ 0.8, which corresponded to a core-shell micellar structure, [Akcasu and Han, 1979; Schuch et al., 2000; Ravi et al., 2003; Yao and Tam, 2011] as revealed by the transmittance data and the bluish color of the polymer solution. At the temperature range of 33 to 39 ^{o}C, the T% transmittance decreased while R_h and R_g/R_h remained constant, which is probably attributed to the changes in the refractive index of core-shell structure. The light scattering count rates with temperature were recorded during the DLS. The light scattering intensities increased significantly beyond 27 ^{o}C (inset of Figure 3.5), even though the particle size began to decrease from 130 to 50 nm. This phenomenon is attributed to the phase transition from random coil to compact globule yielding a more condensed core-shell structure that possessed a higher refractive index. [Zhang, Liu and Li, 2011]

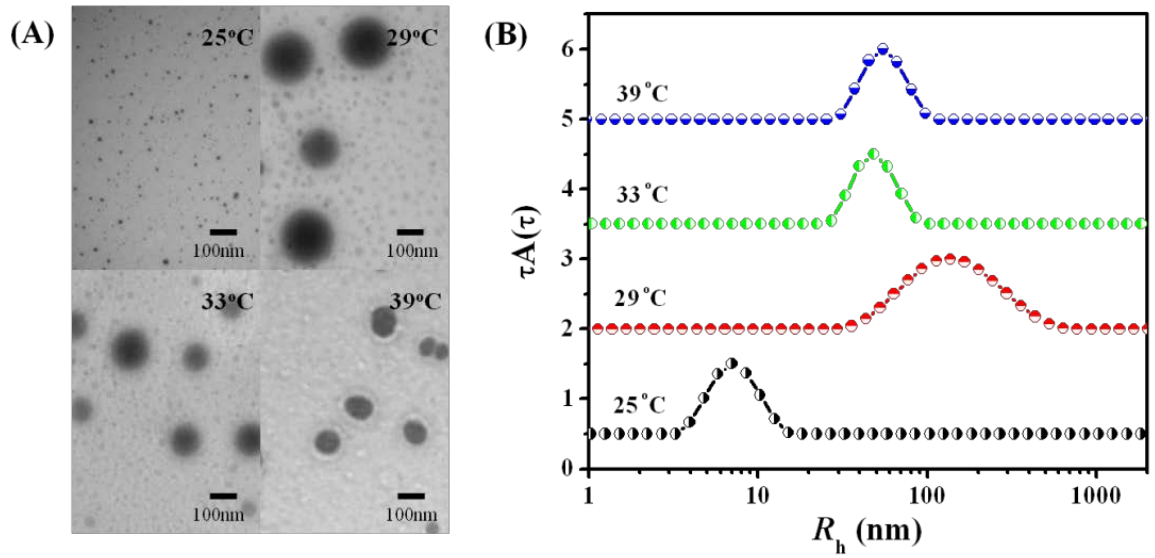

Figure 3.6 (A) TEM images and (B) relaxation time distribution curves of 0.02 wt% P(MEO_2MA-*co*-$PEGMA_{2080}$) solution at different temperatures.

Figures 3.6A and 3.6B show the transmission electron microscopic (TEM) images and relaxation time distribution curves of a 0.02 wt% P(MEO_2MA-*co*-$PEGMA_{2080}$) solution at 25, 29, 33 and 39 ^oC. The average particle size of copolymer nanostructures determined from TEM images was consistent with the DLS measurements, and the morphology corresponded to a core-shell structure.

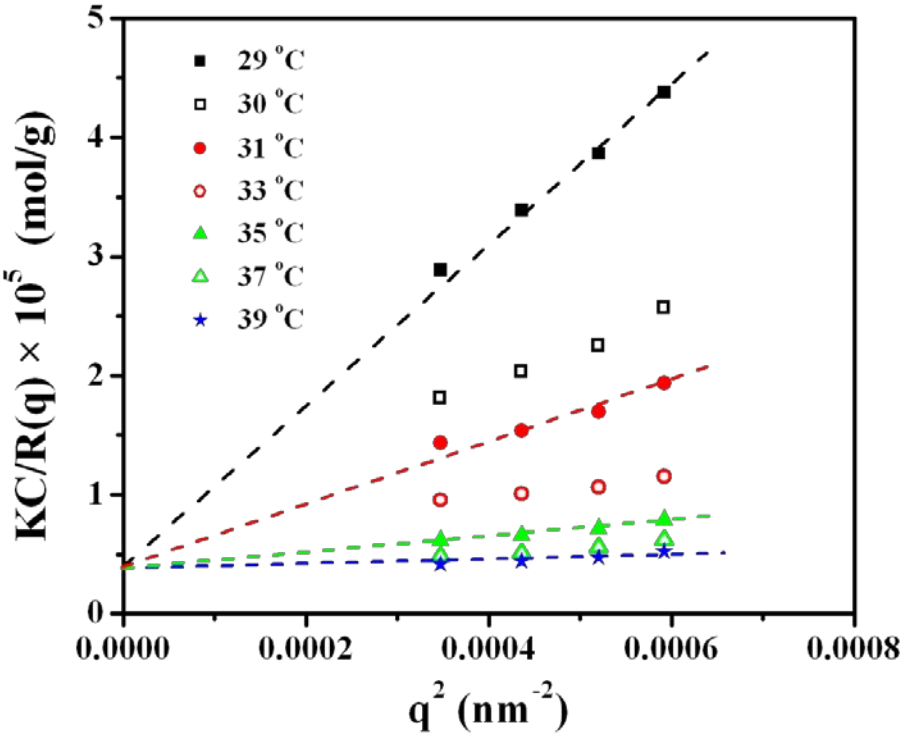

Figure 3.7 KC/R(q) versus the square of the scattering vector (q^2) for 0.02 wt% P(MEO_2MA-*co*-$PEGMA_{2080}$) solution at different temperatures.

The apparent weighted-average molar mass (M_w^{app}) of the micelles can be determined by static light scattering measurements using Equations (2) and (3) in section 3.2.3.4 [Ravi et al., 2003; Chen et al., 2005; Sedlák and Koňák, 2009; Zhao, Zhang and Pispas, 2009; Hao et al., 2010], consequently, the aggregation number of the micelle can be calculated from the equation $Z = M_w^{app}(\text{micelle})/M_w(\text{copolymer})$. Figure 3.7 shows the linear relationship of KC/R(q) versus

q^2 at various temperatures ranging from 29 to 39 °C, and it is interesting that all the data at various temperatures intersected at the same intercept at $q^2=0$. This again confirmed that the molecular weight and hence the aggregation number at the temperature range of 29 to 39 °C remained constant. The M_w^{app} determined from the intercepts was 2.5×10^5 g/mol, giving an average aggregation number Z of 8~9, since the weight average molar mass of the single polymer chain is 2.79×10^4 g/mol. The constant Z values indicated that the micellar aggregates formed at 29 °C were preserved and only conformation changes due to the dehydration of the copolymer chains occurred with increasing temperatures. The schematic describing the mechanism of the two-step thermal transition of the random copolymer P(MEO_2MA-*co*-$PEGMA_{2080}$) is illustrated in Figure 3.8.

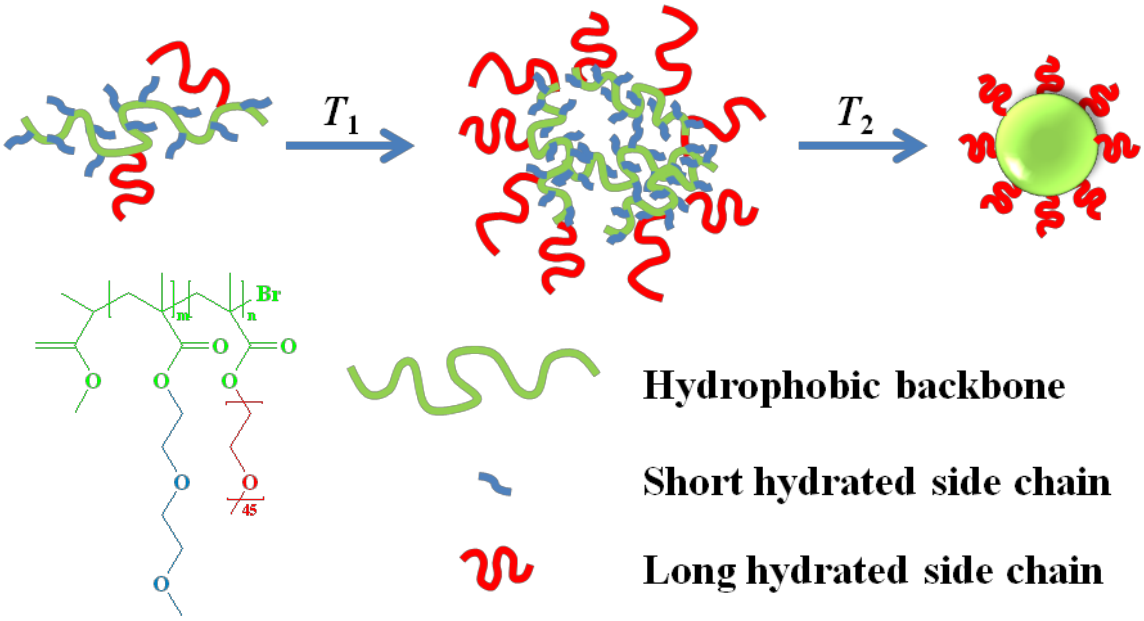

Figure 3.8 Schematic illustration of two-stage thermal induced aggregation process for random copolymer P(MEO_2MA-*co*-$PEGMA_{2080}$) in water.

3.4 Conclusions

In conclusion, a well-defined random copolymer containing 2-(2-Methoxyethoxy) ethyl methacrylate (MEO_2MA, M_n = 188 g/mol) and poly (ethylene glycol) methyl ether methacrylate (PEGMA, M_n = 2080 g/mol) (($P(MEO_2MA\text{-}co\text{-}PEGMA_{2080})$, M_n=17,300 g/mol) was synthesized by ATRP. In comparison to other temperature-sensitive random copolymers based on oligo(ethylene glycol) methacrylates, this copolymer exhibited a unique two-stage thermal induced aggregation process in aqueous solution. By increasing temperature, the copolymer chains phase separate, aggregate and rearrange to produce stable micelles. TEM and light scattering measurements confirmed the formation of large aggregates and micelle structure with increasing temperatures.

Chapter 4 Binding of Cationic Surfactants to a Thermo-sensitive Copolymer Below and Above its Cloud Point

4.1 Introduction

The interactions between surfactants and water-soluble polymers have been extensively studied due to their wide applications, such as in detergents, cosmetic and pharmaceutical products. Mixing surfactants and polymers can generate many interesting functional polymorphic micro or nano-structures, such as micelles, complexes, vesicles, precipitates, liquid crystals, as well as gels, which have a direct impact on the phase behavior, rheological and interfacial properties. [La Mesa, 2005; Tam and Wyn-Jones, 2006; George et al., 2009] Thus, knowledge on the physical properties of mixtures of surfactants and polymers will guide formulators in optimizing the formulation of personal care products. Due to the absence of strong electrostatic forces, the binding interaction between ionic surfactants and nonionic water-soluble polymers displays much simpler behaviour than ionic surfactant/opposite charged polymer systems. In these systems, hydrophobic effects play a significant role as an attractive force producing surfactant micelles that bind to the polymers below their critical micelle concentration (CMC). [Dai, Tam and Li, 2001] In general, the binding interactions between cationic surfactants and neutral polymers are much weaker than the corresponding interactions between similar polymers and anionic surfactants. [Wang and Olofsson, 1995, 1998; Ghoreishi et al. 1999a; Li et al., 2001; Dai and Tam, 2004] For example, an anionic surfactant such as sodium dodecyl sulfate (SDS) displays strong cooperative binding interaction with a diverse range of neutral water-soluble polymers, such as poly(ethylene oxide) (PEO), poly(propylene oxide) (PPO), and poly(vinylpyrrolidone) (PVP), while a cationic surfactant such as

tetradecyltrimethylammonium bromide (TTAB) is more selective and only binds to those polymers with specific hydrophobic groups, such as hydrophobically modified water-soluble polymers. [Ghoreishi et al. 1999a; Li et al., 2001] The binding isotherms and resulting mechanisms for ionic surfactant/neutral polymer systems are also dependent on polymer molecular weight, electrolytes, temperature, and solvent types.

Among these neutral water-soluble polymer/surfactant systems, temperature can play an important role in the binding interactions, particularly for thermo-sensitive polymers that exhibit a lower critical solution temperature (LCST) in aqueous solutions. As we know, poly(*N*-isopropylacrylamide) (PNIPAM) is a thermo-sensitive polymer that undergoes chain conformation transition from an extended coil to a compact globule near the cloud point (C_p). The impacts of ionic surfactants on the phase transition and chain conformation below and above the cloud point have received increasing attentions. [Loh, Teixeira and Lee, 2004; Chee et al., 2011; Chen et al., 2011, 2012] Chee *et al*. [2011] investigated the interactions between SDS and PNIPAM in aqueous solution using time-resolved fluorescence anisotropy measurements, and they found that below the LCST, the PNIPAM chains transformed from an expanded chain conformation to a swollen surfactant-polymer complex with reduced mobility due to the repulsion between the ionic groups of the polymer-bound surfactants. Above the LCST, the addition of SDS transformed the collapsed globule into an expanded surfactant swollen polymer coil. Similar results were observed by Yang and co-workers using nuclear magnetic resonance (NMR), and the effect of surfactant concentration were also studied in detail. [Chen et al., 2011, 2012] The interactions of PNIPAM with cationic surfactants were examined by Loh *et al*. [2004] using isothermal titration calorimetry, where the interactions were significantly affected by temperature due to the changes in the hydration of polymer chains near the LCST. The binding

interactions between ionic surfactants and thermo-sensitive Pluronic triblock copolymers such as PPO-PEO-PPO [Dai, Tam and Li, 2001] and PEO-PPO-PEO [Li et al., 2001; Nambam and Philip, 2012] were also reported. Mixed micelles of Pluronic copolymer and surfactant were produced in aqueous solution, and the percolation transition temperature of the mixture was found to decrease with volume fraction of surfactants. [Nambam and Philip, 2012]

In this chapter, the binding interactions between cationic surfactants and a thermo-responsive statistical copolymer based on oligo(ethylene glycol) methacrylates (OEGMA) were studied by several techniques, such as isothermal titration calorimetry (ITC), surfactant selective electrode (SSE) and dynamic light scattering (DLS). The copolymer possesses a brush-like structure with a relatively hydrophobic methacrylate and hydrophilic ethylene glycol segments, and as reported, OEGMA is touted to be an excellent alternative to PNIPAM due to its biocompatible properties. [Lutz, Akdemir and Hoth, 2006] Three types of cationic surfactants, namely, DoTAB, TTAB, and CTAB, were studied, where the effect of surfactant hydrophobicity on the binding interactions was elucidated. The different binding process below and above the cloud point were examined by analyzing the calorimetric titration and electromotive force (EMF) data, while the microstructure during the binding process was monitored by DLS.

4.2 Experimental

4.2.1 Materials

The well-defined brush-like statistical copolymer containing 2-(2-Methoxyethoxy) ethyl methacrylate (MEO_2MA, M_n = 188 g/mol) and poly (ethylene glycol) methyl ether methacrylate (PEGMA, M_n = 2080 g/mol) (poly(MEO_2MA-*co*-$PEGMA_{2080}$) was prepared via atom transfer radical polymerization (ATRP) to yield a copolymer with M_n =17,300 g/mol and a polydispersity index (PDI) of 1.61. The copolymer possessed a cloud point of 27 ^oC in aqueous solution. The

details of synthetic procedures and characterizations of the copolymer were described in chapter 3 and reported previously. [Peng et al., 2012] Cationic surfactants, such as DoTAB, TTAB, and CTAB of high purity were purchased from Sigma-Aldrich, and used without further purification. The water used was obtained from the Millipore-Q water purification system, which has a resistivity of 18.2 MΩ·cm. The chemical structures of the copolymer and surfactants are shown as below in Scheme 4.1.

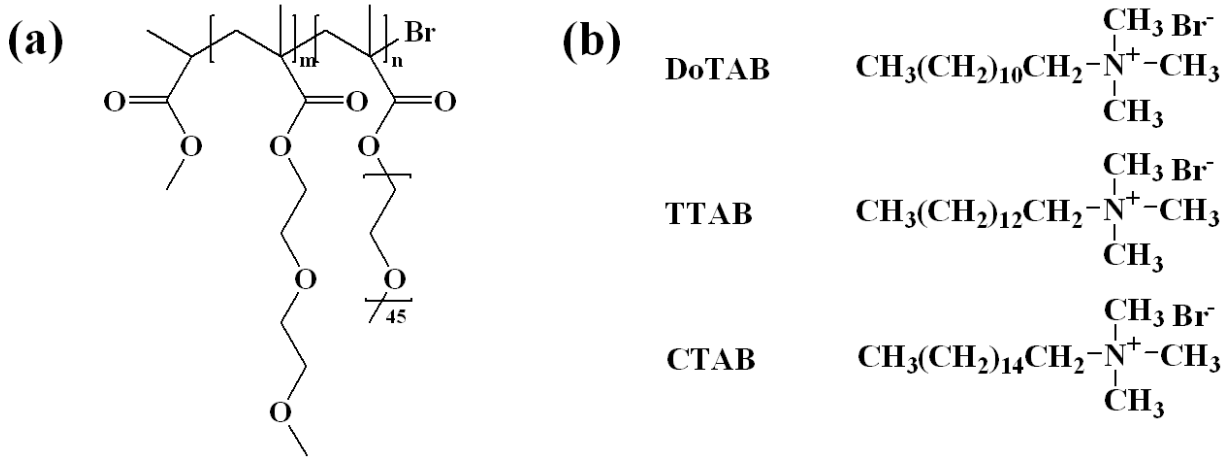

Scheme 4.1 (a) Chemical structure of statistical copolymer with monomer ratio 99 to 1 (m: n). (b) Chemical structures of cationic surfactants: DoTAB, TTAB and CTAB.

4.2.2 Isothermal titration calorimetry (ITC)

The calorimetric data on the binding interactions between cationic surfactants and copolymer poly(MEO_2MA-*co*-$PEGMA_{2080}$) were obtained using a Microcal VP-ITC calorimeter (Northampton, MA). The stock solutions with different concentrations, i.e. CTAB (20 mM), TTAB (100 mM), and DoTAB (200 mM), were selected for each cationic surfactant by considering their different CMCs. The titrations of 0.05, 0.1, and 0.2 wt% copolymer solutions were conducted at both 25.0 and 30.0 °C, which were below and above the cloud point of the copolymer (27.0 °C). A detailed description on this power compensated differential calorimetric

instrument was previously described by Wiseman and co-workers. [1989] The microcalorimeter consists of a reference cell and a sample cell of approximately 1.4 mL in volume, and surfactant solution was injected from a 281.72 μL injection syringe into the sample cell filled with either water or copolymer solutions. The syringe is tailor-made such that the tip acts as a blade-type stirrer to ensure an efficient mixing at 307 rpm. In this study, we utilized identical injection protocol and same time interval between successive injections for all ITC measurements.

4.2.3 Surfactant selective electrode (SSE)

An ionic surfactant electrode (Metrohm 6.0507.120) was used to monitor the binding interactions by measuring changes in the electromotive force (EMF) attributed to changes in the free surfactant concentration. The EMF was measured and recorded on a Metrohm 809 Titrando system equipped with a surfactant selective electrode and a double junction Ag/AgCl reference electrode (Metrohm 6.0750.100). The EMF measurements were designed to complement the ITC experiments using similar copolymer and surfactant concentrations performed at both 25.0 and 30.0 °C. For example, a 20 mM CTAB stock solution was added dropwise to a rapidly stirred 20 mL 0.05, 0.1 and 0.2 wt% copolymer solutions at 25.0 and 30.0 °C. The EMF values were recorded when the equilibrium was achieved after each injection of the surfactant solution. The resulting experimental data was plotted with EMF (mV) versus CTAB concentration, and the critical points for the binding interactions were determined.

4.2.4 Dynamic light scattering (DLS)

Dynamic light scattering measurements were performed on a Brookhaven BI-200SM goniometer system equipped with a PolyScience water-bath. All the samples were filtered through a 0.45 μm filter to remove dust prior to the measurements. For a DLS measurement, the time correlation function of the scattering intensity $G_2(t)$ is defined as $G_2(t) = I(t)\, I(t + \Delta t)$, where

$I(t)$ is the intensity at time t and Δt is the lag time, and the inverse Laplace transform of REPES in the Gendist software package was used to analyze time correlation functions. Thus, the translational diffusion coefficient D of the particle can be determined from the slope of Γ versus q^2, and the apparent hydrodynamic radius R_h was then determined from the Stokes-Einstein equation:

$$R_h = \frac{kT}{6\pi\eta D} = \frac{kTq^2}{6\pi\eta\Gamma} \qquad (1)$$

where k is the Boltzmann constant, η is the solvent viscosity, D is the translational diffusion coefficient, Γ is the decay rate, and q is the scattering vector ($q = 4\pi n \sin(\theta/2)/\lambda$, where n is the refractive index of solvent, θ is the scattering angle, and λ is the wavelength of the incident laser light in vacuum).

4.3 Results and Discussion

4.3.1 ITC results for the binding CTAB to poly(MEO_2MA-*co*-$PEGMA_{2080}$)

Isothermal titration calorimetry has been widely used to study the interactions of many polymer/surfactant systems since it is among one the most sensitive technique for monitoring changes in the differential enthalpy during the binding process. [Bonnaud, Weiss and McClements, 2010; Courtois and Berret, 2010; Fechner, Kosmella and Koetz, 2010] In this study, 20 mM CTAB stock solution was titrated into 0.05, 0.1, and 0.2 wt% copolymer solutions, and the enthalpy profiles at 25.0 and 30.0 °C were plotted in Figures 4.1(a) and 4.1(b), respectively. In Figure 4.1(a), it is obvious that the three titration curves possessed similar trends, but they deviated from the CTAB/water dilution curve (open circle). This difference is attributed to the binding interactions between surfactant and the copolymer. At low surfactant concentration, the enthalpy (ΔH) with large positive values indicated an endothermic process, which corresponded

to the hydrophobic interaction between the alkyl chain of surfactant and hydrophobic backbone of the copolymer. [Li et al., 2001] ΔH then decreased rapidly with increasing CTAB concentration, approaching a minimum that signifies the binding of CTAB molecules to the

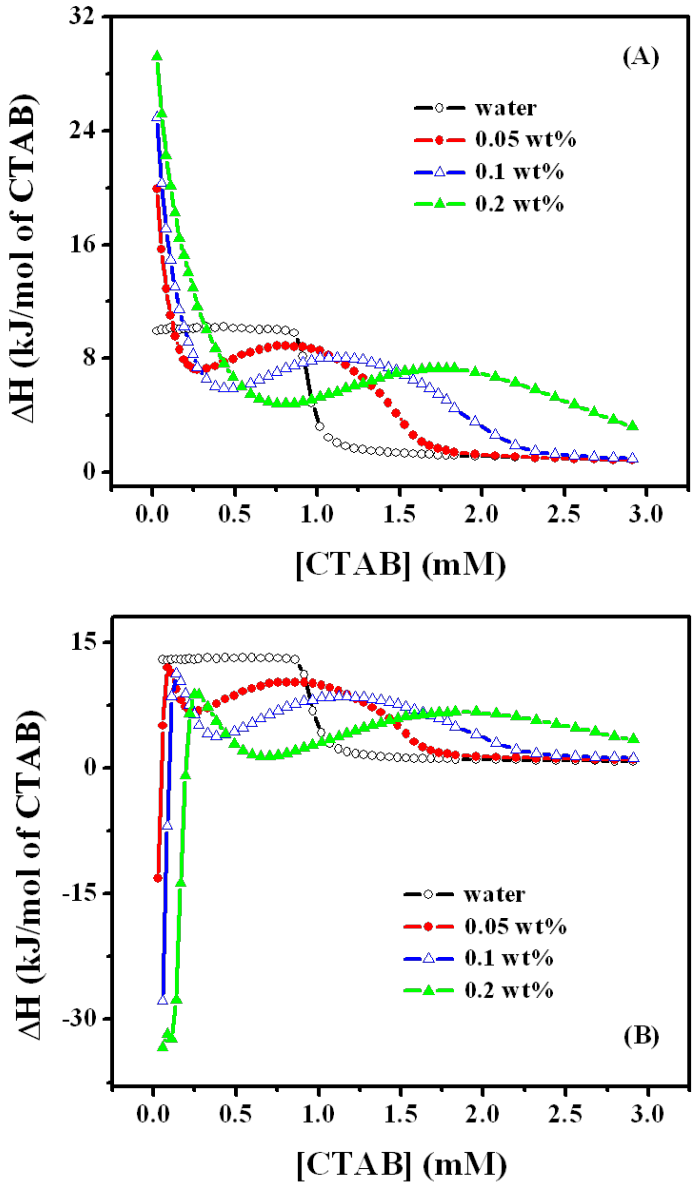

Figure 4.1 ITC curves for titrating 20 mM CTAB into different concentrations of poly(MEO_2MA-*co*-$PEGMA_{2080}$) aqueous solutions at 25.0 °C (a) and 30.0 °C (b).

hydrophobic ethyl methacrylate domains. Beyond this, a very broad endothermic peak at higher CTAB concentrations was observed, which is possibly related to the hydrophobic association of bulk CTAB molecules with the polymer-bound CTAB molecules and formation of CTAB micelles on hydrophobic moieties of the polymer. Finally, at much higher CTAB concentration, the titration curves merged with the CTAB dilution curve, signifying the saturation of the polymer chains with CTAB micelles and the formation of free surfactant micelles after the critical saturation concentration C_2. In this concentration range, the polymer chains/surfactant complexes displayed the properties of a cationic polyelectrolyte. As indicated in Figure 4.1(a), C_2 was dependent on the polymer concentrations, i.e. their values increased with polymer concentrations. This is reasonable as more surfactants are needed to saturate the larger amounts of hydrophobic domains at higher polymer concentrations, which is in accordance to previous observations. [Wang and Olofsson, 1998; Dai and Tam, 2004] A summary of CMC and C_2 for CTAB at different titration conditions is shown in Table 4.1. [Note: C_2 for 0.2 wt% titration curve was not obtained for the present study, because we used a 20 mM CTAB stock solution to yield more data points at the low CTAB concentration region]. However, we expected the C_2 values to be larger than those obtained for 0.05 and 0.1 wt% solutions, which was later confirmed by EMF measurements.

Table 4.1 A summary of CMC and C_2 for CTAB at different conditions obtained from ITC and EMF measurements.

	T (°C)	CMC (mM)	C_2 (mM)		
			0.05 wt%	0.1 wt%	0.2 wt%
ITC	25	0.97	1.73	2.32	--
	30	0.97	1.73	2.32	--
EMF	25	0.94	1.47	2.07	3.03
	30	0.94	1.47	2.07	3.03

The titration curves of CTAB to polymer solutions and its dilution curve at 30.0 °C are presented in Figure 4.1(b). The CMC was determined to be 0.97 mM from the first-order differential curve and equaled to the CMC of CTAB at 25.0 °C. The CMC values are in accordance to those reported in the literature, [Beyer, Leine and Blume, 2006], which indicated that temperature has negligible impact on the CMC in this narrow temperature range. However, the titration curves showed significant divergence with a large negative ΔH values at low CTAB concentration compared to the positive enthalpies observed at 25.0 °C, signifying that the binding process is exothermic. ΔH increased significantly with increasing CTAB concentration, and beyond 0.2-0.5 mM CTAB it exhibited a similar trend to that observed at 25.0 °C (Figure 4.1(a)). This phenomenon is somewhat surprising, but it can be understood by considering the different polymer chain conformation below and above the cloud point of the polymer. Since the temperature exceeded the C_p (27.0 °C) of the copolymer, the polymer chains collapsed to form a compact globular structure induced by intermolecular association of hydrophobic functionalities. The addition of surfactants promoted strong binding between surfactant alkyl tails and polymer aggregates induced by hydrophobic interactions. As more CTAB molecules are absorbed, the enhanced electrostatic repulsion between surfactant ionic head groups exceeded the hydrophobic interactions, leading to the disruption of the aggregates to yield an expanded polymer chains. [Chee et al., 2011] After the dissociation of the polymer chains, the interactions proceeded in a fashion that were identical to that observed at 25.0 °C as signified by the identical profiles of the titration curves as evident in Figures 4.1(a) and 4.1(b) for CTAB concentrations greater than 0.5 mM. Based on the above results, we believe that the exothermic process of the titration curve at 30.0 °C for CTAB concentration less than 0.25 mM is attributed to the heat released from the surfactant binding and disassociation of the insoluble chains resulting in the globule-to-coil

conformational transition of the polymer chains. This observation is consistent with the reverse process for the coil-to-globule conformational transition that was reported to be an endothermic process. [Yao and Tam, 2012] Furthermore, we also observed the values of C_2 measured at 30.0 °C were identical to those obtained at 25.0 °C, as at higher surfactant concentration, the polymer chain conformation with bound surfactant monomers was identical.

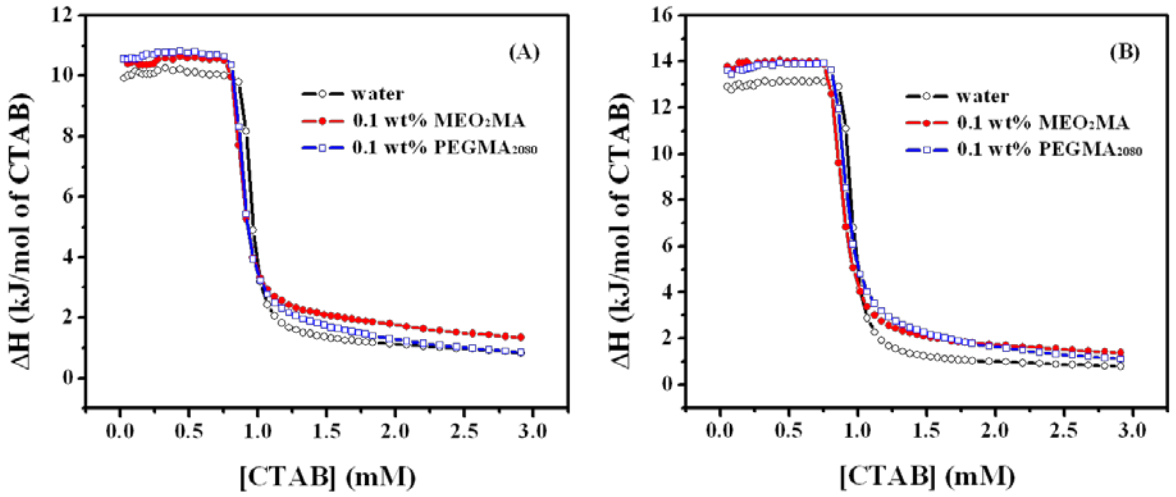

Figure 4.2 ITC curves for titrating 20 mM CTAB into 0.1 wt% monomer MEO_2MA and $PEGMA_{2080}$ aqueous solutions at 25.0 °C (a) and 30.0 °C (b).

In order to further elucidate the nature of binding sites on the polymer chains, we examined the energetics on the interactions between CTAB surfactant and the two respective monomers, i.e. MEO_2MA and $PEGMA_{2080}$ that were used to produce the polymer reported above. The ITC curves for the titration of 20 mM CTAB into 0.1 wt% MEO_2MA and $PEGMA_{2080}$ solutions at both 25.0 and 30.0 °C are shown in Figure 4.2 together with the dilution curve of CTAB in aqueous solution. The titration curves of CTAB to monomer solutions were identical to the CTAB dilution curves at 25.0 and 30.0 °C, respectively, confirming that no or negligible interactions were observed. While the ΔH values for CTAB/monomer systems were slightly

larger than CTAB/water, this small deviation can be attributed to small changes in the solvent environment due to presence of the monomer. Based on these results, we believe that the binding interactions occurred on the hydrophobic backbone of the polymer.

4.3.2 EMF results of binding CTAB to poly(MEO_2MA-*co*-$PEGMA_{2080}$)

The EMF study is another useful and efficient technique to quantify the surfactant-polymer binding by monitoring the monomer concentration of surfactant in solution. [Li, Ma and Hao, 2012] In this study, 20 mM CTAB stock solution was titrated into 20 mL of 0.05, 0.1, and 0.2 wt% copolymer solutions at 25 and 30 °C and the EMFs were measured and plotted as a function of total CTAB concentration (shown in Figure 4.3). Figure 4.3(a) compares the dependence of EMF on CTAB concentrations at 25 °C in the absence and presence of copolymer. In the absence of copolymer, the CMC of CTAB was determined from the EMF calibration curve (open circle), which agreed with the value determined from ITC (shown in Table 4.1). In the presence of copolymer, the EMF deviated from the calibration curve with the first injection of CTAB, indicating the binding of CTAB onto the neutral copolymer as the corresponding free surfactants are lower in bulk solution. Due to the higher hydrophobicity of the polymer, CTAB molecules bind uncooperatively to the polymer at extremely low CTAB concentration, therefore we did not observe the critical aggregation concentration (CAC), and the CTAB monomers bound to the polymer chains as dimers, trimers and small aggregates. [Wang, Tam and Tan, 2004] Uncooperative binding leading to the deviation of the EMF curves at low surfactant concentration were reported for the binding of ionic surfactants to oppositely charged polyelectrolytes [Wang, Tam and Tan, 2004] and hydrophobically modified polymers. [Li et al., 2001; Dai et al., 2004] These EMF results corroborated with the ITC results, where the larger ΔH values at low CTAB concentration are attributed to strong hydrophobic binding interactions.

With increasing CTAB concentration, the EMF curves exhibited an inflection at high CTAB concentration (C_2), denoting the saturation of binding on polymer chains and the formation of free micelles in solution. The C_2 values obtained from EMF measurements were in agreement with the trends observed from the ITC data. In addition, the effects of polymer concentration on the binding behavior were investigated by examining the behavior in 0.05, 0.1, and 0.2 wt% polymer solutions. In Figure 4.3(a), all the three EMF curves deviated from the CTAB/water curve before their inflection points due to the hydrophobic binding. At low CTAB concentration of less than 0.05 mM, the three curves merged, suggesting that concentration effects were negligible at these low concentrations of CTAB. At higher surfactant concentration, more significant deviations from the CTAB/water curve were observed for polymer solutions with high concentration due to the large amount of binding sites on the polymer chains. Finally, as expected, all the binding curves in the presence of polymer merged with the calibration curve as all polymer chains were fully bound by surfactants micelles, and the corresponding surfactant saturation concentration (C_2) increased with increasing polymer concentration. As aforementioned, the EMF measurements for the same polymer solutions were also conducted at 30 °C, which is above the C_p of the polymer in aqueous solution, and the results were plotted in Figure 4.3(b). In comparison to those binding curves at 25 °C, the results at 30 °C showed similar trend as all binding curves displayed a dramatic deviation from the calibration curve, and the deviation is more significant for polymer solutions with higher concentration. However, we observed that the three binding curves were separated at low CTAB concentration instead of overlapping at 25 °C, which could be due to the changes in the polymer chain conformation at high temperature. Above its C_p, the polymer structure became more hydrophobic and even much easier to bind with surfactant molecules due to the hydrophobic interactions. Therefore, even at

low CTAB concentration region, the hydrophobic binding was much more pronounced than those observed at 25 °C.

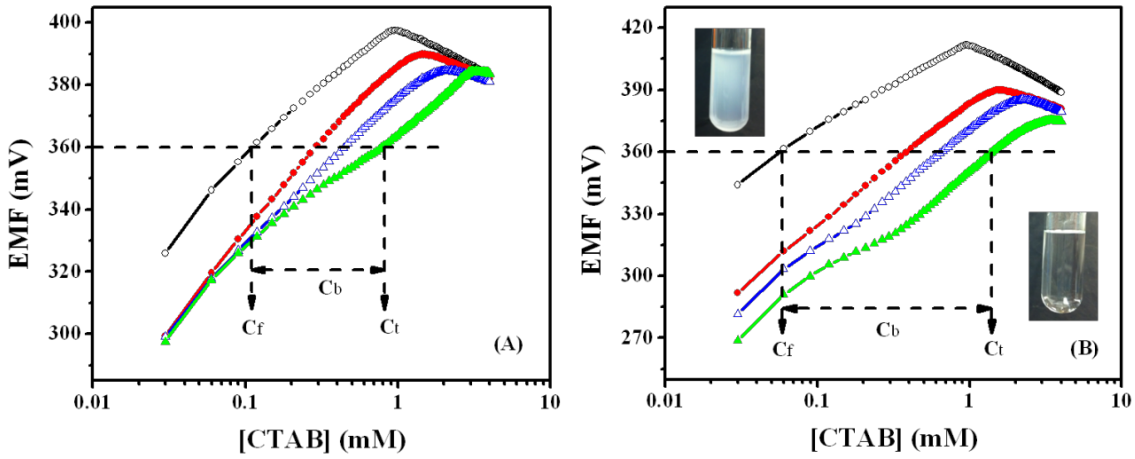

Figure 4.3 EMF curves for titrating 20 mM CTAB into water (—○—), 0.05 (—●—), 0.1 (—△—) and 0.2 (—▲—) wt% of poly(MEO_2MA-*co*-$PEGMA_{2080}$) aqueous solutions at 25.0 °C (a) and 30.0 °C (b). The insets of (b) are the optical pictures of 0.1 wt% polymer aqueous solution before and after adding CTAB at 30.0 °C.

By comparing the EMF data of binding curve and calibration curve, the concentration of polymer-bound surfactant (C_b) can be determined, i.e. the offset between the total surfactant concentration (C_t) and the corresponding free surfactant monomer concentration (C_f), and an example of C_b determination was shown in Figure 4.3(a) and 4.3(b), respectively. Hence, the average values of C_b per gram polymer ($\beta = C_b/C_{polymer}$) can be calculated, and typical binding isotherms showing β versus C_f in the binding region are plotted in Figure 4.4. As expected, it is clearly shown that the β values increased with C_f in the binding region for all polymer concentrations at both 25.0 and 30.0 °C, and the trends became more dramatic at high surfactant concentration, which is in good agreement with the previous results involving ligands binding to macromolecules. [Ghoreishi et al., 1999a, 1999b; Mészáros, Varga and Gilányi, 2005; Rafati and

Ghasemian, 2009] Moreover, we found that the three binding isotherm curves of different concentrations (0.05, 0.1 and 0.2 wt%) overlapped at a certain temperature, suggesting the polymer concentration has no impact on the amount of polymer-bound surfactant, which depends on the polymer dinstinct properties and binding conditions. [Ghoreishi et al., 1999b; Mészáros, Varga and Gilányi, 2005] However, the binding isotherm curves are influenced by temperature, where the interaction at 30.0 °C was initiated at lower surfactant concentration than at 25.0 °C, implying stronger binding affinity at higher temperature, which is due to the changes in polymer conformation. At higher temperature, the polymer chain changes its conformation to a compact globule and forms aggregates with higher hydrophobicity, resulting in the increase of binding affinity. [Rafati and Ghasemian, 2009] However, as more and more surfactant molecules were bound on polymer chains, strong electrostatic repulsion between the bound surfactant ionic heads resulted in the de-compaction of polymer structure, and the polymer chains became less hydrophobic and the binding behaviors became similar to those at 25.0 °C. The C_2 values obtained at these two temperatures were identical, because the amount of hydrophobic binding sites on the polymer chains were similar.

Apparently, all the polymer solutions were transparent at 25.0 °C before and after the addition of surfactant into polymer solution, since the polymer was soluble in aqueous solution below the cloud point. However, at 30.0 °C, the polymer solution became clear when CTAB was titrated into the cloudy polymer solution. As shown in the inset on the top left of Figure 4.3(b), the polymer solution was cloudy when no or minute quantities of CTAB monomers were present. When CTAB was added to the polymer solution, the surfactant monomers bind to the polymer chain via hydrophobic interaction making the polymer chains cationic, which enhances the electrostatic repulsion between polymer-bound surfactant complexes leading to the

disassociation of polymer aggregates. The solution became transparent resulting in a large reduction in the scattering intensity as was confirmed by DLS measurements.

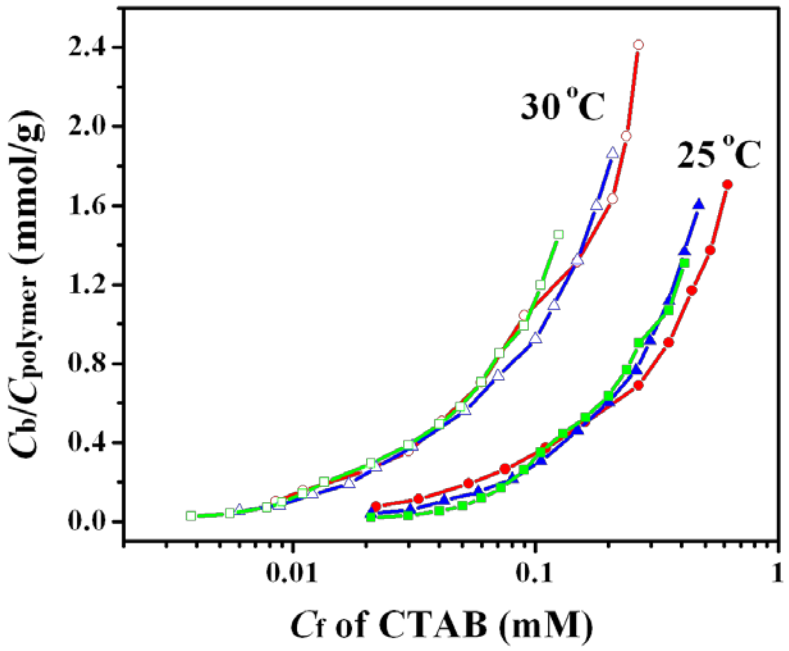

Figure 4.4 Binding isotherms of $C_b/C_{polymer}$ as a function of free CTAB concentration (C_f) for poly(MEO_2MA-*co*-$PEGMA_{2080}$) aqueous solutions at 25 and 30 °C. (Polymer concentrations: circle 0.05 wt%; triangle 0.1 wt%; square 0.2 wt%).

4.3.3 DLS results on the binding CTAB monomers to the copolymer

Dynamic light scattering is widely used to characterize the conformation of surfactant and polymer complexes during the binding process. In this study, the apparent hydrodynamic radii (R_h) of polymer/surfactant complexes were determined from the DLS measurements as a function of surfactant concentration at both 25.0 and 30.0 °C (Figure 4.5). All measurements were repeated three times. Evidently, the R_h value of 0.1 wt% poly(MEO_2MA-*co*-$PEGMA_{2080}$) aqueous solution was about 5.0 nm, and remained relatively constant over the entire surfactant

concentration range at 25.0 °C, suggesting that the polymer chains were solubilized in water below the cloud point. The DLS data confirmed the coil conformation of polymer chains, which expanded slightly when surfactant molecules complexed with the polymer chains due to the repulsive force between the polymer-bound surfactant charged groups. [Barbosa et al., 2006] However, the particle sizes of surfactant/polymer complexes at 30.0 °C displayed significant difference compared to the system at 25.0 °C. In the absence of surfactant, the R_h of 0.02 wt% poly(MEO_2MA-*co*-$PEGMA_{2080}$) aqueous solution was about 82 nm due to the aggregation of the polymer chains. As surfactant was added to the polymer solution, R_h value increased to a maximum of approximately 120 nm, and then decreased to a stable value of 5 nm at CTAB concentration greater than 0.05 mM. The particle size data correlated with the results from both the ITC and EMF measurements.

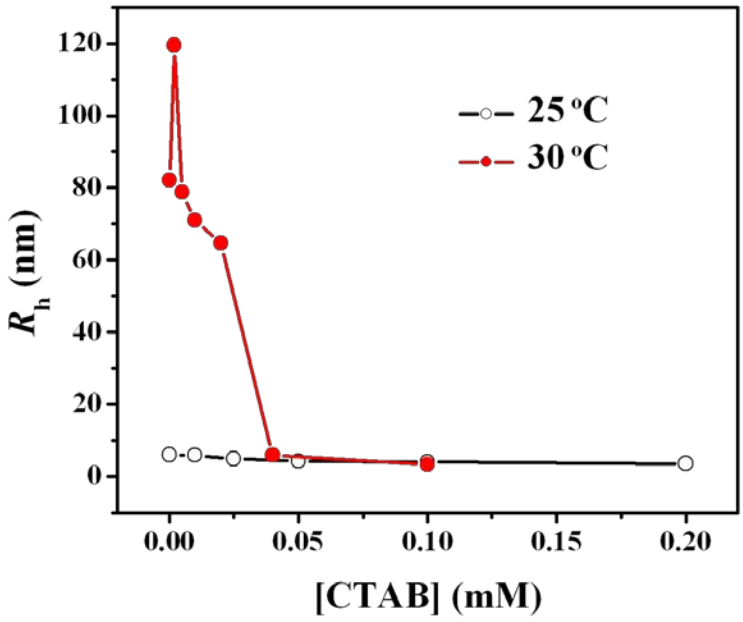

Figure 4.5 The apparent hydrodynamic radius (R_h) of polymer/surfactant complexes as a function of CTAB concentration at 25.0 and 30.0 °C, respectively.

Mechanistically, the surfactant molecules bind uncooperatively to the polymer aggregates at very low surfactant concentration, and the electrostatic repulsion expands the polymer aggregates (size increase from 82 to 120 nm), and further increase in CTAB content induces the dissociation of the aggregates. [Hsu et al., 2006] The enhanced repulsive forces induced the disassociation of polymer aggregates due to the formation of charged polymer chains that mimics the property of as cationic polyelectrolyte. [Mya, Jamieson and Sirivat, 2000; Barbosa et al., 2006; Hsu et al., 2006] This phenomenon is correlated by the visual observation, where the cloudy polymer solution at 30.0 °C became clear with the addition of cationic surfactant (shown in the inset of Figure 4.3(b)).

4.3.4 Effect of surfactant hydrophobicity on the binding interaction

In order to study the effect of surfactant hydrophobicity on the binding interactions between neutral polymer and cationic surfactants, two cationic surfactants with lower hydrophobicity compared to CTAB ($C_{16}H_{33}(CH_3)_3N^+Cl^-$), namely, tetradecyltrimethylammonium bromide (TTAB-$C_{14}H_{29}(CH_3)_3N^+Cl^-$) and dodecytrimethylammonium bromides (DoTAB-$C_{12}H_{25}(CH_3)_3N^+Cl^-$) were examined. The enthalpy profiles for titrating 100 mM TTAB and 200 mM DoTAB stock solution into 0.05, 0.1, and 0.2 wt% copolymer solutions at 25.0 and 30.0 °C are shown in Figure 4.6, respectively. The CMCs of TTAB and DoTAB agreed with previous literature data, and were not significantly affected by temperature. [Wang and Olofsson, 1998; Stodghill, Smith and O'Haver, 2004] The titration curves of TTAB and DoTAB at 25.0 °C are shown in Figure 4.6(a) and (c), and the trends of the enthalpy profiles were identical to CTAB at 25.0 °C, confirming that the binding interactions were identical. At low surfactant concentration, the large positive enthalpy (ΔH) values were attributed to the strong hydrophobic binding interaction. Considering the overall enthalpy of interaction with the polymer, CTAB displayed a

larger enthalpy change, followed by TTAB, while DoTAB exhibited much lower values (shown in Table 4.2). [Loh, Teixeira and Lee, 2004; Mata et al., 2006] These values confirmed that the strength of binding interaction followed the sequence; CTAB > TTAB > DoTAB. This sequence of binding affinity could also be confirmed by the saturation concentration (C_2), which is inversely proportional to the carbon chain length of the hydrophobic alkyl group.

Table 4.2 A comparison of maximum Δ*H* at 25.0 °C and minimum Δ*H* 30.0 °C for titrating CTAB, TTAB and DoTAB into polymer solutions.

Enthalpy (Δ*H*) (kJ/mol)	Polymer Conc. (wt%)	CTAB	TTAB	DoTAB
Max. Δ*H* at 25.0°C	0.05	19.9	8.5	2.8
	0.1	24.9	10.8	3.0
	0.2	29.2	14.4	4.2
Min. Δ*H* at 30.0°C	0.05	-13.2	4.4	1.9
	0.1	-27.7	-3.7	-0.3
	0.2	-33.3	-17.7	-4.7

The ITC titration measurements of TTAB and DoTAB were also conducted at 30.0 °C, and the enthalpy profiles are plotted in Figures 4.6(b) and (d). Similar trends to the CTAB at 30.0 °C were observed, which were consistent to the results observed at 25 ^{o}C. A proposed mechanism describing the binding interaction and the associated microstructural evolution is summarized in Figure 4.7. The schematic illustrates the binding interactions for cationic surfactants and thermo-sensitive poly(MEO_2MA-*co*-$PEGMA_{2080}$) below and above the cloud point. At 25 ^{o}C (which is below the LCST), the polymer chain of poly(MEO_2MA-*co*-$PEGMA_{2080}$) dissolves in water as an expanded water swollen structure, and its conformation changes into a surfactant swollen coil structure by addition of surfactants, ascribing to the hydrophobic interaction between the alkyl chain of cationic surfactant and hydrophobic backbone of the copolymer. As more surfactant molecules are bonded, surfactant micelles formed on hydrophobic moieties of the polymer chain,

and the polymer chain/surfactant complexes displayed the properties of a cationic polyelectrolyte. At temperature in excess of the LCST, the addition of surfactant firstly expands the polymer aggregates to form a loose coil due to electrostatic repulsion between bonded surfactant ionic head groups, and finally the conformation of polymer chain changes from a compact globule to an expanded surfactant swollen coil structure as observed at 25.0 °C.

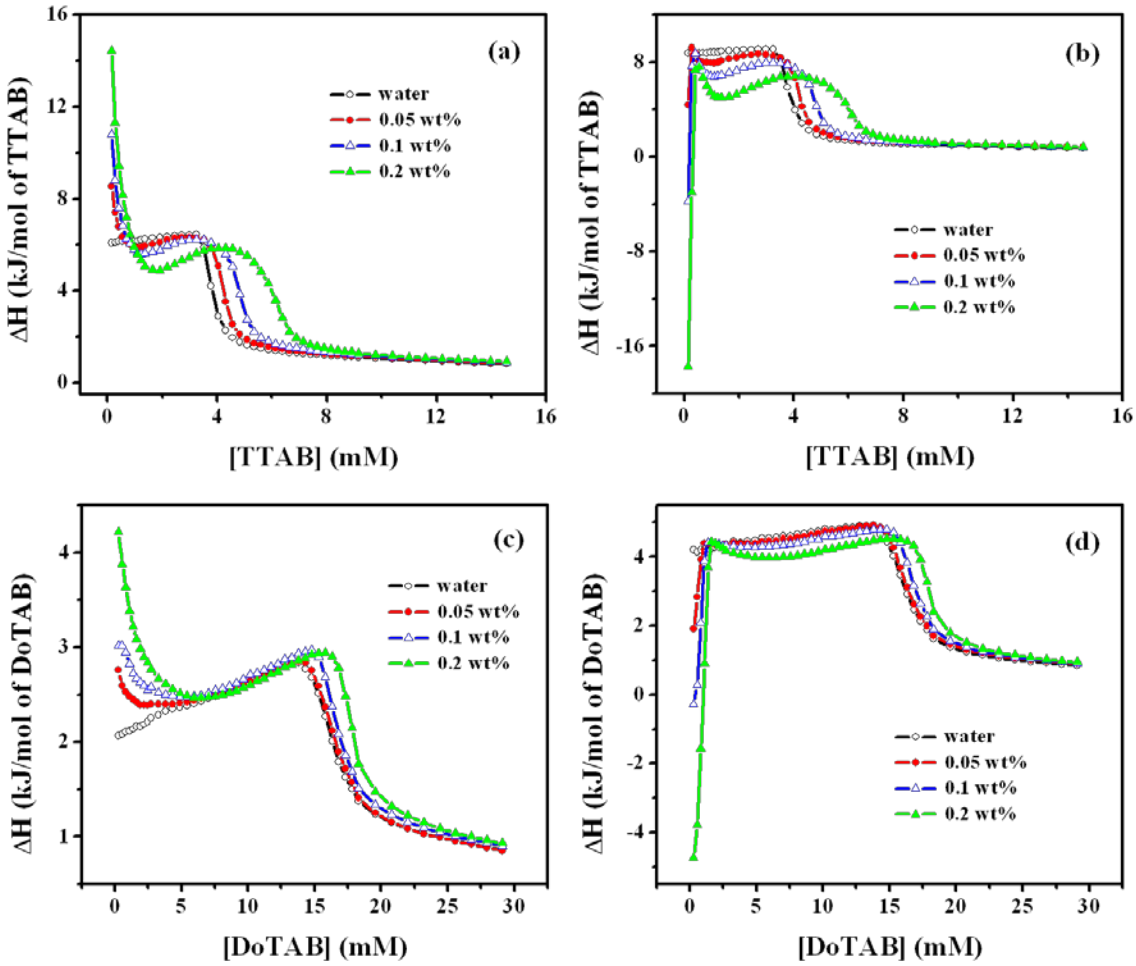

Figure 4.6 ITC curves for titrating 100 mM TTAB and 200 mM DoTAB into different concentrations of poly(MEO_2MA-*co*-$PEGMA_{2080}$) aqueous solutions at 25.0 °C (a, c) and 30.0 °C (b, d), respectively.

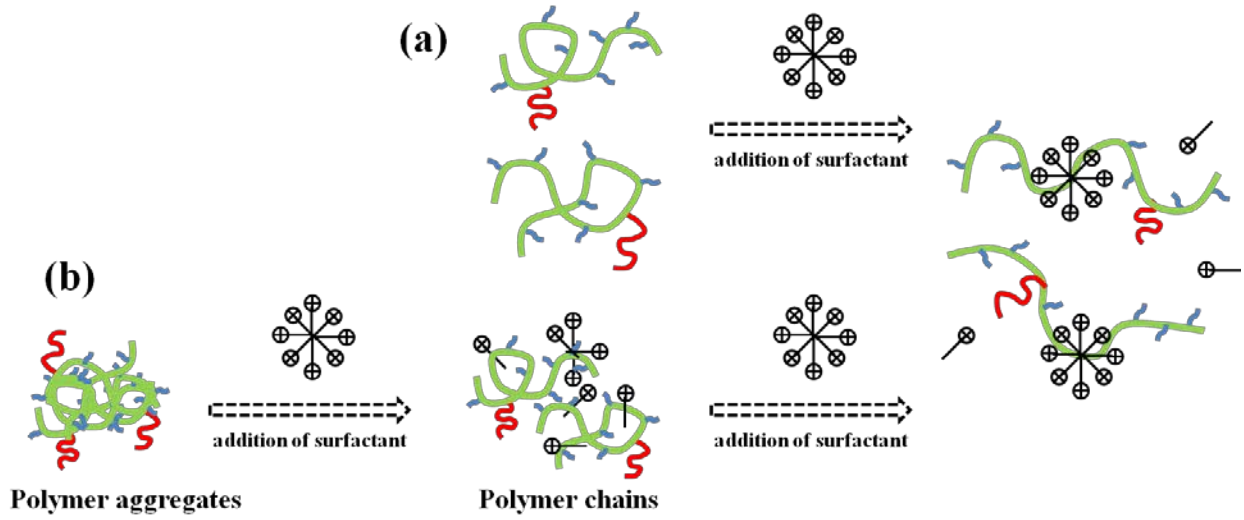

Figure 4.7 Schematic illustration of binding cationic surfactant to thermo-sensitive copolymer below (a) and above (b) its cloud point.

4.4 Conclusions

In this chapter, the binding interactions between cationic surfactants and a statistical thermo-sensitive copolymer based on oligo(ethylene glycol) methacrylates at the temperature below and above its cloud point in aqueous solution were elucidated. By means of ITC, EMF and DLS, we observed significant hydrophobic interactions between cationic surfactants and neutral copolymer, where the binding of surfactant monomers on the polymer backbone is driven by hydrophobic interaction. Below the cloud point, surfactants bind to the individual copolymer chains to form a surfactant-swollen coil, while above the cloud point, surfactants bind to the polymer aggregates that dissociates the aggregate due to the strong electrostatic repulsion between the charged polymer-bound surfactant complexes. The binding between cationic surfactants and the copolymer occurred uncooperatively at low surfactant concentration, as confirmed by surfactant electrode measurements. The surfactant saturation concentration C_2 depended on the polymer concentration and is insensitive to temperature. Moreover, the binding

affinity of the three cationic surfactants in this study follows the sequence: CTAB > TTAB > DoTAB.

Chapter 5 Interactions between Surfactants and Polymer-grafted Cellulose Nanocrystals

5.1 Introduction

Interactions between water-soluble polymers and surfactants in aqueous media have attracted increasing attention in the past decades because of their wide applications in various industrial processes and products, such as in pharmaceutical formulations, rheological control, cosmetic additives and food products. In the polymer/surfactant studies, two critical concentrations are used to describe these interactions i.e. critical aggregation concentration (CAC) and saturation concentration (C_2). The CAC corresponds to the critical surfactant concentration for surfactant-polymer complex formation, while C_2 indicates the saturation of the polymer chains by surfactant molecules. In comparison with CAC and C_2, critical micellization concentration (CMC) is defined as the concentration of the formation of surfactant micelles in the absence of polymer. These critical concentrations can be examined using various instruments, such as ion-selective electrode (ISE), conductometer, isothermal titration calorimeter (ITC), and surface tensiometer. Among these tools, ITC represents the most sensitive technique for studying the binding interactions by monitoring changes in the differential enthalpy. Tam and co-workers [Dai, Tam and Li, 2001; Dai and Tam, 2004; Wang and Tam, 2004] used the ITC to systematically study the interactions between sodium dodecyl sulfate (SDS) and a series of polymers, while McClements and co-workers [Wangsakan, Chinachoti and McClements, 2004; Thongngam and McClements, 2005; Bonnaud, Weiss and McClements, 2010] made important contributions on the elucidation of surfactant/biopolymer interactions via ITC.

Cellulose nanocrystals (CNC) with diameter of 10-20 nm and length of 200-400 nm, derived from native cellulose, is a promising new class of nanomaterials due to its high specific strength, high surface area, unique optical properties, etc. Its attractive physicochemical properties and wide application prospects have attracted significant interest from many industrial and academic researchers. Several reviews on this useful material have been reported. [Habibi, Lucia and Rojas, 2010; Klemm et al., 2011; Eichhorn, 2011; Peng et al., 2011] CNC nanoparticles prepared using sulfuric acid are dispersable in water due to the presence of sulfate groups on CNC surface. Various chemical modifications of CNC were conducted on primary OH groups, such as esterification, [Braun and Dorgan, 2009] cationization, [Hasani et al., 2008] sulfation and carboxylation, [Araki et al., 1999; Habibi, Chanzy and Vignon, 2006] silylation, [Goussé et al., 2002] and polymer grafting. [Morandi, Heath and Thielemans, 2009] Most of these focused on the improvement of its steric stability, dispersability and compatibility in different solvents or matrices. In this study, a commercial cationic polymer (Jeffamine M600) was grafted onto CNC surface via the TEMPO-mediated oxidation and peptidic coupling reaction. This method was first reported in 2001 by Araki et al., [2001] where they grafted poly(ethylene glycol) (PEG) onto cellulose microcrystal to improve its steric stability. Recently two research groups have successfully used this method to modify CNC. [Mangalam, Simonsen and Benight, 2009; Azzam et al., 2010]

Surfactants are used to improve the dispersability of CNC nanoparticles. In 2000, Heux and co-workers introduced their work on the use surfactants to stabilize the cellulose particles in nonpolar solvents. Then Bondeson and Oksman [2007] employed an anionic surfactant to enhance the dispersion of CNC in poly (lactic acid), while non-ionic surfactants were used to disperse CNC particles in polystyrene-based composite fibers as reported by Kim et al. [2009]

and Rojas et al.. [2009] However, studies on the interactions between CNC and surfactants in aqueous media are rare. Since CNC is a low-cost, biodegradable and non-toxic nanomaterial, it could be used as excipient in personal care and pharmaceutical systems, where surfactants play a critical role. Recently, Jackson et al. [2011] reported on the use of CNC and cetyltrimethylammonium bromine (CTAB) for the binding and release of hydrophobic drugs, where the encapsulation and release of drug molecules can be controlled. However, no detailed studies on the interactions of CNC, its derivatives and surfactants have been reported.

In this chapter, an amine-terminated polymer was grafted onto CNC surface. This hydrophilic polymer (consisting of oxypropylene and oxyethylene segments at a ratio of 8 to 1) can enhance the steric stability of CNC particles in aqueous media. FT-IR was used to confirm the amide bond formation between CNC and polymer, while TEM was used to assess the dispersability of CNC and modified CNC samples. The binding interactions between M600-grafted CNC and anionic (SDS), cationic (DoTAB) and non-ionic (Brij 30) surfactants were investigated by ITC.

5.2 Materials and Methods

5.2.1 Materials

Cellulose nanocrystals with an average charge density of 0.26 mmol/g was provided by FPInnovations Canada. All other chemicals were purchased from Sigma-Aldrich, and used as received. The chemicals used in the reaction are: Jeffamine M600, TEMPO reagent, sodium bromide (NaBr), sodium hypochlorite (NaClO), *N*-(3-dimethylaminopropyl)-*N*′-ethylcarbodiimide hydrochloride (EDC), and *N*-hydroxysuccinimide (NHS). The water used was obtained from the Millipore-Q water purification system, which has a resistivity of 18.2 MΩ·cm. The chemical structures of SDS, DoTAB and Brij 30 are shown as below in Scheme 5.1.

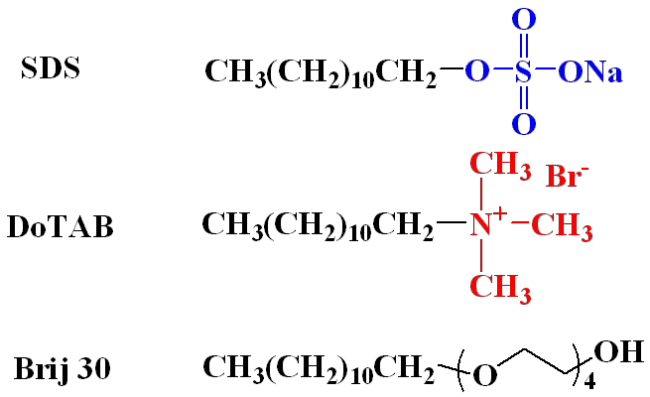

Scheme 5.1 Chemical structures of surfactants: SDS, DoTAB and Brij 30.

5.2.2 Preparation of Jeffamine M600-grafted CNC

The M600-grafted CNC was prepared in two steps (shown in Scheme 5.2): (1) TEMPO-mediated oxidation of CNC and (2) grafting of amine-terminated Jeffamine M600 to oxidized CNC. The oxidation experiments were performed using the reported protocol with some minor modifications. [Saito and Isogai, 2004] In a typical run, 200 mL of a 1.0 wt% CNC suspension was mixed with 150 mg TEMPO and 400 mg NaBr, and slowly stirred for 1h. Then 5 mL of 10-15% sodium hypochlorite solution (NaClO) was added dropwise to initiate the oxidation reaction. The mixture was stirred overnight under room temperature with pH adjusted to 10 using 0.5M NaOH. The oxidized CNC particles were washed with 0.5M HCl and NaCl solution, and then dialyzed against Millipore-Q water. A well-dispersed colloidal suspension was recovered after the dialysis.

Grafting of Jeffamine M600 onto CNC was achieved via the EDC/NHS reaction according to Bulpitt and Aeschlimann. [1999] A desired amount of Jeffamine M600 solution was added dropwise to 100 mL of 1.0 wt% carboxylated CNC suspension and stirred until dissolution. The pH of the mixture was adjusted to 7.5 – 8.0 using either 0.5M NaOH or 0.5M HCl, and then 2 mL of EDC/NHS (ratio of 2: 1) was added to the mixture. The reaction proceeded overnight at

room temperature with the pH of the mixture kept at 7.5 – 8.0. The reacted mixture was adjusted to pH of 1 using HCl and dialyzed against Millipore water (M_w cut-off 12,000-14,000) to remove un-reacted reagents, and the pH of the final solution was neutral (about 7.5). These two reactions were confirmed by FT-IR analysis of freeze-dried CNC product in KBr pellets.

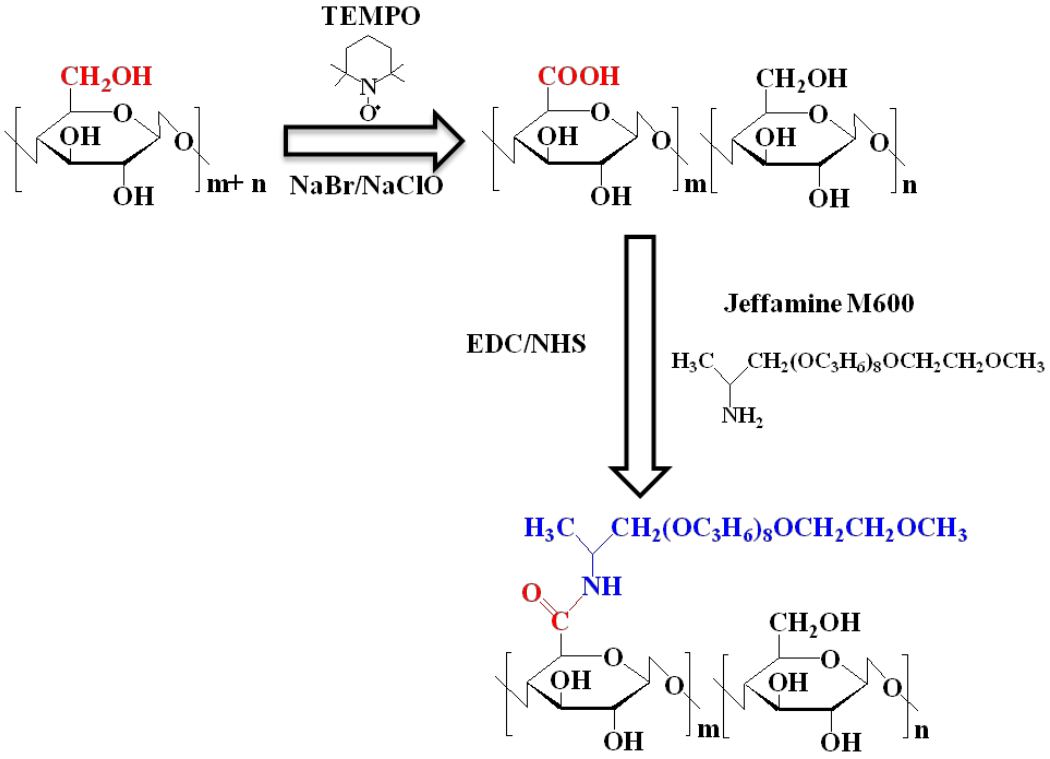

Scheme 5.2 The reaction route of grafting Jeffamine M600 on the CNC surfaces.

5.2.3 Fourier-transform infrared spectroscopy

The FT-IR spectra were measured at room temperature using a Perkin-Elmer 1720 FT-IR spectrometer with a resolution of 4 cm^{-1}. The freeze-dried cellulose particles, namely CNC, oxidized CNC, and M600-grafted CNC were mixed with KBr respectively, and then compressed to form pellets.

5.2.4 Transmission electron microscopy (TEM)

Transmission electron microscopic studies were performed using a Philips CM10 electron microscopy. The TEM samples were prepared by depositing one drop of 0.005 wt% CNC dispersions onto a carbon coated TEM copper grid, which was placed on a filter paper. The excess liquid was removed by the filter paper and the remaining liquid was allowed to air-dry overnight at room temperature.

5.2.5 Conductometric titrator

The carboxylate contents of oxidized CNC and the extent of grafting were determined by the conductometric titration measurements, which were performed on a Metrohm titrator equipped with a water bath to control temperature. The 40 mL of 0.1 wt% aqueous solutions were adjusted to pH 2.7 with 0.1 M HCl, and then titrated with a 0.05 M NaOH solution under stirring. All the tests were conducted at 25 ^{o}C.

5.2.6 Nuclear magnetic resonance (NMR)

The ^{1}H NMR experiments were carried out on a Bruker AV300 NMR spectrometer operating in the Fourier transform mode. D_2O was used as solvent for all measurements. The ^{1}H NMR spectra of 0.2 wt% M600-CNC, 5mM SDS, as well as the mixtures of 0.2 wt% M600-CNC with 5, 10, and 20 mM SDS were recorded in D_2O. All analyses were performed at 25, 45 and 60 °C.

5.2.7 Isothermal titration calorimetry (ITC)

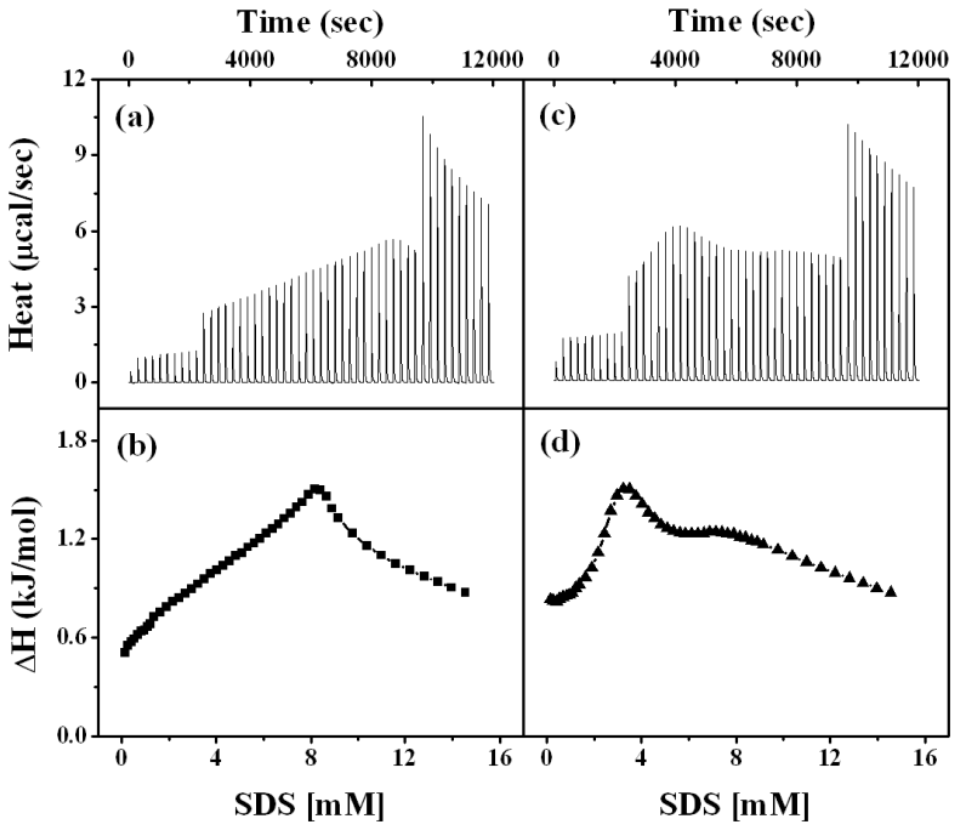

Figure 5.1 Calorimetric titration curves of 100 mM SDS into water (left) and 0.1 wt% M600-grafted CNC (right) at 25 ^{o}C. (a, c) thermogram of raw heats, and (b, d) ITC enthalpy profiles versus real SDS concentration in the sample cell.

The calorimetric data on the binding interactions between surfactants and M600-grafted CNC were obtained using a Microcal VP-ITC calorimeter (Northampton, MA). A detailed description on this power compensated differential calorimetric instrument was previously described. [Wiseman et al., 1989] The microcalorimeter consists of a reference cell and a sample cell of approximately 1.4 mL in volume, and surfactant solution was injected from a 281.72 μL injection syringe into the sample cell filled with either water or CNC suspensions. The syringe is

tailor-made such that the tip acts as a blade-type stirrer to ensure an efficient mixing at 307 rpm. The titration was carried out at 25.0 °C and the sample injections were automatically controlled by an interactive software. In this study, we utilized identical injection protocol, i.e. 2μL for the first 10 injections, 4μL for the next 30 injections, and 10μL for the last 10. The time interval between successive injections was set at 240s. Typical ITC profiles are shown in Figure 5.1 of titrating 100 mM SDS into water at 25 ^{o}C.

5.3 Results and Discussion

5.3.1 Characterization of M600-grafted CNC

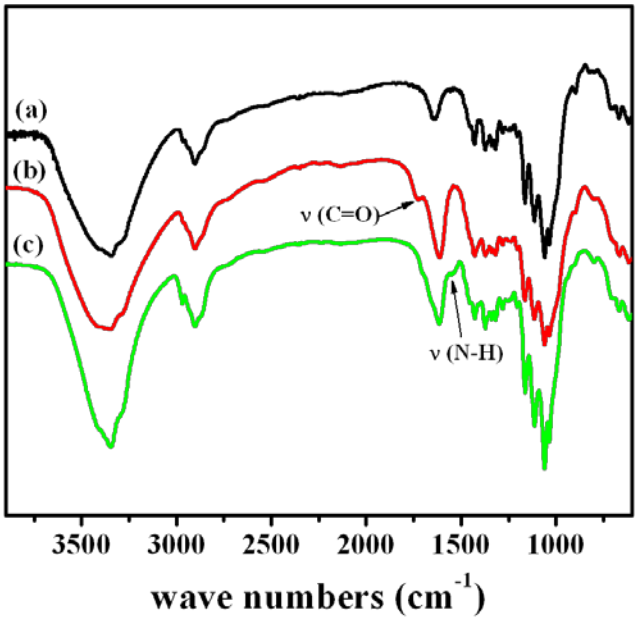

Figure 5.2 FT-IR spectra of (a) cellulose nanocrystals, (b) carboxylated CNC, and (c) M600-grafted CNC.

The grafting of Jeffamine M600 onto CNC surface was confirmed by FT-IR. Figure 5.2 shows the FT-IR spectra of (a) CNC, (b) carboxylated CNC, and (c) M600-grafted CNC. The

spectrum of carboxylated CNC (b) displayed an obvious peak at 1730 cm^{-1} compared to the CNC sample (a). This new peak was assigned to the acidic form of carboxyl groups introduced by the TEMPO-mediated oxidation of primary C_6 hydroxyl groups on CNC surface. [Azzam et al., 2010]

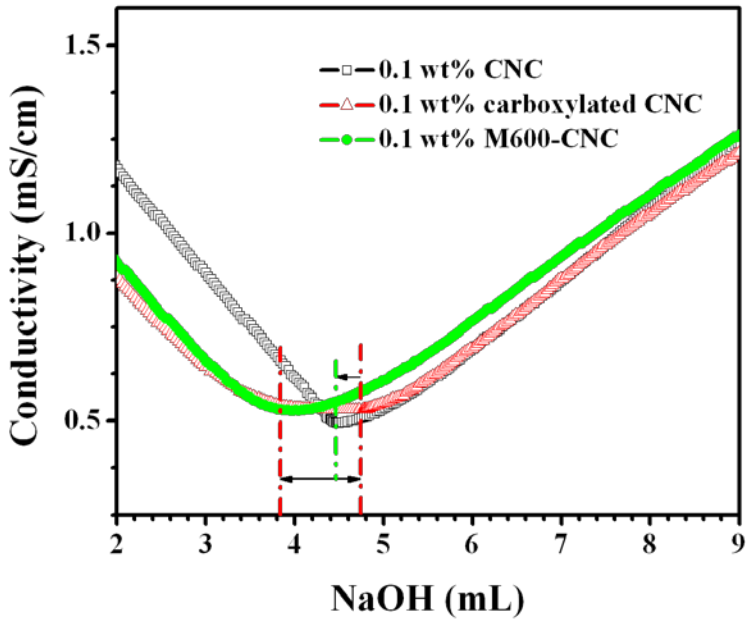

Figure 5.3 Conductometric titration curves of 0.1 wt% of CNC, carboxylated CNC and M600-CNC against 0.05 M NaOH solution.

For the spectrum of M600-grafted CNC, a new peak at 1550 cm^{-1} was observed, which is characteristic of an N-H vibration of the amide bond. Compared to the carboxylated sample, the intensity of 1730 cm^{-1} peak was reduced in Figure 5.2c, suggesting that some of the carboxyl groups have reacted with amine groups of Jeffamine M600. The above analyses from FT-IR spectra supported the formation of covalent amide bond between carboxylated CNC and Jeffamine M600. The density of carboxyl groups on oxidized CNC was calculated to be 1.1

mmol/g based on the conductometric titration results (shown in Figure 5.3), while the extent of grafting was also determined, which is about 0.33 mmol polymers per gram of CNC.

TEM micrographs of CNC and M600-grafted CNC from aqueous dispersion are shown in Figure 5.4, where the CNC and M600-grafted CNC possessed identical size and shape, whose dimensions are in agreement with literature values, i.e. 10 to 20 nm in width and approximately 200 nm in length. [Habibi, Lucia and Rojas, 2010] The CNC rod-like nanoparticles tend to form "bundle-like" aggregates similar to those reported previously, [Orts et al., 1998] while the M600-grafted CNC possessed more individual rod-like nanoparticle with very few aggregates. The better dispersion of the modified CNC can be attributed to the presence of surface grafted M600 chains that generated steric repulsion forces between the nanoparticles. [Azzam et al., 2010]

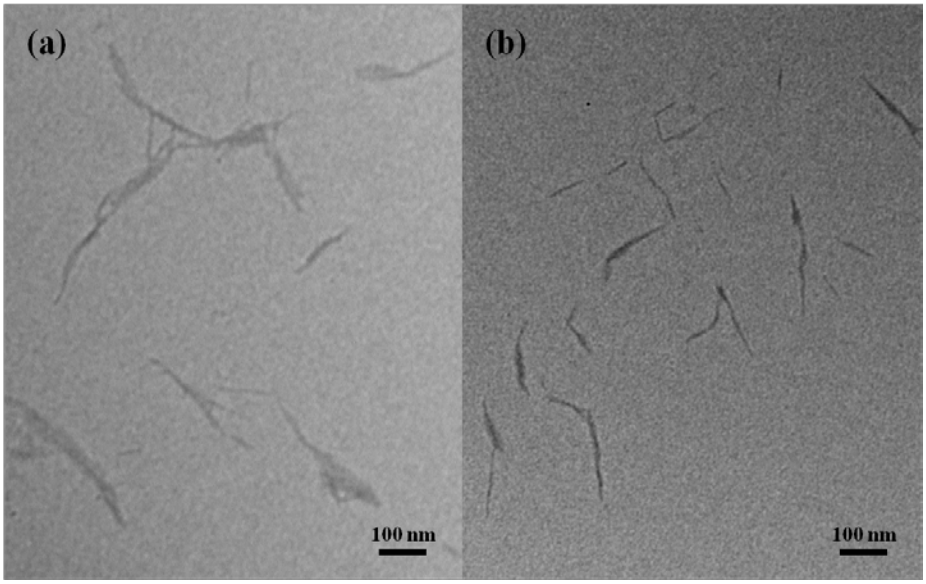

Figure 5.4 TEM images of (a) cellulose nanocrystals, and (b) M600-grafted CNC.

5.3.2 Interactions between M600-grafted CNC and SDS

A typical ITC result for titration of 100 mM SDS into water at 25 ^{o}C is shown in Figure 5.1 (left), which comprises the raw heats (Figure 5.1a) and enthalpy profile (Figure 5.1b) obtained from the integration of each individual peak in Figure 5.1a. The micellar solution of SDS in the

syringe was titrated into water in the sample cell. When the surfactant concentration in the sample cell is lower than the critical micellization concentration (CMC), the SDS micelles will dissociate to produce monomers, and the observed enthalpy contains the heats from surfactant demicellization and dilution of surfactant micelles and monomers. When the concentration of SDS in the sample cell exceeded its CMC, only the surfactant micelle dilution heat was measured. The CMC of SDS was determined from the titration curve to be 8.16 mM, which agreed with literature value. [Dai and Tam, 2004] In the presence of M600-grafted CNC, the enthalpy curve is more complex than SDS dilution process due to onset of polymer/surfactant interactions. At low SDS concentration, SDS molecules bind to oxypropylene segments on M600 chains producing larger endothermic heat compared to the SDS dilution process (shown in Figure 5.1c). When the M600 chains were saturated by SDS micelles at high SDS concentration, only SDS micelle dilution heat was measured.

The calorimetric curves for the titration of 100 mM SDS solution to 0.1 wt% CNC and M600-grafted CNC are plotted in Figure 5.5(a), together with the titration of SDS into water. We observed that the shape of SDS/CNC curve is identical to the SDS/water curve, suggesting that SDS monomers do not bind to CNC. However, at C_{SDS} < CMC, the ΔH values for SDS/CNC system is slightly larger than SDS/water indicating that the presence of CNC slightly alters the solvent environment that has a small effect on the demicellization of SDS micelles. The CMC of SDS in the CNC solution decreased from 8.16 to 7.91 mM due to the electrolyte effect of negative sulfate groups and counterions (Na^+) on CNC surface. The titration curve of SDS to M600-grafted CNC deviated significantly from the SDS/water curve. A distinct endothermic peak was observed at C_{SDS} < CMC followed by a broad shoulder, similar to the results reported previously. [Wang and Olofsson, 1998; Dai, Tam and Li, 2001]

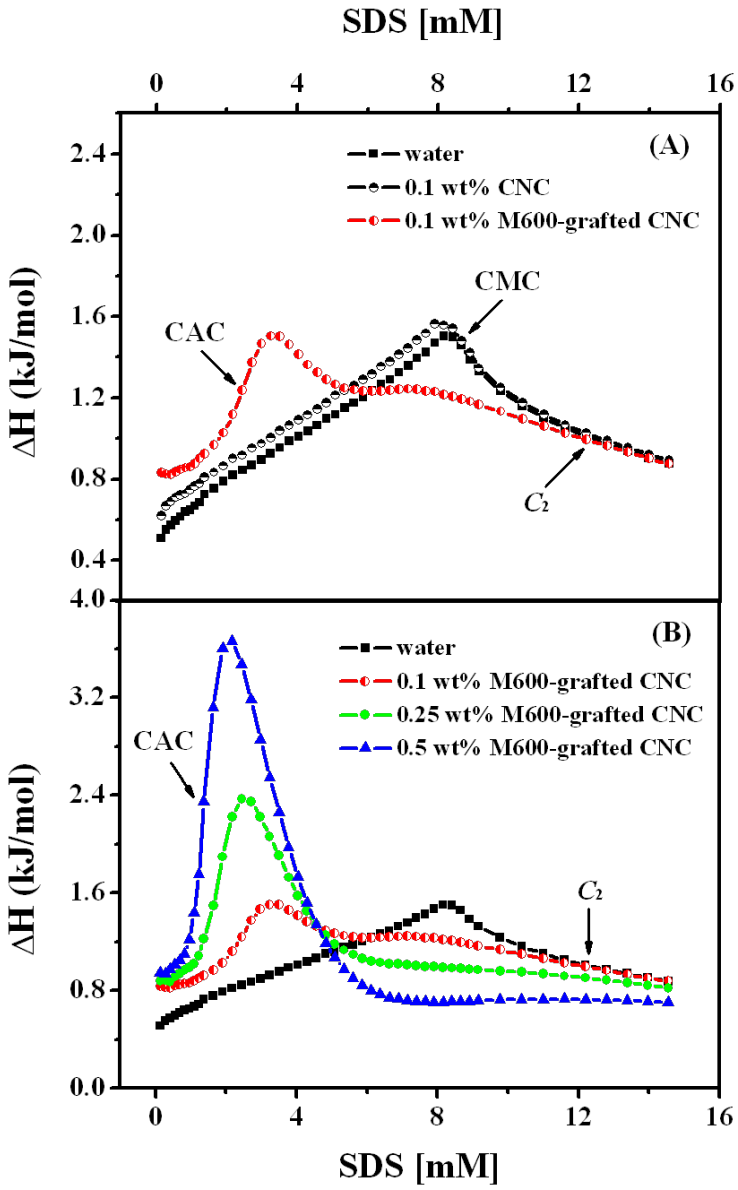

Figure 5.5 (a) Calorimetric titration curves of 100 mM SDS into water, 0.1 wt% CNC suspension, and 0.1 wt% M600-grafted CNC suspensions at 25 ^{o}C. (b) Calorimetric titration curves for titration of 100mM SDS into water and M600-grafted CNC suspensions of various concentrations: 0.1, 0.25, and 0.5 wt% at 25 ^{o}C.

Considering the chain structure of grafted M600 on CNC, the endothermic peak is attributed to the formation of aggregation complexes between SDS and oxypropylene segments on M600

chains. [Dai, Tam and Li, 2001] The onset of binding of SDS monomers to oxypropylene segments is characterized by the critical aggregation concentration (CAC), which is lower than the CMC. A small endothermic "shoulder" (at ~ 8 mM) appeared at a higher SDS concentration, which is related to the formation of SDS micelles on the M600 chains. The titration curve then merged with the SDS dilution curve signifying the saturation of the oxypropylene segments by SDS micelles. We did not observe an exothermic peak corresponding to the re-hydration of polymer chains as reported previously due to the relatively low polymer molecular weight used in this study. [Wang and Olofsson, 1995; Dai and Tam, 2001]

Table 5.1 The CAC, C_2, and thermodynamic parameters from calorimetric titration of 100 mM SDS into 0.1, 0.25, and 0.5 wt% M600-grafted CNC suspensions.

Concentration of M600-grafted CNC	CAC (mM)	C_2 (mM)	ΔH_{agg} (kJ/mol)	ΔG_{agg} (kJ/mol)	$T\Delta S_{agg}$ (kJ/mol)
0.1 wt%	2.44	12.8	0.39	-27.6	28.0
0.25 wt%	1.91	14.6	1.10	-28.7	29.8
0.5 wt%	1.36	--	1.62	-30.3	31.9

The ITC curves for the titration of 100 mM SDS into different concentrations of M600-grafted CNC are shown in Figure 5.5(b). It is evident that the CAC is slightly dependent on polymer concentration, as the CACs for 0.1, 0.25 and 0.5 wt% M600-grafted CNC suspensions are 2.44, 1.91 and 1.36 mM, respectively. The lower CAC corresponds to the earlier onset for the formation of aggregation complexes due to the higher concentration of oxypropylene segments. Furthermore, with the thermodynamic equations derived from the phase separation model, the Gibbs free energy for the formation of polymer/SDS aggregates (ΔG_{agg}) can be described by Equation (1):

$$\Delta G_{agg} = (1 + K)RT \ln(\text{CAC}) \quad (1)$$

where K is the effective micellar charge fraction with a value of 0.85 for SDS. Moreover, the ΔH at CAC comprised of enthalpies contributed by various processes, i.e.: [Meagher, Hatton and Bose, 1998]

$\Delta H = \Delta H$ (dilution of SDS micelles and monomers)

$+ \Delta H$ (demicellization of SDS micelles)

$+ \Delta H$ (binding of SDS monomers to polymer chains) (2)

The measured enthalpy change is mainly attributed to the binding ΔH of SDS/polymer complexes ΔH_{agg}, as the ΔH for the SDS dilution and demicellization is relatively small. Therefore, the entropy ΔS_{agg} can be determined from Equation (3):

$$\Delta G_{agg} = \Delta H_{agg} - T\Delta S_{agg} \quad (3)$$

The values of CAC, ΔG_{agg}, ΔH_{agg}, and ΔS_{agg} for the three M600-grafted CNC samples are summarized in Table 5.1. The thermodynamic parameters suggest that the aggregation process at CAC is an entropically driven process, because ΔH_{agg} is positive, and the Gibbs free energy is dictated by the magnitude of $T\Delta S_{agg}$.

In order to further confirm the binding interaction between SDS and the M600 polymer chains on CNC surface, ^{1}H NMR measurements were conducted on SDS, M600-CNC, and their mixtures. The ^{1}H NMR spectra of 0.2 wt% M600-CNC, 5mM SDS, and their mixtures, i.e. 0.2 wt% M600-CNC with 5, 10, and 20 mM SDS were recorded in D_2O solvent, as shown in Figure 5.6. The peak at 1.04 ppm (Figure 5.6a) was assigned to the $-CH_3$ protons of oxypropylene segments, based on the previous studies, [Ma et al., 2007; Phani Kumar et al., 2011]

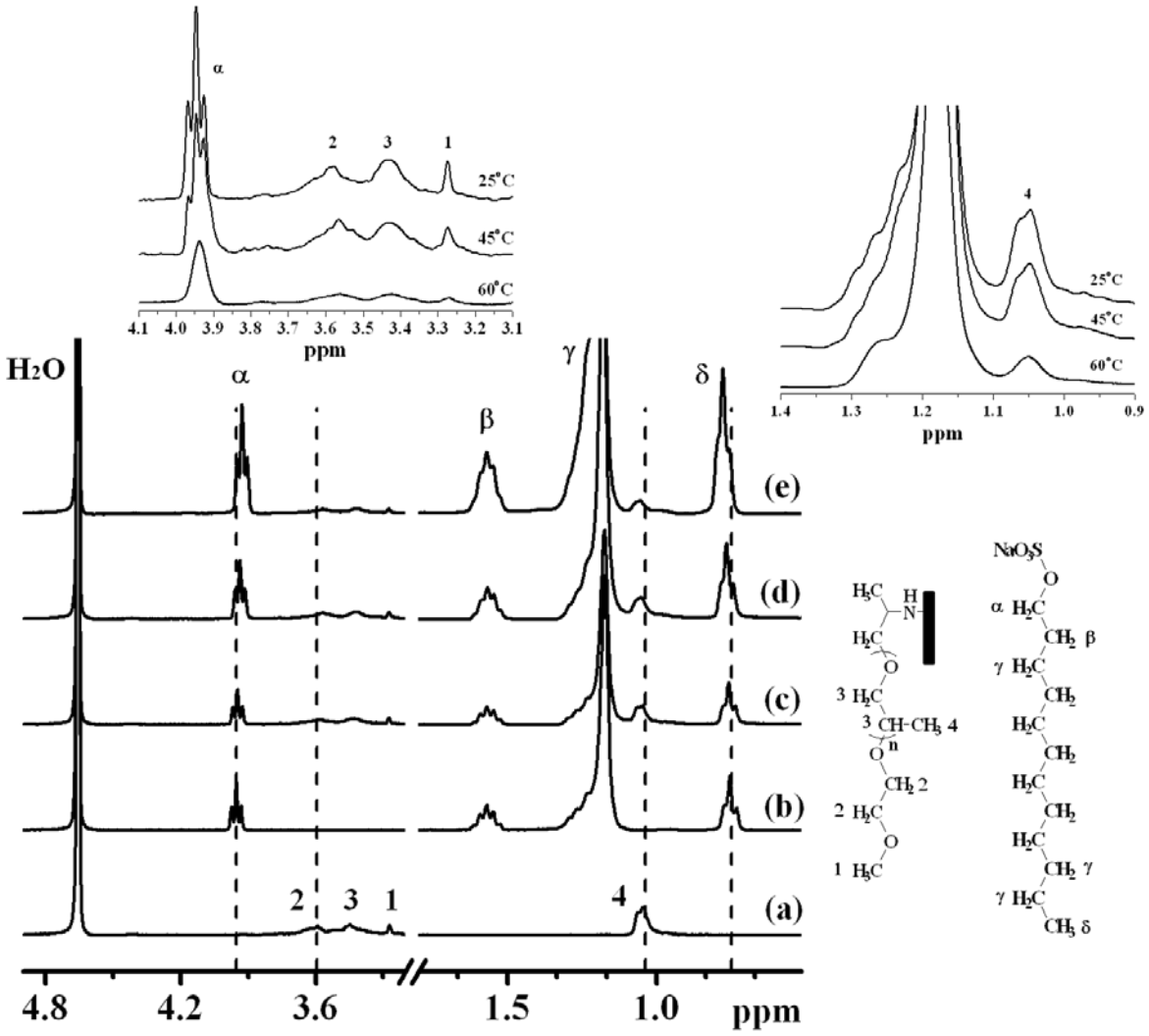

Figure 5.6 ^{1}H NMR spectra of 0.2 wt% M600-CNC (a), 5mM SDS (b), and their mixtures of 0.2 wt% M600-CNC with 5(c), 10(d), and 20 (e) mM SDS in D_2O solvent. The inset shows the ^{1}H NMR spectra of 0.2 wt% M600-grafted CNC with 5 mM SDS in D_2O solvent at 25, 45, and 60 ^{o}C.

and the chemical shift was shifted downfield, from 1.04 (without SDS) to 1.06 ppm in the presence of 20 mM SDS. This is because the microenvironment of polymer segments was altered due to the binding with surfactants, resulting in the change in the chemical shift. [Chen et al.,

2008] On the other hand, as SDS concentration in the mixtures increased from 5 to 20 mM, the chemical shift of $–CH_2$ in the α position near the sulfate group decreased from 3.95 to 3.92 ppm, while the chemical shift of $–CH_3$ in δ position increased from 0.75 to 0.78 ppm. All these results reflect the binding interaction between SDS and M600 polymer chains. The temperature effect on SDS and M600-CNC interactions was studied by ^1H NMR, and the insets of Figure 5.6 (top left and right NMR spectra) show the ^1H NMR spectra of 0.2 wt% M600-grafted CNC with 5 mM SDS in D2O solvent at 25, 45, and 60 ^oC. When the temperature was increased to 60 ^oC, the M600 polymer signals (1–4) undergo apparent broadening due to the reduction in the mobility of most of the oxypropylene segments, and the signal intensity decrease since the polymer chains collapsed and the functional groups were shielded compared to those at low temperatures. The triplets corresponding to α proton of SDS chain at low temperature merged into a singlet at high temperature, ascribing to the enhanced hydration effects of SDS alkyl chain upon heating. [Hsu et al., 2006; Chen et al., 2011]

It is well known that PPGs are thermo-responsive polymeric systems, whose LCST depend on their molecular weights. The LCST for PPG 1 K, 2 K, and 3 K were reported to be 42, 23, and 15.5 ^oC, respectively. [Dai and Tam, 2004] In our study, the M600-CNC system dis-plays a thermo-responsive behavior upon heating. The LCST for this 600 Da polymer was broad and determined to be around 55 ^oC (Figure 5.7), which corresponds to the trend in this refence of [Dai and Tam, 2004]. Above this temperature, the dispersion became cloudy mainly due to the inter-molecule interaction induced by hydrophobic interaction between the dehydrated PPG segments. The dispersion was less turbid at low concentration because the negative charges on the particles surface stabilized the CNC particle and prevented the formation of larger aggregates.

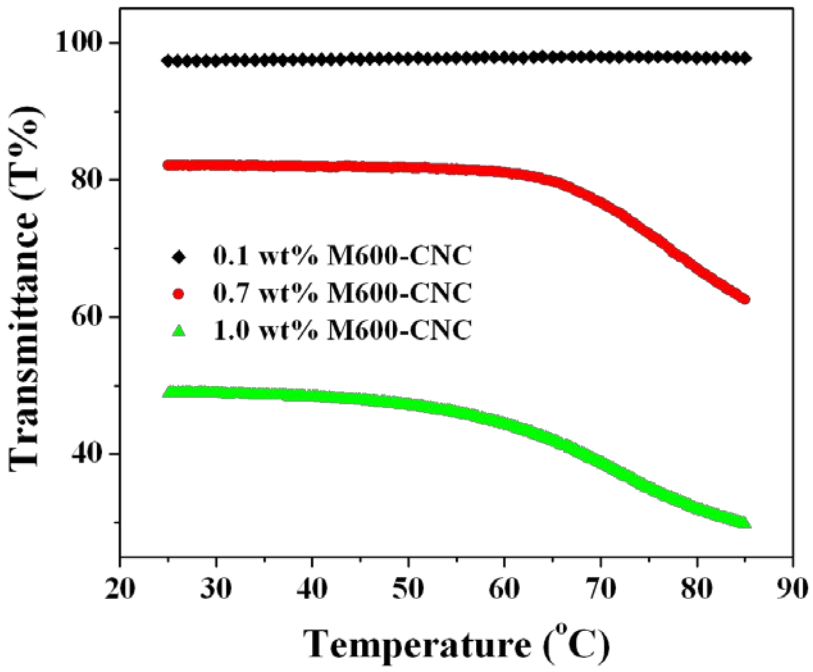

Figure 5.7 Transmittance versus temperature for 0.1, 0.7, and 1.0 wt% M600-CNC aqueous solution at the wavelength of 500 nm.

5.3.3 Interactions between M600-grafted CNC and DoTAB

The calorimetric curves for the titration of 200 mM DoTAB solution into 0.1 wt% CNC and M600-grafted CNC are shown in Figure 5.8(a), together with the dilution curve of DoTAB in water. The DoTAB concentration of 200 mM was chosen to be approximately 12 times the CMC of DoTab at 25 ^{o}C, similar to that used for the titration with SDS solution (i.e. 100 mM). The CMC value of 15.8 mM determined in this study is identical to that reported in the literature. [Guillot et al., 2003]

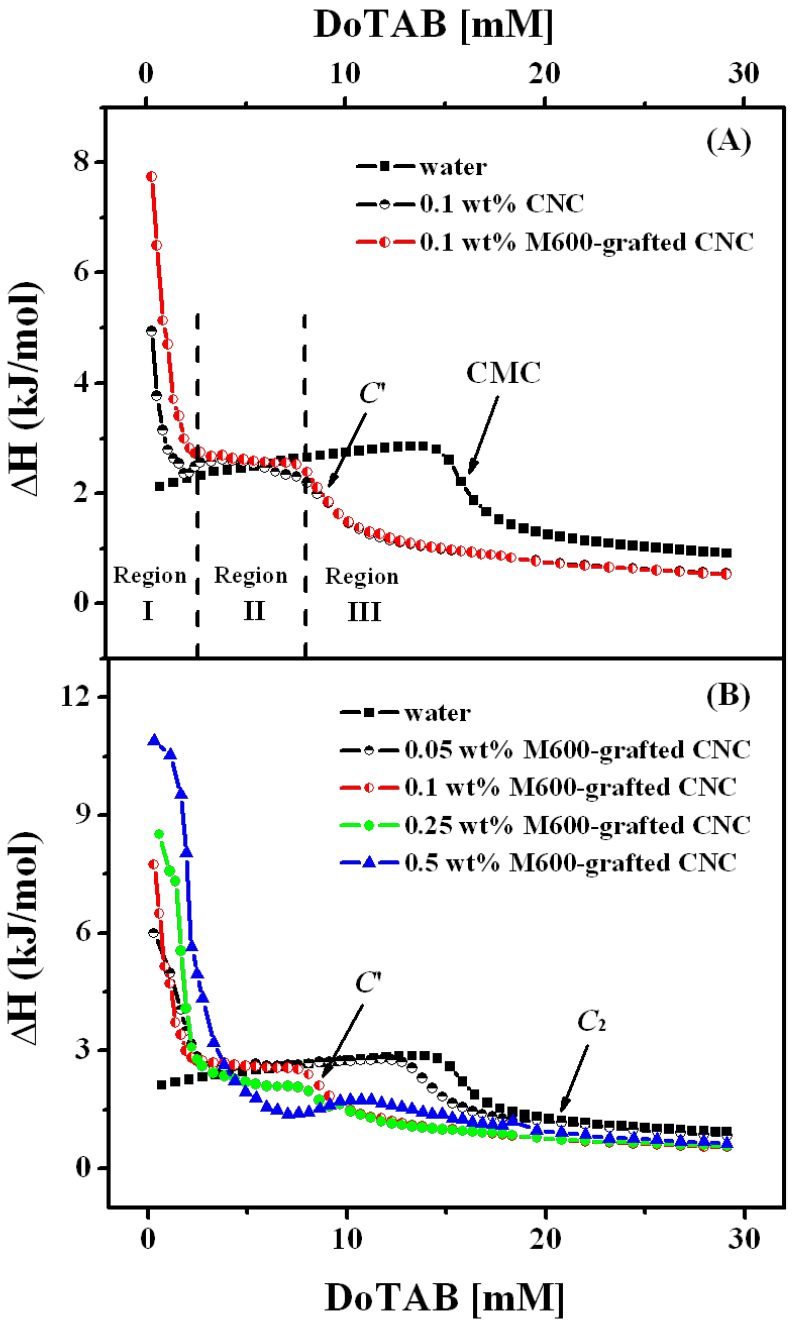

Figure 5.8 (a) Calorimetric titration curves of 200mM DoTAB into water, 0.1 wt% CNC suspension, and 0.1 wt% M600-grafted CNC suspensions at 25 ^{o}C. (b) Calorimetric titration curves for titration of 100mM DoTAB into water and M600-grafted CNC suspensions of various concentrations: 0.05, 0.1, 0.25, and 0.5 wt% at 25 ^{o}C.

The titration curves for DoTAB solution into 0.1 wt% CNC and M600-grafted CNC suspensions are identical, except with some deviation in Region I. In Region I, ΔH decreased rapidly and reached a minimum at DoTAB concentration of ~ 2 mM. Such a trend is attributed to the electrostatic interaction between cationic DoTAB monomers and negative charges on CNC. With increasing surfactant concentration, an increasing proportion of the negative charges become neutralized by DoTAB monomers. [Alila et al., 2005] At low surfactant concentration, the binding enthalpy for DoTAB/M600-grafted CNC system is larger than DoTAB/CNC due to more negative charges on M600-grafted CNC surface produced by the TEMPO oxidative process. In Region II, the two curves merged, where the adsorbed DoTAB monomers on the surface begin to reorganise and associate, induced by hydrophobic interaction between the alkyl chains of the surfactant to form surfactant clusters. [Alila et al., 2005] Region III commences at 8 mM DoTAB till the end of titration curve. A further increase in the surfactant concentration leads to the formation of surfactant micelles on the particle surface, where the critical onset concentration is designated as *C*'. [Wang and Tam, 2002] The micellization of DoTAB in the presence of CNC occurs at a lower concentration due to the polymer induced micellization effect. At much higher surfactant concentration, the titration curve levels off and only the dilution heat of the micelles was measured.

Figure 5.8(b) shows the ITC curves of the titration of 200 mM DoTAB into different concentrations of M600-grafted CNC. The titration curves for 0.05, 0.1, 0.25, and 0.5 wt% exhibited similar profiles with some variations in the enthalpy profiles. The electrostatic interaction between DoTAB and 0.5 wt% M600-grafted CNC is large, and it decreased as the particle concentration was reduced, since the amount of negative charges on the particle surface is proportional to the particle concentration. We observed that the critical concentration (*C*') for

the formation of surfactant micelles on the particle surface decreased with increasing particle concentration; i.e. it decreased from 13.8 to 8.6 mM when the particle concentration was increased from 0.05 to 0.1 wt%. This suggests that the aggregation of surfactant monomers is dependent on the particle concentration.

5.3.4 Interactions between M600-grafted CNC and a non-ionic surfactant (Brij 30)

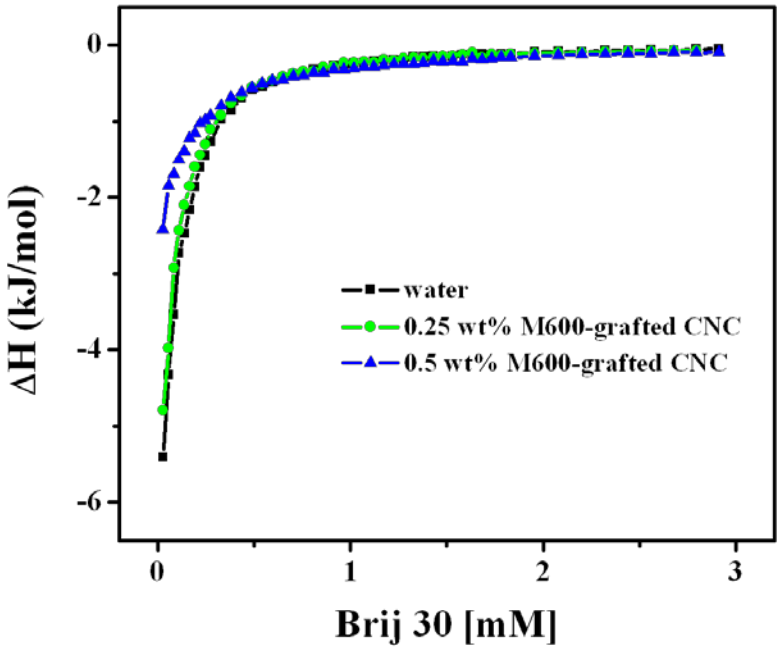

Figure 5.9 Calorimetric titration curves for titration of 20mM Brij 30 into water and M600-grafted CNC suspensions of various concentrations: 0.25, and 0.5 wt% at 25 ^{o}C.

The ITC curves for the titration of 20 mM Brij 30 into water, 0.25 and 0.5 wt% of M600-grafted CNC are plotted in Figure 5.9. The CMCs for nonionic surfactant (Brij series) are quite low, and it was reported the CMC of Brij 30 is about 0.004 mM at 25 ^{o}C. [Hait and Moulik, 2001] In the dilution curve of Brij 30, the enthalpy changes became less negative at low surfactant concentration ranging from 0 to 0.54 mM, and approached zero at higher surfactant

concentration. The titration curve of Brij 30/M600-grafted CNC is identical to the Brij 30 dilution curve. However, their enthalpy changes are considerably less exothermic at low surfactant concentration, especially for the 0.5 wt% M600-grafted CNC system, which could be due to changes in the solvent environment with the addition of modified CNC that impacts the disassociation process of Brij 30 micelles. In addition, Brij 30 monomers may bind to the hydrophobic segments of the nanoparticles at relatively high particle concentration.

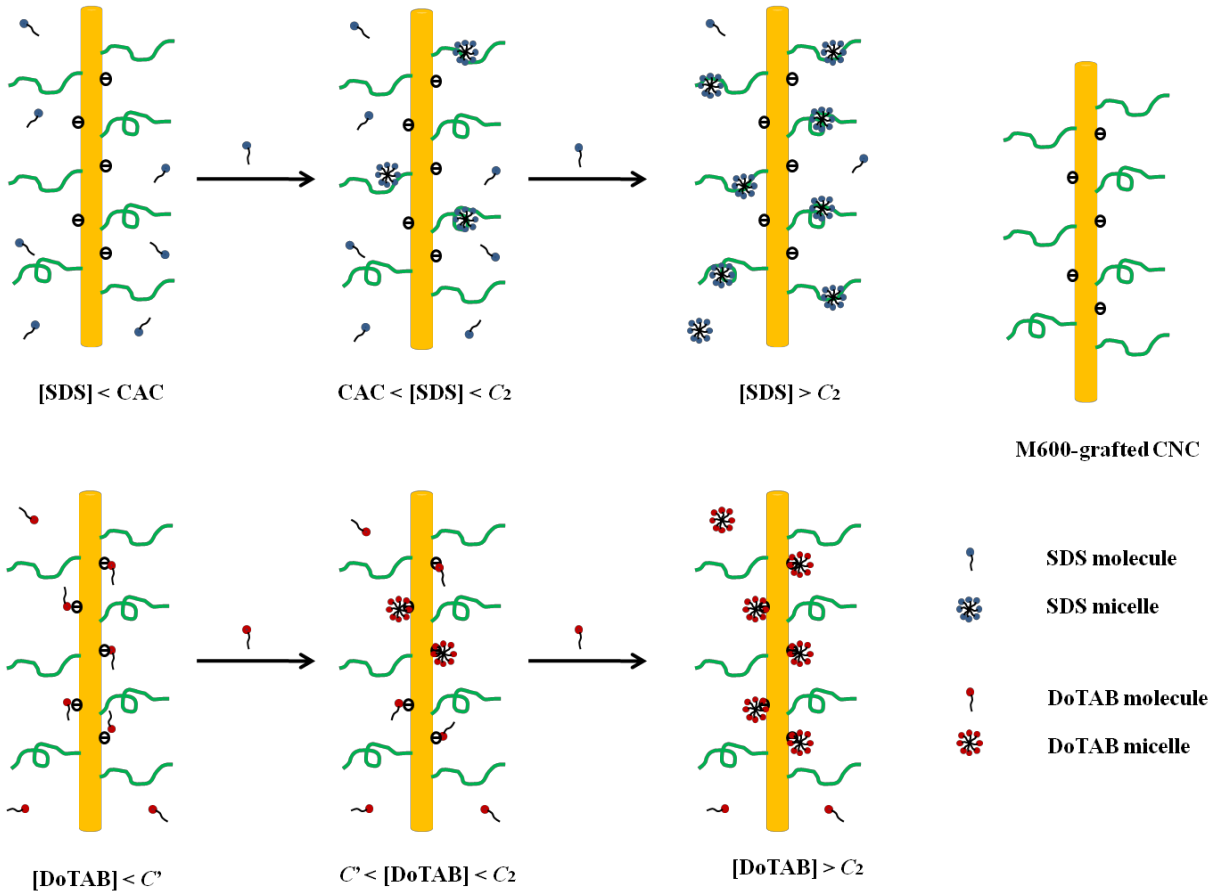

Figure 5.10 Schematic diagrams describing the binding interactions for SDS/M600-grafted CNC and DoTAB/ M600-grafted CNC systems in aqueous media.

A schematic mechanism describing the binding interactions of SDS/M600-grafted CNC and DoTAB/M600-grafted CNC systems in aqueous media is shown in Figure 5.10. For the SDS/M600-grafted CNC, at low concentration, SDS molecules bind to oxypropylene segments

via hydrophobic interactions, and they form micelles above the CAC. With increasing SDS concentration up to C_2, all the oxypropylene segments become saturated with SDS micelles and free SDS micelles begin to form in the bulk. Similarly, in the DoTAB/M600-grafted CNC system, DoTAB molecules are initially attracted to the negative charged sites, and they reorganize and associate with adjacent DoTAB molecules forming clusters of surfactant monomers when the concentration reached *C*'. At concentration greater than C_2, free surfactant micelles are formed in the bulk solution.

5.4 Conclusions

This chapter describes that a commercial cationic polymer (Jeffamine M600) was successfully grafted onto CNC surface via TEMPO oxidation and peptidic coupling reactions. The formation of covalent amide bond between polymer and CNC was confirmed by FT-IR. The interactions between M600-grafted CNC and anionic (SDS), cationic (DoTAB) and non-ionic (Brij 30) surfactants were investigated by ITC. A large endothermic peak was found for SDS and M600-grafted CNC system, indicating strong hydrophobic interaction between the surfactant tails and oxypropylene segments. DoTAB and M600-grafted CNC exhibited strong ionic interaction due to the neutralization of opposite charges. Titration of Brij 30 into M600-grafted CNC and water showed identical curves, implying the absence of significant interaction. Possible applications of modified CNC in personal care products and pharmaceuticals are being explored.

Chapter 6 Aggregation behavior of *N*-carboxyethylchitosan in aqueous solution: effects of pH, polymer concentration, and presence of a gemini surfactant

6.1 Introduction

Chitosan is an important polysaccharide, derived from the abundant organic resource chitin. Because of its intrinsic biocompatibility and biodegradability, [Onishi and Machida, 1999; VandeVord et al., 2002] chitosan has attracted considerable attention in biological and industrial applications, such as tissue engineering, transplant and cell regeneration, encapsulation, and wastewater treatment. [Schulz et al., 1998; Ishaug-Riley et al., 1999; Niklason et al., 1999] In acidic media, chitosan is water soluble mainly because of the presence of amino groups at the C-2 position (p*K*a ~ 6.3-7). At pH < 4, most of the amino groups are protonated, and the strong electrostatic interactions among the cations make the molecular chains expanded and promote the solubility. On the other hand, at high pH values, the amino groups become deprotonated, which induces an insoluble chitosan in basic media. Since some applications of chitosan are restricted by the solubility of the polymer in basic media, many polyampholyte derivatives of chitosan, which can be soluble in both acidic and basic media, are used. These modified chitosans are synthesized with carboxylate or sulfo groups on the reactive functional groups along the polymer backbone. [Sashiwa et al., 2003a, 2003b; Ravi Kumar et al., 2004]

Among the numerous water-soluble derivatives, *N*-carboxyethylchitosan (CECh), synthesized by adding the acrylic acid (AA) onto -NH_2 groups by Michael addition, is one of the most attractive derivatives. Due to the modification of COOH, CECh presents some significant properties, such as improved water solubility, higher biocompatibility, and better

biodegradability in comparison with chitosan. [Yancheva et al., 2007] Moreover, the conformation and the dimensions of the molecular chains in aqueous solution are also different from those of chitosan. Depending on the numbers of AA units attached to the $-NH_2$ groups, i.e. the degree of substitution (DS), CECh possesses distinct zwitterionic properties with different isoelectric points (IEPs). The zwitterionic properties play an important role in the aggregation behavior of polyampholyte, which had attracted great interest of many researchers. [Neyret et al., 1995; Lowe, Billingham and Armes, 1998; Bütün et al., 1999; Patrickios et al., 1999; Braun, Selb and Candau, 2001; Liu and Armes, 2003; Ciferri and Kudaibergenov, 2007; Kudaibergenov and Ciferri, 2007] A series of block and random polyampholytes have been synthesized and their self-assembly properties under different conditions have been investigated by Armes and co-workers [1998; 1999; 2003] and Candau and co-workers, [1995; 2001] respectively. Meanwhile, the aggregation behaviors of proteins and nucleic acids, two typical ampholytic macromolecules in nature, were studied under different conditions, such as different pHs, [Linden and Venema, 2007] ionic strengths, [Li et al., 2009] concentrations, [Boulet, Britten and Lamarche, 2000] and in the presence of a surfactant. [Pi et al., 2006; Wu et al., 2007] However, CECh is quite different from those polyampholytes, due to its unique rigid backbone, which can promote molecular steric stability. Mincheva and co-workers [2008] performed a systematic study on the formation of nanosized structures of CECh solution near the IEP, and obtained well-regulated structures. Zhu et al. [2005] investigated the self-aggregation behavior of *O*-carboxymethylchitosan (OCMCS) in dilute aqueous solution. However, there are few papers on the zwitterionic properties of CECh until now, especially those on the effects of pH, polymer concentration, and the presence of a gemini surfactant. As we know, the interaction between polymer and surfactant is a very interesting subject, which is the focus of many researchers. [Lim

et al., 2003; Berret et al., 2004; Nizri et al., 2004, 2009] Under different ratios of polymer and surfactant, the rheological properties changed considerably, and many charming conformations that formed in the solution were detected. One characteristic of the interaction is the existence of a critical aggregation concentration (CAC), where surfactants start to bind onto polymer chains. In most reports, traditional surfactants were employed. However, if a cationic gemini surfactant is added to the CECh solution in basic media, the solution must exhibit some novel behavior. The fundamental knowledge developed from such studies will provide the information necessary for the development of new and novel systems for applications in the biomedical and chemical fields.

In this chapter, fluorescence-probe spectroscopy, viscometry, surface tensiometry, as well as turbidity and zeta potential measurements, were used to investigate the influence of pH, polymer concentration and a gemini surfactant on the aggregation behavior of *N*-carboxyethylchitosan in aqueous solution. In order to provide more details on the aggregation mechanism, the effect of surfactant spacer length on the interaction between gemini surfactant and CECh was also explored simultaneously.

6.2 Experimental

6.2.1 Materials

Chitosan powder (M_w = 2.3 × 10^5 g/mol) with a degree of deacetylation ≥ 90% was supplied by Shanghai Reagent Co. Ltd, China. Acrylic acid (Shanghai LinFeng Reagent Co. Ltd) was distilled under reduced pressure before use. CECh was prepared by a Michael addition reaction as described by Sashiwa et al., [2003b] and the degree of substitution (DS) of CECh was 0.21, based on ^{1}H NMR analysis referred to relevant literature. [Kang et al., 2006] The CECh product was precipitated in anhydrous EtOH and was rinsed three times to remove the low-

molecular-weight component. The precipitate was dissolved in water and dialyzed against distilled water for three days using a dialysis tube (M_w cut-off $\leq$ 3500), and the solution was then lyophilized. Cationic gemini surfactants (12-*n*-12) were synthesized by a reaction of α, ω-dibromoalkanes with *N*, *N*-dodecyldimethylamine. Pyrene for the fluorescence probe studies was purchased from Sigma-Aldrich Chemical Co., and used as received. Fresh doubly distilled water was used in all experiments.

6.2.2 Sample preparation

A stock CECh solution of 0.2 wt% was prepared and diluted to solutions with various concentrations (0.01-0.1 wt%). The pH of the solution at 0.05 wt% was adjusted to 3-11 (monitored by a Sartorius PB-10 pH meter) by either dilute aq. HCl or aq. NaOH. By mixing the surfactant and CECh solutions, we obtained various 12-*n*-12/CECh samples with a constant CECh concentration of 0.05 wt%, and a series of surfactant concentration (10^{-7}-10^{-3} mol/L) in basic media. All samples were kept at 25.0 ^{o}C for 24h before each experiment to ensure complete dissolution.

6.2.3 Characterizations

6.2.3.1 Fluorescence emission spectroscopy

Samples for fluorescence spectroscopy measurements were prepared by using a saturated pyrene water solution as the solvent. The fluorescence measurements were conducted on an F4500 fluorescence spectrophotometer (Hitachi) equipped with a thermostated water circulating bath, and the excitation wavelength was fixed on 335 nm, while the slit widths of excitation and emission were settled at 10.0 and 2.5 nm, respectively.

6.2.3.2 Viscosity measurements

A Brookfield LVDV3 rheometer with a cone spindle of SC-18 was employed for the viscosity measurements. The viscosity value reported below was an average one of three times at a fixed shear rate 264 s^{-1}.

6.2.3.3 Surface tension measurements

The surface tension measurements were performed with a Radian series tensiometer from Thermo Cahn. Surface tensions (γ) were determined by employing the Wilhelmy plate technique. The tensiometer was calibrated against water before measurements.

6.2.3.4 Turbidity measurements

The spectrophotometer used in this work was a Shimadzu 2450-UV UV/Vis spectrophotometer, and all measurements were made in a quartz cuvette (1 cm width) at wavelength of 500 nm at 25.0 ^{o}C.

6.2.3.5 Zeta potential

The zeta potential was conducted on a Nano-ZS (Malvern) using Doppler velocimetry and phase analysis light scattering. The scattering angle was 173^{o}, while the laser wavelength was 633 nm. Each measurement was repeated at least three times.

6.3 Results and Discussion

6.3.1 Influence of pH on the aggregation behavior of CECh

The pH of solution plays an important role in inducing polyelectrolyte aggregation, i.e. at different pH values, the solubility of different functional groups changed, resulting in the formation of aggregation. Turbidity measurements can easily detect the polymer conformation

transformation from aggregates to particles or molecular chains by recording the transmittance values. [Neto et al., 2005; de Vasconcelos et al., 2006] The transmittance dependence on pH of 0.05 wt% CECh aqueous solutions at λ = 500 nm is shown in Figure 6.1. It is evident that CECh possessed the typical characteristics of a polyampholyte, because at either high or low pH, the solutions were almost transparent with nearly 100% transmittance, while the transmittance decreased rapidly in the middle range of pH 6-7, which can be defined as the isoelectric point (IEP) range. In this case, the IEP of CECh with DS = 0.21 is ca. 6.65 (= (pHa + pHb)/2).

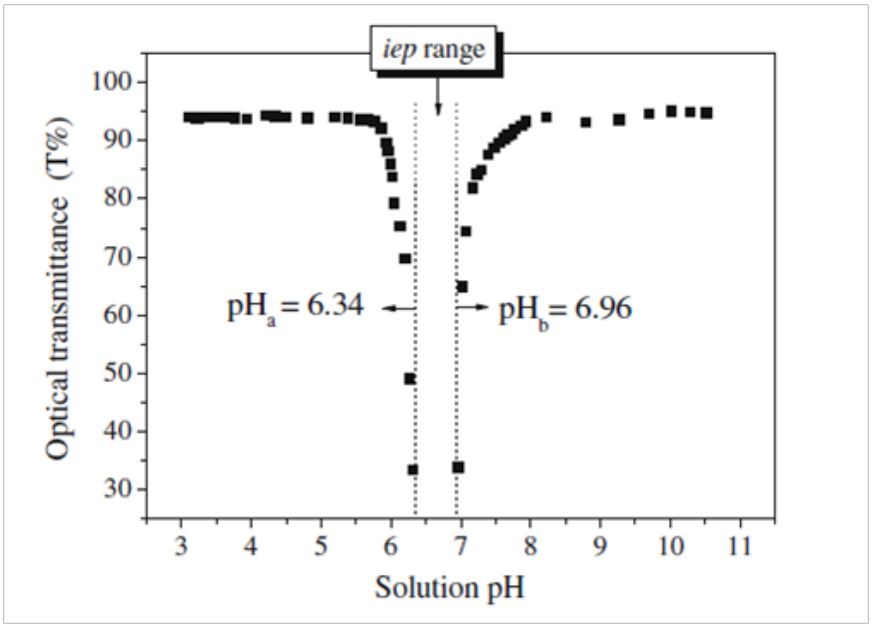

Figure 6.1 The optical transmittance (T%) of CECh aqueous solution at λ = 500 nm under various pHs.

Similar phenomena were also observed in block copolymer systems, such as poly(2-(dimethylamino)ethyl methacrylate-block-methacrylic acid) (poly(DMA-*b*-MAA)) and poly(2-(diethylamino)ethyl methacrylateblock-methacrylic acid) (poly(DEA-*b*-MAA)). [Creutz et al., 1997; Dai et al., 2003] At low pH, CECh molecules possessed uncharged carboxylic groups (-COOH) and positively protonated -NH_3^+ groups, which could be considered as a positive polyelectrolyte that can be molecularly dissolved in aqueous solution due to the repulsion

between -NH_3^+ groups. Although the amino groups were deprotonated and rendered hydrophobic at high pH, CECh molecules were solubilized in aqueous solution due to the ionization of carboxylic groups (-COOH). At almost neutral pH, obvious precipitation occurred because of the coexistence of positive and negative charges, and the electrostatic attractions between intra- and intermolecules resulted in a rapid decrease in the light transmittance.

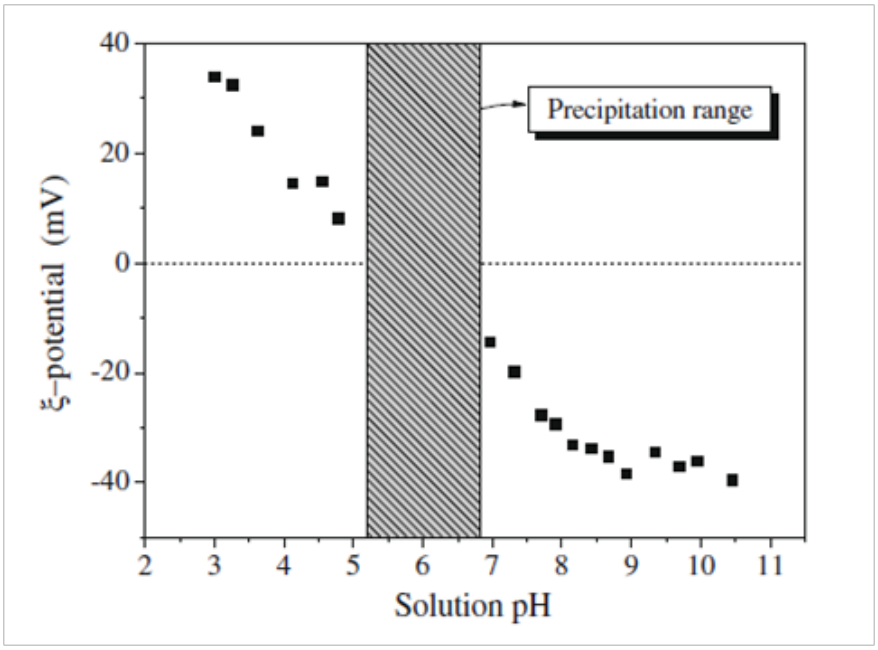

Figure 6.2 The zeta potential of CECh aqueous solution under various values of pH.

The zeta potential was used to characterize the charge density of the particles and the electrostatic interactions among charged particles. Herein, the zeta potential experiments were performed under the same condition as those in the turbidity measurements on CECh solutions with different pHs. With increasing pH, the zeta potential (ζ) decreased from +34 mV at pH 3.00 to -40 mV at pH 10.45 (shown in Figure 6.2), indicating the surface charge changed from net positive to net negative. Either at low or high pH, CECh dissolved in aqueous media, due to the electrostatic repulsion between the abundant charges distributed on the molecular chains. Experimentally, the aggregation would not occur when $|\zeta| > 30$ mV, which is in agreement with

the data from the turbidity measurements. During the whole process from acidic to basic conditions, the zeta potential approached to zero at pH between 5.2 and 6.8, and the phase separation occurred due to the electrostatic attraction between positive amino groups and negative carboxylic moieties.

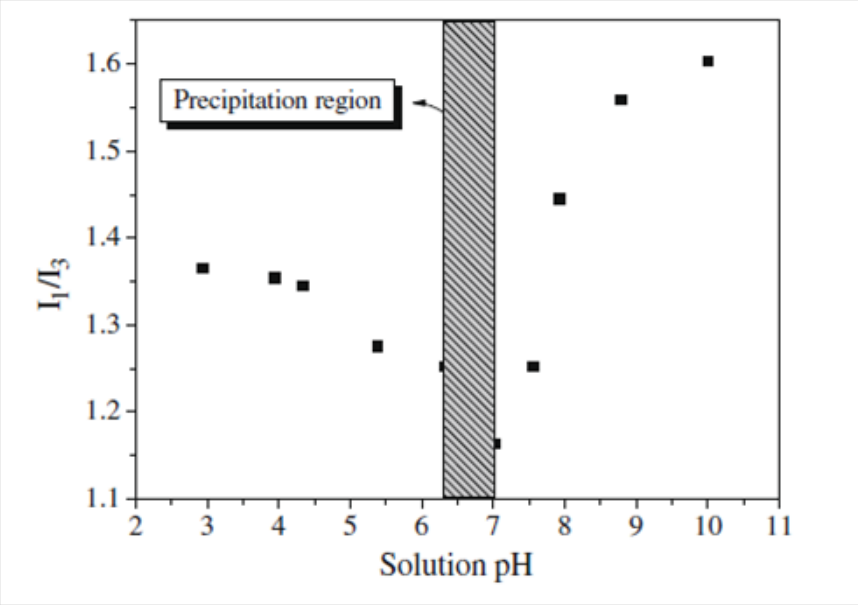

Figure 6.3 Fluorescence spectroscopy of CECh aqueous solution at different values of pH by using pyrene as a fluorescent probe.

The aggregation behavior of CECh was also investigated by recording the fluorescence intensities of the first and third vibronic peaks (I_1/I_3) of pyrene. The ratio of I_1/I_3 as a function of solution pH is illustrated in Figure 6.3. From this figure, it is obvious that at pH 6.3-7.0, the I_1/I_3 values were smaller than those at low or high pHs, implying a more hydrophobic environment where pyrene is located, i.e. the CECh aggregates in aqueous solution. As expected, the driving force for the hydrophobic aggregation near the IEP region was attributed to the charge compensation between positive amino groups and negative carboxylic moieties according to the previous measurements. Moreover, it is also an evidence for the existence of intermolecular

interactions, because the I_1/I_3 values at both low and high pHs were slightly lower than that in pure water (I_1/I_3 = 1.726).

6.3.2 Influence of polymer concentration on the aggregation behavior of CECh

As mentioned above, the aggregation of CECh in aqueous solution was driven by inter- and intramolecular interactions. Among the intramolecular forces, the electrostatic attraction is the dominant force at or near the IEP, even though the aggregation behaviors were different at low and high pHs according to the fluorescence measurements. Potentiometric and conductivity titrations were further conducted by titrating 0.1 M NaOH to 0.05 wt% CECh solution at 25 ^{o}C, which was adjusted to pH 3 at first. Herein, the two transition points at pH 4 and 10 were considered as examples of full protonation of NH_2 and full ionization of COOH, [Skorik et al., 2003] respectively.

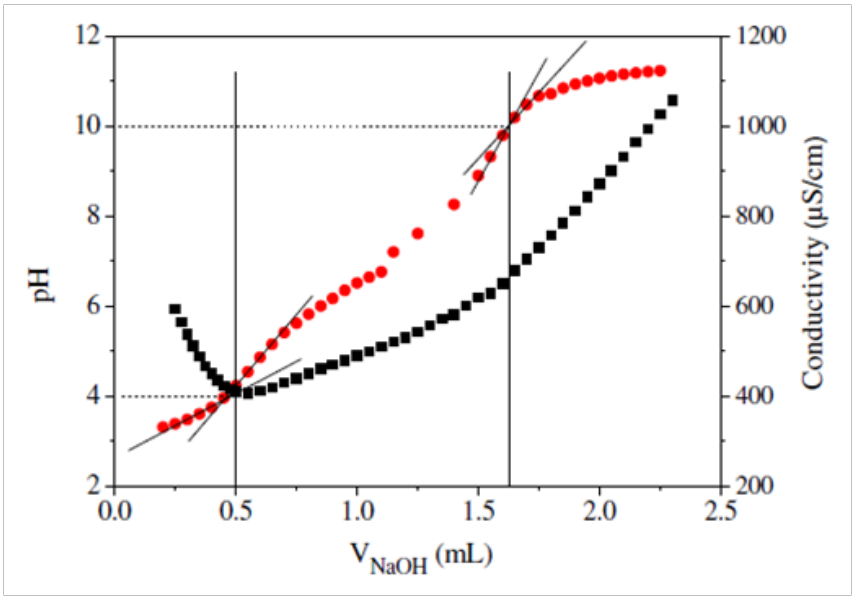

Figure 6.4 Potentiometric and conductivity titration of 0.05 wt% CECh with 0.1 M NaOH at 25 ^{o}C. Square-filled symbols represent conductivity, and circle-filled symbols represent pH.

The titration curves are shown in Figure 6.4. In this section, the aggregation behavior at pH 4 and 10 with a series of polymer concentrations between 0.01 and 0.1 wt% were compared to further

investigate the aggregation mechanism using viscosity measurements and fluorescence emission spectroscopy. Viscosity measurements are considered to be an effective method to explore the properties of polymer solution, and these have already been used to study the aggregation behavior of chitosan and its derivatives. [Onésippe and Lagerge, 2008; Chytil and Pekař, 2009] The concentration dependence of viscosity is illustrated in Figure 6.5, and it indicated the viscosity increased linearly with the CECh concentration at both pH 4 and 10 when concentration above 0.02 wt%. It is understood that the intermolecular association is enhanced at high polymer concentrations. At low concentrations before 0.02 wt%, the viscosities were almost the same, and then at higher concentrations, the viscosities at pH 4 distinctly exceeded those at pH 10. Considering the degree of substitution and the pH, the charge density of polymer chains at pH 4 is three times larger than that at pH 10. According to Manning counterion condensation theory, [Ray and Manning, 2000] the counterion may be condensed on the polymer chains as the charge density parameter increased with n > 1, consequently, the electrostatic interaction among the polymer chains was driven by the release of condensed counterions. Therefore, in our case, the counterion condensed on the polymer chains probably occurred at pH 4, and significant intermolecular association produced a higher viscosity than that at pH 10, which could also explain the difference of I_1/I_3 values at pH 4 and pH 10.

To further compare the aggregation behavior at different CECh concentrations at pH 4 and 10, fluorescence emission spectroscopy was employed to study on the same samples prepared as those for viscosity measurements. Figure 6.6 illustrates the change of the I_1/I_3 ratios as a function of CECh concentration. Both the two profiles at pH 4 and 10 decreased with CECh concentration, implying the microenvironment where pyrene was located became more hydrophobic due to intermolecular aggregation. At CECh concentrations lower than 0.02 wt%, the I_1/I_3 values were

both near 1.726 at pH 4 and 10, which indicated that the polymer chains were molecularly dissolved in aqueous solution and had little impact on each other. As expected, the I_1/I_3 values at pH 4 were still lower than those at pH 10, signifying enhanced aggregation behavior at pH 4.

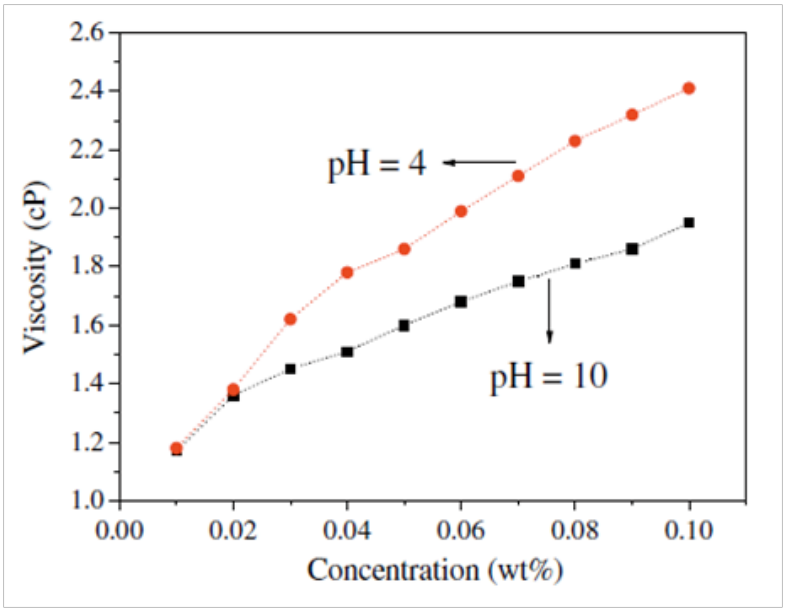

Figure 6.5 The solution viscosity as a function of CECh concentration at pH 4 and 10.

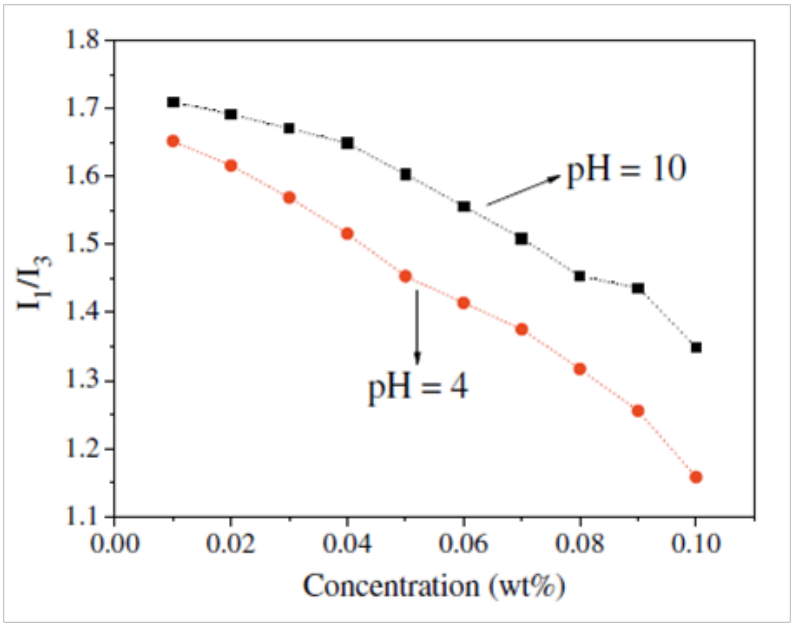

Figure 6.6 The I_1/I_3 values as a function of CECh concentration at pH 4 and 10.

6.3.3 Influence of a gemini surfactant on the aggregation behavior of CECh

The interaction between surfactant and polymer has evoked great interest for many years due to the interesting changes in rheology, morphology, and other solution properties of the polymer. Herein, a series of mixing samples consisting of CECh (0.05 wt%) and a gemini surfactant with different concentrations (*C*s) from 10^{-7} to 10^{-3} mol/L were prepared in basic media to study the critical aggregation concentration (CAC) of gemini surfactant and CECh complexes and the effect of spacer length on the interactions of gemini surfactant and CECh.

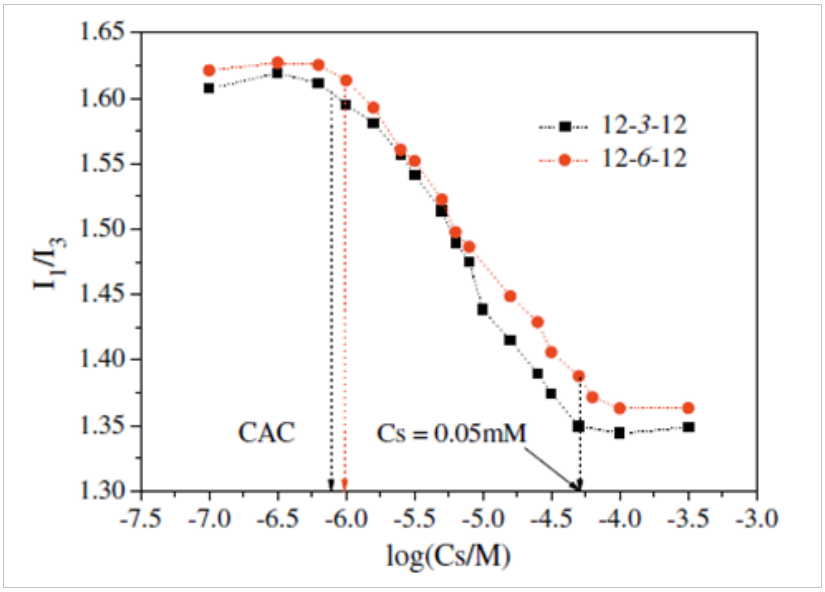

Figure 6.7 Surfactant concentration dependence of the micropolarity in 12-*n*-12/CECh solution (C_{CECh} = 0.05 wt%) in basic media.

As aforementioned, the carboxyl groups (-COOH) ionized in basic media, hence the addition of cationic gemini surfactant could certainly induce some unique conformations of the CECh/12-*n*-12 (*n* = 3, 6) system by the strong electrostatic interaction between the two kinds of oppositely charged species and the hydrophobic interaction among the CECh backbones. The profile of I_1/I_3 values versus log*C*s in the presence of 0.05 wt% CECh is shown in Figure 6.7. It shows that the I_1/I_3 values were almost constant at ~1.6 at very low *C*s (<0.001 mmol/L),

implying that such a small amounts of surfactant had an impact on the CECh molecules. However, the values were lower than those of pyrene in pure water solution (I_1/I_3 = 1.726), which is probably related to the hydrophobic interaction between CECh backbones. The I_1/I_3 values started to decrease at *C*s = 0.001 mmol/L, and this concentration is defined as the CAC of CECh/surfactant systems, i.e., the onset concentration for the formation of a micelle-like structure near the binding site of the polyion chain. [Pi et al., 2006] In the range of *C*s = 0.001-0.05 mmol/L, a sharp decrease in I_1/I_3 was observed, suggesting the decrease of the micropolarity around pyrene due to the formation of surfactant/polymer aggregates. When *C*s reached 0.05 mmol/L, the I_1/I_3 values finally level off at ~1.36 and no longer decreased with the addition of surfactant. It is suggested that the -COO^- groups are completely bound with positive surfactant head groups, and the excessive surfactant begins to form micelles on their own, [Kang et al., 2009] in which the pyrene molecules locate in and lead to a constant value of I_1/I_3. The critical micellization concentration (CMC) of gemini surfactants 12-*3*-12 and 12-*6*-12 that we used in the measurements were 0.93 and 1.17 mmol/L, respectively. Obviously, the addition of polymer molecules resulted in the formation of free micelles at lower surfactant concentration. Furthermore, by comparing the two mixing systems, we found that the I_1/I_3 values of CECh/12-*3*-12 were always slightly lower than those of CECh/12-*6*-12 in the investigated surfactant concentration range. It could be interpreted that the CECh/12-*3*-12 aggregates were more compact since 12-*3*-12 possessed a higher charge density.

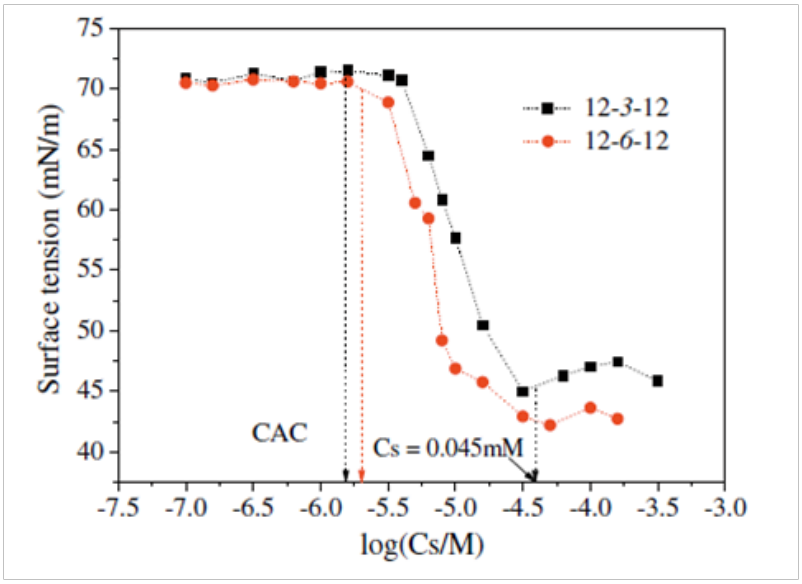

Figure 6.8 The surface tension of CECh/12-*n*-12 aqueous solution as a function of log*C*s in basic media.

Surface tension measurement is an efficient method to highlight the influence of surfactant on the polymer aggregation behavior, which has been applied in many studies. [Dėdinaitė and Ernstsson, 2003; Pepić, Filipović-Grčić and Jalšenjak, 2008] The surface tension of the two mixing systems is plotted versus log(*C*s/M) in Figure 6.8. At very low *C*s (< 0.0015 mmol/L), the surface tension values were almost constant and consistent with that of pure water (ca. 71.97 mN/m), suggesting that the CECh molecules themselves had no surface activity as a random polyampholyte. [Babak et al., 1999] Moreover, it was also demonstrated that all the surfactant molecules bound to carboxyl groups via electrostatic attraction, and no distribution at the air/solution interface to decrease the surface tension. The surface tension began to decrease at *C*s = 0.0015 mmol/L, in accordance with the results of fluorescence measurements, which implied that surfactant molecules started to disperse at the air/solution interface. This effect took place at a lower surfactant concentration, where pure surfactant alone did not affect the surface tension of the pure solvent. [Onésippe and Lagerge, 2008] The surface tension exhibited a significant

decrease in the range of *C*s = 0.0015-0.045 mmol/L, due to the dispersion of surfactant molecules at the surface and their interaction with CECh as well. Furthermore, the ongoing binding process induced the aggregating of the surfactant/polymer system in this concentration region. When *C*s was above 0.045 mmol/L, the surface tension gradually levelled off at 46 and 43 mN/m for the CECh/12-*3*-12 and CECh/12-*6*-12 systems, respectively, which was attributed to the saturation of surfactant molecules at the air/solution interface in the presence of CECh and the formation of free micelles in bulk. It is surmised that in the range of *C*s = 0.0015-0.045 mmol/L, the surfactant molecules tended to disperse at the air/solution interface to reduce the interfacial energy, and simultaneously bound to CECh chains driven by the electrostatic attraction. The surface tension results corresponded to those from the fluorescence measurements. It is evident that the surface tension of CECh/12-*6*-12 was lower than that of CECh/12-*3*-12 above *C*s = 0.0015 mmol/L. This is because surfactant 12-*6*-12 presents a higher surface activity than 12-*3*-12, which is in accordance with studies reported in the literature. [Zana, Benrraou and Rueff, 1991; Huang et al., 2008]

Figure 6.9 presents the viscosities as a function of log*C*s for surfactant/CECh aqueous solutions. As expected, the addition of a gemini surfactant could alter the rheological properties of the polymer solution due to the formation of surfactant/CECh aggregates. It showed that solution viscosities remained constant as *C*s < 0.045 mmol/L, suggesting the interaction between CECh and surfactant had little impact on the solution viscosity, while the hydrophobic interaction among the CECh backbones played a dominate role. By increasing the *C*s to 0.045 mmol/L, a decrease of viscosity from 1.56 to 1.12 cP was observed, which is attributed to the changes in the CECh/surfactant complex conformation. As mentioned before, the free micelles started to form above Cs > 0.045 mmol/L, and simultaneously the CECh chains collapsed and

wrapped around the free micelles, which might reduce the intermolecular interactions, resulting in a decrease in the viscosity. Another reason could be ascribed to the lower dimensions of the macromolecular chains, because the surfactant molecules may shield the repulsion between ionic groups on CECh chains. Furthermore, there was no phase separation occurring during the whole experiment under a shear rate 264 s^{-1}, which is the optimum shear rate for this polymer concentration. When complexes of the CECh/surfactant were formed, the co-ions, Na^+ and Br^- in our experiments, could be liberated and became more homogeneously distributed in the continuous phase. This process will result in a strong increase in entropy, which also plays an important role in the interaction between CECh and the surfactant.

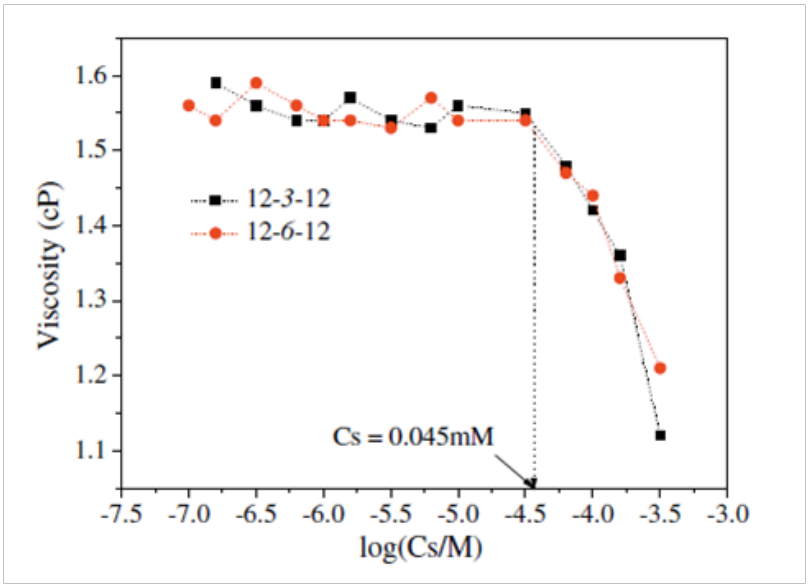

Figure 6.9 Surfactant concentration log*C*s dependence of viscosity of CECh/12-*n*-12 aqueous solution in basic media.

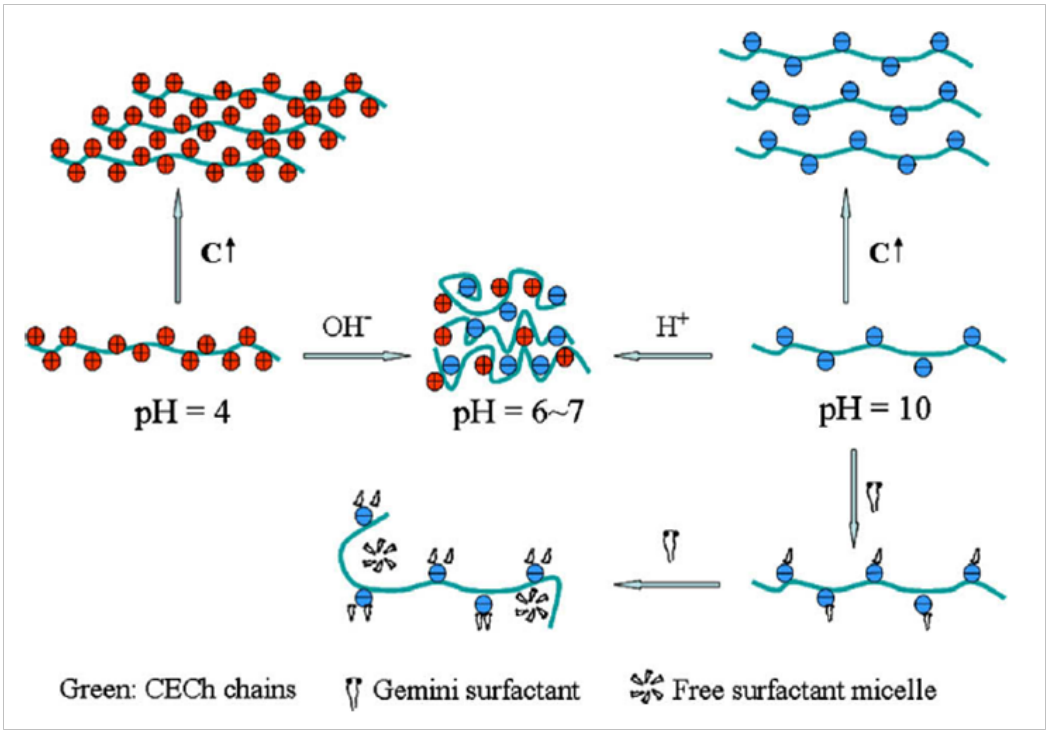

Figure 6.10 The proposed model for CECh aggregation behavior under different conditions.

6.4 Conclusions

Combining the measurements of turbidity, zeta potential, fluorescence spectroscopy, viscosity, and surface tension, we have studied the aggregation behavior of CECh under different pH values, and polymer concentrations, as well as in the presence of a gemini surfactant. Specially, as shown in Figure 6.10, the aggregation mechanism under different conditions is proposed. The CECh molecules are dissolved in water as molecular chains at either low or high pH, ascribing to the protonation of -NH_2 and ionization of -COOH, and the charge neutralization near IEP results in the phase separation of the CECh solution. The intermolecular interaction at pH 4 is stronger than that at pH 10 during the whole CECh concentration region, which can be interpreted by the counterion condensation theory as the higher charge density at pH 4. The critical aggregation concentrations of CECh/12-*n*-12 (*n* = 3, 6) systems in basic media can be determined to be 0.001-0.0015 mmol/L, and the values estimated from fluorescence and surface

tension are in good agreement. The CECh/12-*n*-12 interactions were affected by the spacer length of gemini surfactant, i.e., the binding affinity between gemini surfactant and CECh is inversely proportional to the spacer length.

Chapter 7 Conclusions and Recommendations

7.1 General Contributions

In the thesis, a random copolymer P(MEO_2MA-*co*-$PEGMA_{2080}$) was synthesized and characterized, while a unique two-stage thermal induced aggregation behavior was found in copolymer aqueous solution (Chapter 3). The binding interactions between cationic surfactants and the copolymer at the temperature below and above its cloud point in aqueous solution were elucidated and significant hydrophobic interactions were observed (Chapter 4). The interactions between surfactants and two biodegradable natural materials, i.e. CNC and chitosan derivative were investigated (Chapter 5 & 6).

Interactions between surfactants and three different polymeric nanostructures were summarized based on this study: namely cationic surfactants (CTAB, TTAB and DoTAB) and neutral polymer system; anionic (SDS), cationic (DoTAB) and non-ionic (Brij 30) surfactants with polymer-grafted CNC; and gemini surfactant and one chitosan derivative system. The key understandings between these nanostructures and surfactants are reported. These interactions will induce the restructuring of polymer chains and the occurrence of precipitation. In the presence of charged polymers and oppositely charged surfactants, electrostatic attraction dominates the binding interactions, which could induce phase separation due to charge neutralization. In the uncharged polymers and surfactants systems, the interactions are mainly controlled by the hydrophobic effect. The following conclusions can be drawn from this study.

7.1.1 Thermo-responsive oligo (ethylene glycol) methacrylates copolymer

A well-defined random copolymer P(MEO_2MA-*co*-$PEGMA_{2080}$) was synthesized by ATRP, and it exhibited a unique two-stage thermal induced aggregation process in aqueous

solution. The copolymer chains associated at the first thermal transition followed by a rearrangement process at the second thermal transition to produce a stable core-shell micellar structure, which was stabilized by the longer ethylene glycol segments (M_n = 2080 g/mol) shell. The results of concentration studies confirmed the occurrence of multiple thermal transitions, and the phase transitions of this copolymer in water were insensitive to polymer concentration. It was proven that the length of the side chain could significantly alter the solution properties. By using poly(ethylene glycol) methyl ether methacrylate with a molecular weight of 2080 g/mol instead of 475 g/mol, unusual solution properties were observed in comparison to previous results on copolymers of oligo(ethylene glycol) methacrylates, where only one sharp transition was reported. The copolymer chains phase separate, aggregate and rearrange to produce stable micelles by increasing temperature, while the large aggregates and micelle structure was confirmed by TEM and light scattering measurements.

7.1.2 Binding interactions between cationic surfactants and neutral copolymer

The binding interactions between cationic surfactants and poly(MEO_2MA-*co*-$PEGMA_{2080}$) in aqueous solution were elucidated at the temperature below and above its cloud point. Below the cloud point, surfactants bind to the individual copolymer chains to form a surfactant-swollen coil. While above the cloud point, surfactants bind to the polymer aggregates that dissociate the aggregate due to the strong electrostatic repulsion within the charged polymer-bound surfactant complexes. Significant hydrophobic interactions were observed between surfactant monomers and the polymer backbone, however, the binding interactions between cationic surfactants and neutral polymers were reported to be weak previously and cationic surfactants were very selective and only bind to those polymers with specific hydrophobic groups. The binding occurred uncooperatively at low surfactant concentration, which was confirmed by EMF

measurements. The surfactant saturation concentration C_2 depended on the polymer concentration and was insensitive to temperature. Moreover, the binding affinity of the three cationic surfactants in this study follows the sequence: CTAB > TTAB > DoTAB.

7.1.3 Interactions between surfactants and TRP-modified CNC

Cellulose Nanocrystals (CNC) had been reported as a very promising new class of nanomaterials due to its high specific strength, high surface area, unique optical properties, etc. Its attractive physicochemical properties and wide application prospects had attracted significant interest, and most of researchers focused on the improvement of its steric stability, dispersability and compatibility in different solvents or matrices by conducting chemical modifications on CNC surface or physical interactions. In this study, a commercial cationic polymer (Jeffamine M600) was successfully grafted onto CNC surface via TEMPO oxidation and peptidic coupling reactions. The better dispersion of the modified CNC in water was demonstrated, and the interactions between M600-grafted CNC and anionic (SDS), cationic (DoTAB) and non-ionic (Brij 30) surfactants were investigated by ITC. Strong electrostatic interaction was only observed between M600-grafted CNC and DoTAB, due to the binding of opposite charges. Hydrophobic interaction was displayed for the M600-grafted CNC/SDS system, and negligible interaction between M600-grafted CNC and Brij 30 was observed.

7.1.4 Interactions between gemini surfactant and *N*-carboxyethylchitosan

A biocompatible derivative of chitosan, *N*-carboxyethylchitosan (CECh), was synthesized by Michael addition reaction, which possesses high solubility in both acidic and basic media due to the modification by carboxyl groups. The aggregation behavior of CECh under different pH values, polymer concentrations, as well as in the presence of a gemini surfactant was investigated by means of turbidity, zeta potential, fluorescence spectroscopy, viscosity, and surface tension.

The CECh molecules dissolved in both acidic and basic water conditions and the intermolecular interaction at pH 4 was stronger than that at pH 10 due to the high charge density at low pH. The CECh/12-*n*-12 interactions were affected by the spacer length of gemini surfactant, i.e. the binding affinity between gemini surfactant and CECh was inversely proportional to the spacer length.

7.2 Recommendations for Future work

On the basis of the results obtained thus far, the impact of factors such as polymer properties, salt, pH, solvents etc. on the surfactants/polymeric nanostructures should be investigated. The effect of small molecules (surfactants, salt, ionic liquid etc.) and monomer composition on LCST behaviors is anticipated, and the following recommendations for future studies are proposed:

7.2.1 Effect of solvent conditions and polymer properties on surfactants/polymeric nanostructures

More types of thermo-responsive polymers with different molecular weight should be grafted onto CNC surface, and a comparison between surfactants with these TRPs in bulk and at CNC surface is necessary and woud present an interesting study. In this thesis, only one commercial Jeffamine polymer with M_w of 600 Da was grafted onto CNC surface using the "grafting-to" approach, hence only limited insights on the impact of polymer M_w on the interactions was achieved. Future studies should focus on a series of Jeffamine polymers with different M_w to study the impact of molecular weights on the thermal transition and binding interactions. Moreover, the CNC surface can be modified by many other thermo-responsive polymers using the "grafting-from" approach, an example is shown in Scheme 7.1. As discussed

earlier, the thermo-responsive behaviors of these polymers have been widely investigated in bulk solution in the presence and absence of surfactant molecules. However, studies on CNC surface modification with TRPs and especially studies on the interaction between TRPs and surfactants on CNC surface are rare. Since the polymer chains are grafted onto CNC surface, they may display different chain conformation compared to their behaviors in bulk solution, and the interactions with surfactants may also be different, and a comparison study is needed. On the other hand, the solvent conditions, such as salts, pH, co-solvents, also have great influence on the surfactant//polymeric nanostructures interactions, and a detailed study considering different conditions is recommended.

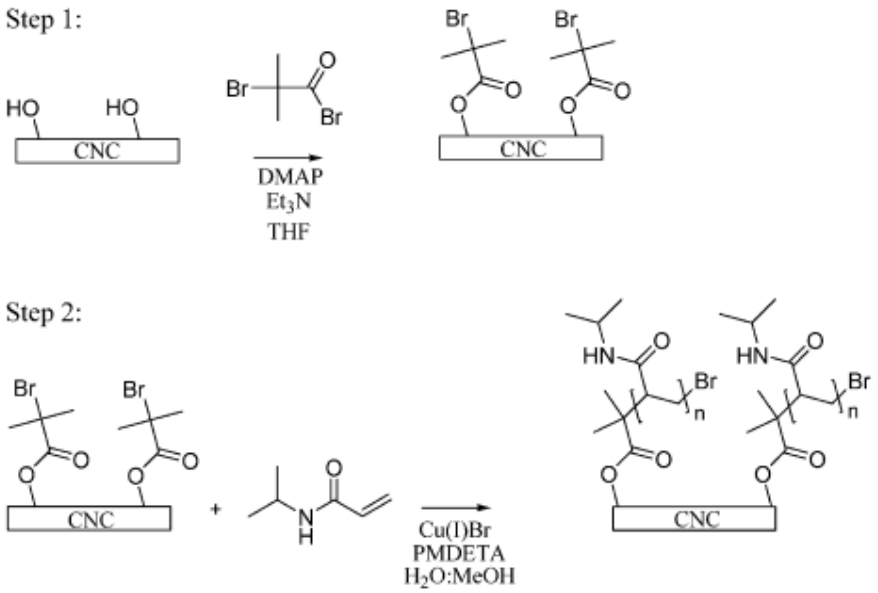

Scheme 7.1 Synthesis route for the grafting of PNIPAM from the surface of CNC. [Zoppe et al., 2010]

7.2.2 Rheological properties of TRPs-modified CNC in the presence of surfactant

CNCs are rigid rod-like crystals that process very interesting rheological and phase behavior properties, depending on their concentrations. At low concentration, CNC particles are

randomly oriented (isotropic) in aqueous solution, and when the concentration reaches a critical value, they align to form a chiral nematic ordering with the phase changing from an isotropic to an anisotropic chiral nematic liquid crystalline phase. As the concentration is increased further, aqueous CNC suspensions display a shear birefringence phenomenon. Meanwhile, the gelling properties of CNC suspensions also depend on their concentrations. In comparison with spherical particles, the shear rheology of rod-like particles is more complex considering the anisotropy of the system. Hence, on the basis of the unique properties of CNC suspensions, the addition of surfactants may alter their phase and rheological properties in suspensions and the types of surfactants (anionic, cationic and non-ionic) will have an important influence due to the negative charges on CNC surface. Therefore, studies on effect of surfactant on the rheological properties of CNC suspensions and also the TRPs-modified CNC suspensions could be very interesting and meaningful.

7.2.3 Effect of small molecules and composition on LCST

The LCST of copolymers could be varied by the addition of small molecules and changing the composition of the monomers. Lutz and co-workers [2006] synthesized a series of copolymers with tunable LCSTs of between 26 and 90 ^{o}C by varying the monomer composition, similarly, Hoogenboom et al. [2008] prepared poly(2-oxazoline)s with tunable LCSTs from 25 ^{o}C to 100 ^{o}C by varying molecular weights and compositions. The relatively higher LCST for the copolymers was attributed to the high proportion of hydrophilic monomers due to their hydrophobic-hydrophilic characteristics. In this thesis, we only examined the thermo-responsive behavior of copolymer with 1% $PEGMA_{2080}$, which exhibited an unusual two-stage thermal induced aggregation behavior in aqueous solution. Therefore, studying the effect of polymer

compositions on the thermal induced aggregation behavior would be very interesting as the hydrophobic-hydrophilic balance of the copolymers depends on the composition.

Another simpler approach to manipulate the LCST of thermoresponsive polymers has been introduced to use small molecule additives, such as salt, ionic liquid, saccharides or surfactants. It is known that salts have a significant impact on the LCST of aqueous solutions of thermoresponsive polymers, because the introduction of salt in the solution could disrupt the hydration structure surrounding the polymer chains, leading to decrease the quality of the solvent for polymer chains and favor their aggregation at a lower temperature compared with pure water. In the TRPs/surfactants systems, the surfactant hydrophobicity will play an important role in the interaction with these copolymers, since the associative behavior is driven by hydrophobic interactions. When surfactants bind to the polymer, the hydrophobic/hydrophilic balance of polymers may alter, resulting in changes in the phase transition behavior.

References

Akcasu, A. Z. and C. C. Han, "Molemlar Weight and Temperature Dependence of Polymer Dimensions in Solution," *Macromolecules* **12**, 276-280 (1979).

Alila, S., S. Boufi, M. N. Belgacem and D. Beneventi, "Adsorption of a Cationic Surfactant onto Cellulosic Fibers I. Surface Charge Effects," *Langmuir* **21**, 8106-8113 (2005).

Antunes, F. E., E. F. Marques, M. G. Miguel and B. Lindman, "Polymer-vesicle association," *Adv. Colloid Interface Sci.* **147-148**, 18-35 (2009).

Araki, J., M. Wada and S. Kuga, "Steric Stabilization of a Cellulose Microcrystal Suspension by Poly(ethylene glycol) Grafting," *Langmuir* **17**, 21-27 (2001).

Araki, J., M. Wada, S. Kuga and T. Okano, "Influence of surface charge on viscosity behavior of cellulose microcrystal suspension," *J. Wood Sci.* **45**, 258-261 (1999).

Aseyev, V., H. Tenhu and F. M. Winnik, "Non-ionic Thermoresponsive Polymers in Water," *Adv. Polym. Sci.* **242**, 29-89 (2011).

Azzam, F., L. Heux, J. L. Putaux, and B. Jean, "Preparation By Grafting Onto, Characterization, and Properties of Thermally Responsive Polymer-Decorated Cellulose Nanocrystals *Biomacromolecules* **11**, 3652-3659 (2010).

Babak, V., I. Lukina, G. Vikhoreva, J. Desbrières and M. Rinaudo, "Interfacial properties of dynamic association between chitin derivatives and surfactants," *Colloids Surf. A* **147**, 139-148 (1999).

Bao, H., L. Li, L. H. Gan and H. Zhang, "Interactions between Ionic Surfactants and Polysaccharides in Aqueous Solutions," *Macromolecules* **41**, 9406-9412 (2008).

Barbosa, S., P. Taboada, E. Castro and V. Mosquera, "Influence of SDS and two anionic hydrotropes on the micellized state of the triblock copolymer $E_{71}G_7E_{71}$," *J. Colloid Interface Sci.* **296**, 677-684 (2006).

Becer, C. R., S. Hahn, M. W. M. Fijten, H. M. L. Thijs, R. Hoogenboom and U. S. Schubert, "Libraries of Methacrylic Acid and Oligo(ethylene glycol) Methacrylate Copolymers with LCST Behavior," *J. Polym. Sci. Polym. Chem.* **46**, 7138-7147 (2008).

Beck-Candanedo, S., D. Viet and D. G. Gray, "Triphase Equilibria in Cellulose Nanocrystal Suspensions Containing Neutral and Charged Macromolecules," *Macromolecules* **40**, 3429-3436 (2007).

Beck-Candanedo, S., D. Viet and D. G. Gray, "Induced phase separation in cellulose nanocrystal suspensions containing ionic dye species," *Cellulose* **13**, 629-635 (2006).

Berlioz, S., S. Molina-Boisseau, Y. Nishiyama and L. Heux, "Gas-Phase Surface Esterification of Cellulose Microfibrils and Whiskers," *Biomacromolecules* **10**, 2144-2151 (2009).

Berret, J. F., B. Vigolo, R. Eng, P. Hervé, I. Grillo and L. Yang, "Electrostatic Self-Assembly of Oppositely Charged Copolymers and Surfactants: A Light, Neutron, and X-ray Scattering Study," *Macromolecules* **37**, 4922-4930 (2004).

Beyer, K., D. Leine and A. Blume, "The demicellization of alkyltrimethylammonium bromides in 0.1M sodium chloride solution studied by isothermal titration calorimetry," *Colloids Surf. B* **49**, 31-39 (2006).

Bloor, D. M., H. K. O. Mwakibete and E. Wyn-Jones, "EMF Studies Associated with the Binding of Cetyltrimethylammonium Bromide to the Polymers Poly(propylene oxide), Poly(vinylmethylether), and Ethyl(hydroxyethyl) Cellulose," *J. Colloid Interface Sci.* **178**, 334-338 (1996).

Bondeson, D. and K. Oksman, “Dispersion and characteristics of surfactant modified cellulose whiskers nanocomposites,” *Compos. Interfaces* **14**, 617-630 (2007).

Bonnaud, M., J. Weiss and D. J. McClements, “Interaction of a Food-Grade Cationic Surfactant (Lauric Arginate) with Food-Grade Biopolymers (Pectin, Carrageenan, Xanthan, Alginate, Dextran, and Chitosan),” *J. Agric. Food Chem.* **58**, 9770-9777 (2010).

Bordel, D., J. Putaux and L. Heux, “Orientation of Native Cellulose in an Electric Field,” *Langmuir* **22**, 4899-4901 (2006).

Boulet, M., M. Britten and F. Lamarche, “Aggregation of some food proteins in aqueous dispersions: effects of concentration, pH and ionic strength,” *Food Hydrocolloids* **14**, 135-144 (2000).

Braun, B. and J. R. Dorgan, “Single-Step Method for the Isolation and Surface Functionalization of Cellulosic Nanowhiskers,” *Biomacromolecules* **10**, 334-341 (2009).

Braun, O., J. Selb and F. Candau, “Synthesis in microemulsion and characterization of stimuli-responsive polyelectrolytes and polyampholytes based on *N*-isopropylacrylamide,” *Polymer* **42**, 8499-8510 (2001).

Brazel, C. S., “Magnetothermally-responsive Nanomaterials: Combining Magnetic Nanostructures and Thermally-Sensitive Polymers for Triggered Drug Release,” *Pharm. Res.* **26**, 644-656 (2009).

Bu, H., A. -L. Kjøniksen and B. Nyström, “Rheological Characterization of Photochemical Changes of Ethyl(hydroxyethyl)cellulose Dissolved in Water in the Presence of an Ionic Surfactant and a Photosensitizer,” *Biomacromolecules* **5**, 610-617 (2004).

Bulpitt, P. and D. Aeschlimann, “New strategy for chemical modification of hyaluronic acid: Preparation of functionalized derivatives and their use in the formation of novel biocompatible hydrogels,” *J. Biomed. Mater. Res.* **47**, 152-169 (1999).

Bütün, V., A. B. Lowe, N. C. Billingham and S. P. Armes, “Synthesis of Zwitterionic Shell Cross-Linked Micelles,” *J. Am. Chem. Soc.* **121**, 4288-4289 (1999).

Cao, Y., X. X. Zhu, J. T. Luo and H. Y. Liu, “Effects of substitution groups on the RAFT polymerization of N-alkylacrylamides in the preparation of thermosensitive block copolymers,” *Macromolecules* **40**, 6481-6488 (2007).

Casettaria, L., D. Vllasaliu, E. Castagnino, S. Stolnik, S. Howdle and L. Illum, “PEGylated chitosan derivatives: Synthesis, characterizations and pharmaceutical applications,” *Prog. Polym. Sci.* **37**, 659-685 (2012).

Çetin, N. S., P. Tingaut, N. Özmen, N. Henry, D. Harper, M. Dadmun and G. Sèbe, “Acetylation of Cellulose Nanowhiskers with Vinyl Acetate under Moderate Conditions,” *Macromol. Biosci.* **9**, 997-1003 (2009).

Chakraborty, T., I. Chakraborty and S. Ghosh, “Sodium Carboxymethylcellulose-CTAB Interaction: A Detailed Thermodynamic Study of Polymer-Surfactant Interaction with Opposite Charges,” *Langmuir* **22**, 9905-9913 (2006).

Chan, Y. -H. M., R. Schweiss, C. Werner and M. Grunze, “Electrokinetic Characterization of Oligo- and Poly(ethylene glycol)-Terminated Self-Assembled Monolayers on Gold and Glass Surfaces,” *Langmuir* **19**, 7380-7385 (2003).

Chee, C. K., S. Rimmer, I. Soutar and L. Swanson, “Time-resolved fluorescence anisotropy studies of the interaction of N-isopropyl acrylamide based polymers with sodium dodecyl sulphate,” *Soft Matter* **7**, 4705-4714 (2011).

Cheng, N., W. G. Liu, Z. Q. Cao, W. H. Ji, D. C. Liang, G. Guo and J. Y. Zhang, "A study of thermoresponsive poly(N-isopropylacrylamide)/polyarginine bioconjugate non-viral transgene vectors," *Biomaterials* **27**, 4984-4992 (2006).

Chen, H. W., J. F. Li, Y. W. Ding, G. Z. Zhang, Q. J. Zhang and C. Wu, "Folding and Unfolding of Individual PNIPAM-*g*-PEO Copolymer Chains in Dilute Aqueous Solutions," *Macromolecules* **38**, 4403-4408 (2005).

Chen, G., A. Dufresne, J. Huang and P. R. Chang, "A Novel Thermoformable Bionanocomposite Based on Cellulose Nanocrystal-graft-Poly(ε-caprolactone)," *Macromol. Mater. Eng.* **294**, 59-67 (2009).

Chen, J. Q., H. J. Xue, Y. F. Yao, H. Yang, A. M. Li, M. Xu, Q. Chen and R. S. Cheng, "Effect of Surfactant Concentration on the Complex Structure of Poly(*N*-isopropylacrylamide)/Sodium *n*-Dodecyl Sulfate in Aqueous Solutions," *Macromolecules* **45**, 5524-5529 (2012).

Chen, J. Q., X. L. Gong, H. Yang, Y. F. Yao, M. Xu, Q. Chen and R. S. Cheng, "NMR Study on the Effects of Sodium n-Dodecyl Sulfate on the Coil-to-Globule Transition of Poly(N-isopropylacrylamide) in Aqueous Solutions," *Macromolecules* **44**, 6227-6231 (2011).

Chen, K. -S., J. -C. Tsai, C. -W. Chou, M. -R. Yang and J. -M. Yang, "Effects of additives on the photo-induced grafting polymerization of *N*-isopropylacrylamide gel onto PET film and PP nonwoven fabric surface," *Mater. Sci. Eng. C* **20**, 203-208 (2002).

Chen, S., B. Yang, C. Guo, J. H. Ma, L. R. Yang, X. F. Liang, C. Hua and H. Z. Liu, "Spontaneous Vesicle Formation of Poly(ethylene oxide)-Poly(propylene oxide)-Poly(ethylene oxide) Triblock Copolymer," *J. Phys. Chem. B* **112**, 15659-15665 (2008).

Chen, X. R., X. B. Ding, Z. H. Zheng and Y. X. Peng, "Thermosensitive polymeric vesicles self-assembled by PNIPAAm-b-PPG-b-PNIPAAm triblock copolymers," *Colloid Polym. Sci.* **283**, 452-455 (2005).

Chiefari, J., Y. K. Chong, F. Ercole, J. Krstina, J. Jeffery, T. P. T. Le, R. T. A. Mayadunne, G. F. Meijs, C. L. Moad, G. Moad, E. Rizzardo and S. H. Thang, "Living Free-Radical Polymerization by Reversible Addition-Fragmentation Chain Transfer: The RAFT Process," *Macromolecules* **31**, 5559-5562 (1998).

Choi, S. H., S. H. Lee and T. G. Park, "Temperature-Sensitive Pluronic/Poly(ethylenimine) Nanocapsules for Thermally Triggered Disruption of Intracellular Endosomal Compartment," *Biomacromolecules* **7**, 1864-1870 (2006).

Chytil, M. and M. Pekař, "Effect of new hydrophobic modification of hyaluronan on its solution properties: evaluation of self-aggregation," *Carbohydr. Polym.* **76**, 443-448 (2009).

Ciferri, A. and S. Kudaibergenov, "Natural and Synthetic Polyampholytes, Theory and Basic Structures," *Macromol. Rapid Commun.* **28**, 1953-1968 (2007).

Convertine, A. J., N. Ayres, C. W. Scales, A. B. Lowe and C. L. McCormick, "Facile, Controlled, Room-temperature RAFT Polymerization of *N*-isopropylacrylamide," *Biomacromolecules* **5**, 1177-1180 (2004).

Convertine, A. J., B. S. Lokitz, Y. Vasileva, L. J. Myrick, C. W. Scales, A. B. Lowe and C. L. McCormick, "Direct synthesis of thermally responsive DMA/NIPAM diblock and DMA/NIPAM/DMA triblock copolymers via aqueous, room temperature RAFT polymerization," *Macromolecules* **39**, 1724-1730 (2006).

Couderc, S. M., G. A. Fox, D. M. Bloor, J. F. Holzwarth and E. Wyn-Jones, "EMF and Microcalorimetry Studies Associated with the Binding of the Cationic Surfactants to Neutral Polymers," *Langmuir* **15**, 5474-5479 (1999).

Courtois, J. and J. -F. Berret, "Probing Oppositely Charged Surfactant and Copolymer Interactions by Isothermal Titration Microcalorimetry," *Langmuir* **26**, 11750-11758 (2010).

Crespy, D. and R. M. Rossi, "Temperature-responsive polymers with LCST in the physiological range and their applications in textiles," *Polym. Int.* **56**, 1461-1468 (2007).

Creutz, S., J. van Stam, S. Antoun, F. C. De Schryver and R. Jérôme, "Exchange of Polymer Molecules between Block Copolymer Micelles Studied by Emission Spectroscopy. A Method for the Quantification of Unimer Exchange Rates," *Macromolecules* **30**, 4078-4083 (1997).

Cunliffe, D., C. de las Heras Alarcón, V. S. J. R. Peters and C. Alexander, "Thermoresponsive Surface-Grafted Poly(*N*-isopropylacrylamide) Copolymers: Effect of Phase Transitions on Protein and Bacterial Attachment," *Langmuir* **19**, 2888-2899 (2003).

Dai, S., K. C. Tam, E. Wyn-Jones and R. D. Jenkins, "Isothermal Titration Calorimetric and Electromotive Force Studies on Binding Interactions of Hydrophobic Ethoxylated Urethane and Sodium Dodecyl Sulfate of Different Molecular Masses," *J. Phys. Chem. B* **108**, 4979-4988 (2004).

Dai, S. and K. C. Tam, "Isothermal Titration Calorimetric Studies on the Temperature Dependence of Binding Interactions between Poly(propylene glycol)s and Sodium Dodecyl Sulfate," *Langmuir* **20**, 2177-2183 (2004).

Dai, S. and K. C. Tam, "Isothermal Titration Calorimetry Studies of Binding Interactions between Polyethylene Glycol and Ionic Surfactants," *J. Phys. Chem. B* **105**, 10759-10763 (2001).

Dai, S., K. C. Tam and L. Li, "Isothermal Titration Calorimetric Studies on Interactions of Ionic Surfactant and Poly(oxypropylene)-Poly(oxyethylene)-Poly(oxypropylene) Triblock Copolymers in Aqueous Solutions," *Macromolecules* **34**, 7049-7055 (2001).

Dai, S., P. Ravi, K. C. Tam, B. W. Mao and L. H. Gan, "Novel pH-Responsive Amphiphilic Diblock Copolymers with Reversible Micellization Properties," *Langmuir* **19**, 5175-5177 (2003).

Dai, S., P. Ravi and K. C. Tam, "Thermo- and photo-responsive polymeric systems," *Soft Matter* **5**, 2513-2533 (2009).

Dėdinaitė, A. and M. Ernstsson, "Chitosan-SDS Interactions at a Solid-Liquid Interface: Effects of Surfactant Concentration and Ionic Strength," *J. Phys. Chem. B* **107**, 8181-8188 (2003).

de Rodriguez, N. L. G., W. Thielemans and A. Dufresne, "Sisal cellulose whiskers reinforced polyvinyl acetate nanocomposites," *Cellulose* **13**, 261-270 (2006).

de Vasconcelos, C. L., P. M. Bezerril, D. E. S. dos Santos, T. N. C. Dantas, M. R. Pereira and J. L. C. Fonseca, "Effect of Molecular Weight and Ionic Strength on the Formation of Polyelectrolyte Complexes Based on Poly(methacrylic acid) and Chitosan," *Biomacromolecules* **7**, 1245-1252 (2006).

Dimitrov, I., B. Trzebicka, A. H. E. Müller, A. Dworak and C. B. Tsvetanov, "Thermosensitive water-soluble copolymers with doubly responsive reversibly interacting entities," *Prog. Polym. Sci.* **32**, 1275-1343 (2007).

Dimitrov, P., S. Rangelov, A. Dworak and C. B. Tsvetanov, "Synthesis and Associating Properties of Poly(ethoxyethyl glycidyl ether)/Poly(propylene oxide) Triblock Copolymers," *Macromolecules* **37**, 1000-1008 (2004).

Dong, S. P. and M. Roman, "Fluorescently Labeled Cellulose Nanocrystals for Bioimaging Applications," *J. Am. Chem. Soc.* **129**, 13810-13811 (2007).

Dong, X. M., T. Kimura, J. -F. Revol and D. G. Gray, "Effects of Ionic Strength on the Isotropic-Chiral Nematic Phase Transition of Suspensions of Cellulose Crystallites," *Langmuir* **12**, 2076-2082 (1996).

Dong, X. M. and D. G. Gray, "Effect of Counterions on Ordered Phase Formation in Suspensions of Charged Rodlike Cellulose Crystallites," *Langmuir* **13**, 2404-2409 (1997).

Dreher, M. R., D. Raucher, N. Balu, O. M. Colvin, S. M. Ludeman and A. Chilkoti, "Evaluation of an elastin-like polypeptide-doxorubicin conjugate for cancer therapy," *J. Control. Release* **91**, 31-43 (2003).

Dubief, D., E. Samain and A. Dufresne, "Polysaccharide Microcrystals Reinforced Amorphous Poly(*β*-hydroxyoctanoate) Nanocomposite Materials," Macromolecules **32**, 5765-5771 (1999).

Dufresne, A., "Polysaccharide nanocrystal reinforced nanocomposites," *Can. J. Chem.* **86**, 484-494 (2008).

Du, F. -S., Y. Wang, R. Zhang and Z. -C. Li, "Intelligent nucleic acid delivery systems based on stimuli-responsive polymers," *Soft Matter* **6**, 835-848 (2010).

Edgar, C. D. and D. G. Gray, "Influence of Dextran on the Phase Behavior of Suspensions of Cellulose Nanocrystals," *Macromolecules* **35**, 7400-7406 (2002).

Eichhorn, S. J., "Cellulose nanowhiskers: promising materials for advanced applications," *Soft Matter* **7**, 303-315 (2011).

Elazzouzi-Hafraoui, S., J. Putaux and L. Heux, "Self-assembling and Chiral Nematic Properties of Organophilic Cellulose Nanocrystals," *J. Phys. Chem. B* **113**, 11069-11075 (2009).

Elazzouzi-Hafraoui, S., Y. Nishiyama, J. Putaux, L. Heux, F. Dubreuil and C. Rochas, "The Shape and Size Distribution of Crystalline Nanoparticles Prepared by Acid Hydrolysis of Native Cellulose," *Biomacromolecules* **9**, 57-65 (2008).

Evertsson, H. and S. Nilsson, "Microstructures formed in aqueous solutions of a hydrophobically modified nonionic cellulose derivative and sodium dodecyl sulfate: a fluorescence probe investigation," *Carbohydrate Polymers* **40**, 293-298 (1999).

Fan, Y. X., Y. Liu, J. Q. Xi and R. Guo "Vesicle formation with amphiphilic chitosan derivatives and a conventional cationic surfactant in mixed systems," *J. Colloid Interface Sci.* **360**, 148-153 (2011).

Favier, V., H. Chanzy and J. Y. Cavaille, "Polymer Nanocomposites Reinforced by Cellulose Whiskers," *Macromolecules* **28**, 6365-6367 (1995).

Fechner, M., S. Kosmella and J. Koetz, "pH-dependent polyampholyte SDS interactions," *J. Colloid Interface Sci.* **345**, 384-391 (2010).

Fleming, K., D. G. Gray, S. Prasannan and S. Matthews, "Cellulose Crystallites: A New and Robust Liquid Crystalline Medium for the Measurement of Residual Dipolar Couplings," *J. Am. Chem. Soc.* **122**, 5224-5225 (2000).

Ganachaud, F., M. J. Monteiro, R. G. Gilbert, M. A. Dourges, S. H. Thang and E. Rizzardo, "Molecular weight characterization of poly(Nisopropylacrylamide) prepared by living free-radical polymerization," *Macromolecules* **33**, 6738-6745 (2000).

Gan, D. J. and L. A. Lyon, "Synthesis and Protein Adsorption Resistance of PEG-Modified Poly(N-isopropylacrylamide) Core/Shell Microgels," *Macromolecules* **35**, 9634-9639 (2002).

Gao, X., N. Kučerka, M. -P. Nieh, J. Katsaras, S. P. Zhu, J. L. Brash and H. Sheardown, "Chain Conformation of a New Class of PEG-Based Thermo-responsive Polymer Brushes Grafted on Silicon as Determined by Neutron Reflectometry," *Langmuir* **25**, 10271-10278 (2009).

George, J., P. Sudheesh, P. N. Reddy and L. Sreejith, "Influence of Salt on Cationic Surfactant-Biopolymer Interactions in Aqueous Media," *J. Solution Chem.* **38**, 373-381 (2009).

Ghoreishi, S. M., Y. Li, D. M. Bloor, J. Warr and E. Wyn-Jones, "Electromotive Force Studies Associated with the Binding of Sodium Dodecyl Sulfate to a Range of Nonionic Polymers," *Langmuir* **15**, 4380-4387 (1999).

Gil, E. S., D. J. Frankowski, R. J. Spontak and S. M. Hudson, "Swelling Behavior and Morphological Evolution of Mixed Gelatin/Silk Fibroin Hydrogels," *Biomacromolecules* **6**, 3079-3087 (2005).

Gil, E. S. and S. M. Hudson, "Stimuli-reponsive polymers and their bioconjugates," *Prog. Polym. Sci.* **29**, 1173-1222 (2004).

Goussé, C., H. Chanzy, G. Excoffier, L. Soubeyrand and E. Fleury, "Stable suspensions of partially silylated cellulose whiskers dispersed in organic solvents," *Polymer* **43**, 2645-2651 (2002).

Grunert, M. and W. T. Winter, "Nanocomposites of Cellulose Acetate Butyrate Reinforced with Cellulose Nanocrystals," *J. Polym. Environ.* **10**, 27-30 (2002).

Guillot, S., M. Delsanti, S. Désert and D. Langevin, "Surfactant-Induced Collapse of Polymer Chains and Monodisperse Growth of Aggregates near the Precipitation Boundary in Carboxymethylcellulose-DTAB Aqueous Solutions," *Langmuir* **19**, 230-237 (2003).

Habibi, Y., A. Goffin, N. Schiltz, E. Duquesne, P. Dubois and A. Dufresne, "Bionanocomposites based on poly(ε-caprolactone)-grafted cellulose nanocrystals by ring-opening polymerization," *J. Mater. Chem.* **18**, 5002-5010 (2008).

Habibi, Y., H. Chanzy and M. Vignon, "TEMPO-mediated surface oxidation of cellulose whiskers," *Cellulose* **13**, 679-687 (2006).

Habibi, Y., I. Hoeger, S. S. Kelley and O. J. Rojas, "Development of Langmuir-Schaeffer Cellulose Nanocrystal Monolayers and Their Interfacial Behaviors," *Langmuir* **26(2)**, 990-1101 (2010).

Habibi, Y., L. A. Lucia and O. J. Rojas, "Cellulose Nanocrystals: Chemistry, Self-Assembly, and Applications," *Chem. Rev.* **110**, 3479-3500 (2010).

Habibi, Y., L. Foulon, V. Aguié-Béghin, M. Molinari and R. Douillard, "Langmuir-Blodgett films of cellulose nanocrystals: Preparation and characterization," *J. Colloid Interface Sci.* **316**, 388-397 (2007).

Habibi, Y., T. Heim and R. Douillard, "AC electric field-assisted assembly and alignment of cellulose nanocrystals," *J. Polym. Sci. B Polym. Phys.* **46**, 1430-1436 (2008).

Ha, C. S. and J. A. Gardella, "Surface Chemistry of Biodegradable Polymers for Drug Delivery Systems," *Chem. Rev.* **105**, 4205-4232 (2005).

Hait, S. K. and S. P. Moulik, "Determination of Critical Micelle Concentration (CMC) of Nonionic Surfactants by Donor-Acceptor Interaction with Iodine and Correlation of CMC with Hydrophile-Lipophile Balance and Other Parameters of the Surfactants," *J. Surfact. Deterg.* **4**, 303-309 (2001).

Han, S., M. Hagiwara and T. Ishizone, "Synthesis of Thermally Sensitive Water-Soluble Polymethacrylates by Living Anionic Polymerizations of Oligo(ethylene glycol) Methyl Ether Methacrylates," *Macromolecules* **36**, 8312-8319 (2003).

Hansson, P. and B. Lindman, "Surfactant-polymer interactions," *Curr. Opin. Colloid Interface Sci.* **1**, 604-613 (1996).

Hao, J. K., Z. Y. Li, H. Cheng, C. Wu and C. C. Han, "Kinetically Driven Intra- and Interchain Association of Hydrophobically and Hydrophilically Modified Poly(acrylic acid) in Dilute Aqueous Solutions," *Macromolecules* **43**, 9534-9540 (2010).

Hasan, E., M. Zhang, A. H. E. Müller and Ch. B. Tsvetanov, "Thermoassociative Block Copolymers of Poly(*N*-Isopropylacrylamide) and Poly(Propylene Oxide)," *J. Macromol. Sci. A* **41**, 467-486 (2004).

Hasani, M., E. D. Cranston, G. Westman and D. G. Gray, "Cationic surface functionalization of cellulose nanocrystals," *Soft Matter* **4**, 2238-2244 (2008).

He, C. L., S. W. Kim and D. S. Lee, "*In situ* gelling stimuli-sensitive block copolymer hydrogels for drug delivery," *J. Control. Release* **127**, 189-207 (2008).

Heux, L., G. Chauve and C. Bonini, "Nonflocculating and Chiral-Nematic Self-ordering of Cellulose Microcrystals Suspensions in Nonpolar Solvents," *Langmuir* **16**, 8210-8212 (2000).

Hinrichs, W. L. J., N. M. E. Schuurmans-Nieuwenbroek, P. van de Wetering and W. E. Hennink, "Thermosensitive polymers as carriers for DNA delivery," *J. Control. Release* **60**, 249-259 (1999).

Hirsch, S. G. and R. J. Spontak, "Temperature-dependent property development in hydrogels derived from hydroxypropylcellulose," *Polymer* **43**, 123-129 (2002).

Hoff, E., B. Nyström and B. Lindman, "Polymer-Surfactant Interactions in Dilute Mixtures of a Nonionic Cellulose Derivative and an Anionic Surfactant," *Langmuir* **17**, 28-34 (2001).

Holmberg, K., B. Jönsson, B. Kronberg, B. Lindman Surfactants and Polymers in Aqueous Solution 2nd edition, Wiley-Blackwell, 2002

Hoogenboom, R., H. M. L. Thijs, M. J. H. C. Jochems, B. M. van Lankvelt, M. W. M. Fijten and U. S. Schubert, "Tuning the LCST of poly(2-oxazoline)s by varying composition and molecular weight: alternatives to poly(N-isopropylacrylamide)?" *Chem. Commun.* **44**, 5758-5760 (2008).

Hou, J., Z. Liu, S. Zhang, X. Yue and J. Yang, "The role of viscoelasticity of alkali/surfactant/polymer solutions in enhanced oil recovery," *J. Petrol. Sci. Eng.* **47**, 219-235 (2005).

Hsu, Y. H., W. H. Chiang, M. C. Chen, C. S. Chern and H. C. Chiu, "Effects of SDS on the Thermo- and pH-Sensitive Structural Changes of the Poly(acrylic acid)-Based Copolymer Containing Both Poly(*N*-isopropylacrylamide) and Monomethoxy Poly(ethylene glycol) Grafts in Water," *Langmuir* **22**, 6764-6770 (2006).

Hua, F., X. Jiang and B. Zhao, "Temperature-Induced Self-Association of Doubly Thermosensitive Diblock Copolymers with Pendant Methoxytris(oxyethylene) Groups in Dilute Aqueous Solutions," *Macromolecules* **39**, 3476-3479 (2006).

Huang, X., Y. Han, Y. Wang, M. Cao and Y. Wang, "Aggregation properties of cationic gemini surfactants with dihydroxyethylamino headgroups in aqueous solution," *Colloids Surf. A* 325, 26-32 (2008).

Hurtgen, M., J. Liu, A. Debuigne, C. Jerome and C. Detrembleur, "Synthesis of Thermo-Responsive Poly(*N*-vinylcaprolactam)-Containing Block Copolymers by Cobalt-Mediated Radical Polymerization," *J. Polym. Sci. Polym. Chem.* **50**, 400-408 (2012).

Ishaug-Riley, S. L., L. E. Okun, G. Prado, M. A. Applegate and A. Ratcliffe, "Human articular chondrocyte adhesion and proliferation on synthetic biodegradable polymer films," *Biomaterials* **20**, 2245-2256 (1999).

Ishizone, T., A. Seki, M. Hagiwara, S. Han, H. Yokoyama, A. Oyane, A. Deffieux and S. Carlotti, "Anionic Polymerizations of Oligo(ethylene glycol) Alkyl Ether Methacrylates: Effect of Side Chain Length and ω-Alkyl Group of Side Chain on Cloud Point in Water," *Macromolecules* **41**, 2963-2967 (2008).

Isogai, N., J. P. Gong and Y. Osada, "Thermosensitive Polymer Gel by Reversible Surfactant Binding," *Macromolecules* **29**, 6803-6806 (1996).

Ito, S., K. Ogawa, H. Suzuki, B. L. Wang, R. Yoshida and E. Kokufuta, "Preparation of Thermosensitive Submicrometer Gel Particles with Anionic and Cationic Charges," *Langmuir* **15**, 4289-4294 (1999).

Jackson, J. K., K. Letchford, B. Z. Wasserman, L. Ye, W. Y. Hamad and H. M. Burt, "The use of nanocrystalline cellulose for the binding and controlled release of drugs," *Int. J. Nanomedicine* **6**, 321-330 (2011).

Jelesarov, I. and H. R. Bosshard, "Isothermal titration calorimetry and differential scanning calorimetry as complementary tools to investigate the energetics of biomolecular recognition," *J. Mol. Recognit.* **12**, 3-18 (1999).

Jiang, B., C. Liu, C. Zhang, B. Wang and Z. Wang, "The effect of non-symmetric distribution of fiber orientation and aspect ratio on elastic properties of composites," *Composites Part B* **38**, 24-34 (2007).

Jiang, X, G., C. A. Lavender, J. W. Woodcock and B. Zhao, "Multiple Micellization and Dissociation Transitions of Thermo- and Light-Sensitive Poly(ethylene oxide)-b-poly(ethoxytri(ethylene glycol) acrylate-co-o-nitrobenzyl acrylate) in Water," *Macromolecules* **41**, 2632-2643 (2008).

Jonas, A. M., K. Glinel, R. Oren, B. Nysten and W. T. S. Huck, "Thermo-Responsive Polymer Brushes with Tunable Collapse Temperatures in the Physiological Range," *Macromolecules* **40**, 4403-4405 (2007).

Junior de Menezes, A., G. Siqueira, A. A. S. Curvelo and A. Dufresne, "Extrusion and characterization of functionalized cellulose whiskers reinforced polyethylene nanocomposites," *Polymer* **50**, 4552-4563 (2009).

Kang, H. M., B. L. Peng, Y. Y. Liang, X. Han and H. L. Liu, "Study of the interaction between a diblock polyelectrolyte PDMA-*b*-PAA and a gemini surfactant 12-*6*-12 in basic media," *J. Colloid Interface Sci.* **333**, 135-140 (2009).

Kang, H. M., Y. L. Cai, J. J. Deng, H. J. Zhang, Y. F. Tang and P. S. Liu, "Synthesis and aqueous solution behavior of phosphonate-functionalized chitosans," *Eur. Polym. J.* **42**, 2678-2685 (2006).

Kim, J., G. Montero, Y. Habibi, J. P. Hinestroza, J. Genzer, D. S. Argyropoulos and O. J. Rojas, "Dispersion of cellulose crystallites by nonionic surfactants in a hydrophobic polymer matrix," *Polym. Eng. Sci.* **49**, 2054-2061 (2009).

Kitano, H., T. Hirabayashi, M. Gemmei-Ide and M. Kyogoku, “Effect of Macrocycles on the Temperature-Responsiveness of Poly[(methoxydiethylene glycol methacrylate)-*graft*-PEG],” *Macromol. Chem. Phys.* **205**, 1651-1659 (2004).

Kjøniksen, A. -L., B. Nyström and B. Lindman, “Dynamic Viscoelasticity of Gelling and Nongelling Aqueous Mixtures of Ethyl(hydroxyethyl)cellulose and an Ionic Surfactant,” *Macromolecules* **31**, 1852-1858 (1998).

Kjøniksen, A. -L., K. D. Knudsen and B. Nyström, “Phase separation and structural properties of semidilute aqueous mixtures of ethyl(hydroxyethyl)cellulose and an ionic surfactant,” *Eur. Polym. J.* **41**, 1954-1964 (2005).

Kjøniksen, A. -L., N. Beheshti, H. K. Kotlar, K. Zhu and B. Nyström, “Modified polysaccharides for use in enhanced oil recovery applications,” *Eur. Polym. J.* **44**, 959-967 (2008).

Klemm, D., F. Kramer, S. Moritz, T. Lindström, M. Ankerfors, D. Gray and A. Dorris, “Nanocelluloses: A New Family of Nature-Based Materials,” *Angew. Chem. Int. Ed.* **50**, 2-31 (2011).

Kloser, E. and D. G. Gray, “Surface Grafting of Cellulose Nanocrystals with Poly(ethylene oxide) in Aqueous Media,” *Langmuir* **26**, 13450-13456 (2010).

Kovacs, T., V. Naish, B. O’Connor, C. Blaise, F. Gagne, L. Hall, V. Trudeau and P. Martel “An ecotoxicological characterization of nanocrystalline cellulose (NCC),” *Nanotoxicology* **4(3)**, 255-270, (2010).

Kresge, C. T., M. E. Leonowicz, W. J. Roth, J. C. Vartuli and J. S. Beck, “Ordered mesoporous molecular sieves synthesized by a liquid-crystal template mechanism,” *Nature* **359**, 710-712 (1992).

Kudaibergenov, S. and A. Ciferri, “Natural and Synthetic Polyampholytes, Functions and Applications,” *Macromol. Rapid Commun.* **28**, 1969-1986 (2007).

Kurisawa, M., M. Yokoyama and T. Okano, “Gene expression control by temperature with thermo-responsive polymeric gene carriers,” *J. Control. Release* **69**, 127-137 (2000).

Kwak, J. C. T., Polymer-Surfactant Systems, Surfactant Science Series, ed., Marcel Dekker, New York, 1998, vol. 77.

La Mesa, C. “Polymer-surfactant and protein-surfactant interactions,” *J. Colloid Interface Sci.* **286**, 148-157 (2005).

Lee, S. H., S. H. Choi, S. H. Kim and T. G. Park, “Thermally sensitive cationic polymer nanocapsules for specific cytosolic delivery and efficient gene silencing of siRNA: Swelling induced physical disruption of endosome by cold shock,” *J. Control. Release* **125**, 25-32 (2008).

Levis, S. R. and P. B. Deasy, “Pharmaceutical applications of size reduced grades of surfactant co-processed microcrystalline cellulose,” *Int. J. Pharmaceut.* **230**, 25-33 (2001).

Li, C. C., C. Lavigueur and X. X. Zhu, “Aggregation and Thermoresponsive Properties of New Star Block Copolymers with a Cholic Acid Core,” *Langmuir* **27**, 11174-11179 (2011).

Li, C. M., N. J. Buurma, I. Haq, C. Turner, S. P. Armes, V. Castelletto, I. W. Hamley and A. L. Lewis, “Synthesis and Characterization of Biocompatible, Thermoresponsive ABC and ABA Triblock Copolymer Gelators,” *Langmuir* **21**, 11026-11033 (2005).

Li, G. B., H. M. Ma and J. C. Hao, “Surfactant ion-selective electrodes: A promising approach to the study of the aggregation of ionic surfactants in solution,” *Soft Matter* **8**, 896-909 (2012).

Lim, P. F. C., L. Y. Chee, S. B. Chen and B. H. Chen, "Study of Interaction between Cetyltrimethylammonium Bromide and Poly(acrylic acid) by Rheological Measurements," *J. Phys. Chem. B* **107**, 6491-6496 (2003).

Linden, van der E. and P. Venema, "Self-assembly and aggregation of proteins," *Curr. Opin. Colloid Interface Sci.* **12**, 158-165 (2007).

Lindman, B., A. Carlsson, G. Karlström and M. Malmsten, "Nonionic Polymers and Surfactants -some Anomalies in Temperature Dependence and in Interactions with Ionic Surfactants," *Adv. Colloid Interface Sci.* **32**, 183-203 (1990).

Lin, N., G. Chen, J. Huang, A. Dufresne and P. R. Chang, "Effects of polymer-grafted natural nanocrystals on the structure and mechanical properties of poly(lactic acid): A case of cellulose whisker-graft-polycaprolactone," *J. Appl. Polym. Sci.* **113**, 3417-3425 (2009).

Liu, F. and M. W. Urban, "Recent advances and challenges in designing stimuli-responsive polymers," *Prog. Polym. Sci.* **35**, 3-23 (2010).

Liu, J. Q., M. L. Zhai and H. F. Ha, "Pre-irradiation grafting of temperature sensitive hydrogel on cotton cellulose fabric," *Radiat. Phys. Chem.* **55**, 55-59 (1999).

Liu, S. and S. P. Armes, "Synthesis and Aqueous Solution Behavior of a pH-Responsive Schizophrenic Diblock Copolymer," *Langmuir* **19**, 4432-4438 (2003).

Li, X., Y. Cheng, C. Yi, Y. Hua, C. Yang and S. Cui, "Effect of ionic strength on the heat-induced soy protein aggregation and the phase separation of soy protein aggregate/dextran mixtures," *Food Hydrocolloids* **23**, 1015-1023 (2009).

Li, Y., R. Xu, S. Couderc, D. M. Bloor, E. Wyn-Jones and J. F. Holzwarth, "Binding of Sodium Dodecyl Sulfate (SDS) to the ABA Block Copolymer Pluronic F127 ($EO_{97}PO_{69}EO_{97}$): F127 Aggregation Induced by SDS," *Langmuir* **17**, 183-188 (2001).

Li, Y., R. Xu, S. Couderc, D. M. Bloor, J. F. Holzwarth and E. Wyn-Jones, "Binding of Tetradecyltrimethylammonium Bromide to the ABA Block Copolymer Pluronic F127 (EO_{97} $PO_{69}EO_{97}$): Electromotive Force, Microcalorimetry, and Light Scattering Studies," *Langmuir* **17**, 5742-5747 (2001).

Li, Z. M., Q. H. He, D. Ma and H. W. Chen, "On-chip integrated multi-thermo-actuated microvalves of poly(*N*-isopropylacrylamide) for microflow injection analysis," *Anal. Chim. Acta* **665**, 107-112 (2010).

Ljungberg, N., C. Bonini, F. Bortolussi, C. Boisson, L. Heux and J. Y. Cavaillé, "New Nanocomposite Materials Reinforced with Cellulose Whiskers in Atactic Polypropylene: Effect of Surface and Dispersion Characteristics," *Biomacromolecules* **6**, 2732-2739 (2005).

Ljungberg, N., J. -Y. Cavaillé and L. Heux, "Nanocomposites of isotactic polypropylene reinforced with rod-like cellulose whiskers," *Polymer* **47**, 6285-6292 (2006).

Loh, W., L. A. C. Teixeira and L. -T. Lee, "Isothermal Calorimetric Investigation of the Interaction of Poly(N-isopropylacrylamide) and Ionic Surfactants," *J. Phys. Chem. B* **108**, 3196-3201 (2004).

Lowe, A. B., N. C. Billingham and S. P. Armes, "Synthesis and Characterization of Zwitterionic Block Copolymers," *Macromolecules* **31**, 5991-5998 (1998).

Lutz, J. -F. and A. Hoth, "Preparation of Ideal PEG Analogues with a Tunable Thermosensitivity by Controlled Radical Copolymerization of 2-(2-Methoxyethoxy)ethyl Methacrylate and Oligo(ethylene glycol) Methacrylate," *Macromolecules* **39**, 893-896 (2006).

Lutz, J.-F., K. Weichenhan, Ö. Akdemir and A. Hoth, "About the Phase Transitions in Aqueous Solutions of Thermoresponsive Copolymers and Hydrogels Based on 2-(2-

methoxyethoxy)ethyl Methacrylate and Oligo(ethylene glycol) Methacrylate," *Macromolecules* **40**, 2503-2508 (2007).

Lutz, J. -F., Ö. Akdemir and A. Hoth, "Point by Point Comparison of Two Thermosensitive Polymers Exhibiting a Similar LCST: Is the Age of Poly(NIPAM) Over?" *J. Am. Chem. Soc.* **128**, 13046-13047 (2006).

Lutz, J. -F., "Polymerization of Oligo(Ethylene Glycol) (Meth)Acrylates: Toward New Generations of Smart Biocompatible Materials," *J. Polym. Sci. Polym. Chem.* **46**, 3459-3470 (2008).

Lutz, J. -F., "Thermo-Switchable Materials Prepared Using the OEGMA-Platform," *Adv. Mater.* **23**, 2237-2243 (2011).

Mahmoud, K. A., K. B. Male, S. Hrapovic and J. H. T. Luong, "Cellulose Nanocrystal/Gold Nanoparticle Composite as a Matrix for Enzyme Immobilization," *ACS Appl. Mater. Interfaces* **1**, 1383-1386 (2009).

Ma, H. W., M. Wells, T. P. Beebe, Jr. and A. Chilkoti, "Surface-Initiated Atom Transfer Radical Polymerization of Oligo(ethylene glycol) Methyl Methacrylate from a Mixed Self-Assembled Monolayer on Gold," *Adv. Funct. Mater.* **16**, 640-648 (2006).

Ma, J. H., C. Guo, Y. L. Tang and H. Z. Liu, "^{1}H NMR Spectroscopic Investigations on the Micellization and Gelation of PEO-PPO-PEO Block Copolymers in Aqueous Solutions," *Langmuir* **23**, 9596-9605 (2007).

Makhaeva, E. E., H. Tenhu and A. R. Khokhlov, "Conformational Changes of Poly(vinylcaprolactam) Macromolecules and Their Complexes with Ionic Surfactants in Aqueous Solution," *Macromolecules* **31**, 6112-6118 (1998).

Mangalam, A. P., J. Simonsen and A. S. Benight, "Cellulose/DNA Hybrid Nanomaterials," *Biomacromolecules* **10**, 497-504 (2009).

Mano, J. F., "Stimuli-Responsive Polymeric Systems for Biomedical Applications," *Adv. Eng. Mater.* **10**, 515-527 (2008).

Mata, J., J. Patel, N. Jain, G. Ghosh and P. Bahadur, "Interaction of cationic surfactants with carboxymethylcellulose in aqueous media," *J. Colloid Interface Sci.* **297**, 797-804 (2006).

Mao, Z. W., L. Ma, J. Yan, M. Yan, C. Y. Gao and J. C. Shen, "The gene transfection efficiency of thermoresponsive N,N,N-trimethylchitosan chloride-g-poly(N-isopropylacrylamide) copolymer," *Biomaterials* **28**, 4488-4500 (2007).

Marchessault, R. H., G. Bremner and G. Chauve, "Fishing for Proteins with Magnetic Cellulosic Nanocrystals," in "Polysaccharides for Drug Delivery and Pharmaceutical Applications," Anonymous American Chemical Society (2006), pp. 3-17.

McLoughlin, D., M. Impéror-Clerc and D. Langevin, "A New Cubic Phase Containing DNA and a Surfactant," *ChemPhysChem* **5**, 1619-1623 (2004).

Meagher, R. J. and T. A. Hatton, "Enthalpy Measurements in Aqueous SDS/DTAB Solutions Using Isothermal Titration Microcalorimetry," *Langmuir* **14**, 4081-4087 (1998).

Mészáros, R., I. Varga and T. Gilányi, "Effect of Polymer Molecular Weight on the Polymer/Surfactant Interaction," *J. Phys. Chem. B* **109**, 13538-13544 (2005).

Meyer, D. E., B. C. Shin, G. A. Kong, M. W. Dewhirst and A. Chilkoti, "Drug targeting using thermally responsive polymers and local Hyperthermia," *J. Control. Release* **74**, 213-224 (2001).

Mincheva, R., F. Bougard, D. Paneva, M. Vachaudez, N. Manolova, P. Dubois and I. Rashkov, "Self-Assembly of *N*-Carboxyethylchitosan Near the Isoelectric Point," *J. Polym. Sci.: Part A: Polym. Chem.* **46**, 6712-6721 (2008).

Montanari, S., M. Roumani, L. Heux and M. R. Vignon, "Topochemistry of Carboxylated Cellulose Nanocrystals Resulting from TEMPO-Mediated Oxidation," *Macromolecules* **38**, 1665-1671 (2005).

Morandi, G., L. Heath and W. Thielemans, "Cellulose Nanocrystals Grafted with Polystyrene Chains through Surface-Initiated Atom Transfer Radical Polymerization (SI-ATRP)," *Langmuir* **25**, 8280-8286 (2009).

Morris, C., B. Szczupak, A. S. Klymchenko and A. G. Ryder, "Study of Water Adsorption in Poly(N-isopropylacrylamide) Thin Films Using Fluorescence Emission of 3-Hydroxyflavone Probes," *Macromolecules* **43**, 9488-9494 (2010).

Mothé, C. G., D. Z. Correia, F. P. de França and A. T. Riga, "Thermal and Rheological Study of Polysaccharides for Enhanced Oil Recovery," *J. Therm. Anal. Calorim.* **85**, 31-36 (2006).

Mya, K. Y., A. M. Jamieson and A. Sirivat, "Effect of Temperature and Molecular Weight on Binding between Poly(ethylene oxide) and Cationic Surfactant in Aqueous Solutions," *Langmuir* **16**, 6131-6135 (2000).

Nagase, K., J. Kobayashi and T. Okano, "Temperature-responsive intelligent interfaces for biomolecular separation and cell sheet engineering," *J. R. Soc. Interface* **6**, 293-309 (2009).

Nambam, J. S. and J. Philip, "Effects of Interaction of Ionic and Nonionic Surfactants on Self-Assembly of PEO−PPO−PEO Triblock Copolymer in Aqueous Solution," *J. Phys. Chem. B* **116**, 1499-1507 (2012).

Naves, A. F. and D. F. S. Petri, "The effect of molecular weight and degree of substitution on the interactions between carboxymethyl cellulose and cetyltrimethylammonium bromide," *Colloids Surf. A* **254**, 207-214 (2005).

Neto, C. G. T., A. L. P. Fernandes, A. I. B. Santos, W. A. Morais, M. V. M. Navarro, T. N. C. Dantas, M. R. Pereira and J. L. C. Fonseca, "Preparation and characterization of chitosan-based dispersions," *Polym. Int.* **54**, 659-666 (2005).

Neyret, S., L. Ouali, F. Candau and E. Pefferkorn, "Adsorption of Polyampholytes on Polystyrene Latex: Effect on Colloid Stability," *J. Colloid Interface Sci.* **176**, 86-94 (1995).

Niklason, L. E., J. Gao, W. M. Abbott, K. K. Hirschi, S. Houser, R. Marini and R. Langer, "Functional Arteries Grown in Vitro," *Science* **284**, 489-493 (1999).

Nizri, G., A. Makarsky, S. Magdassi and Y. Talmon, "Nanostructures Formed by Self-Assembly of Negatively Charged Polymer and Cationic Surfactants," *Langmuir* **25**, 1980-1985 (2009).

Nizri, G., S. Magdassi, J. Schmidt, Y. Cohen and Y. Talmon, "Microstructural Characterization of Micro- and Nanoparticles Formed by Polymer-Surfactant Interactions," *Langmuir* **20**, 4380-4385 (2004).

Nyström, B., A. -L. Kjøniksen and C. Iversen, "Characterization of association phenomena in aqueous systems of chitosan of different hydrophobicity," *Adv. Colloid Interface Sci.* **79**, 81-103 (1999).

Nyström, B., A. -L. Kjøniksen, N. Beheshti, K. Zhu and K. D. Knudsen, "Rheological and structural aspects on association of hydrophobically modified polysaccharides," *Soft Matter* **5**, 1328-1339 (2009).

Okano, T., N. Yamada, M. Okuhara, H. Sakai and Y. Sakurai, “Mechanism of cell detachment from temperature-modulated, hydrophilichydrophobic polymer surfaces,” *Biomaterials* **16**, 297-303 (1995).

Onésippe, C. and S. Lagerge, “Studies of the association of chitosan and alkylated chitosan with oppositely charged sodium dodecyl sulfate,” *Colloids Surf. A* **330**, 201-206 (2008).

Onishi, H. and Y. Machida, “Biodegradation and distribution of water-soluble chitosan in mice,” *Biomaterials* **20**, 175-182 (1999).

Orts, W. J., L. Godbout, R. H. Marchessault and J. -F. Revol, “Enhanced Ordering of Liquid Crystalline Suspensions of Cellulose Microfibrils: A Small Angle Neutron Scattering Study,” *Macromolecules* **31**, 5717-5725 (1998).

Ostrovskii, D., A. -L. Kjøniksen, B. Nyström and L. M. Torell, “Association and Thermal Gelation in Aqueous Mixtures of Ethyl(hydroxyethyl)cellulose and Ionic Surfactant: FTIR and Raman Study,” *Macromolecules* **32**, 1534-1540 (1999).

Oupický, D., T. Reschel, C. Koňák and L. Oupická, “Temperature-Controlled Behavior of Self-Assembly Gene Delivery Vectors Based on Complexes of DNA with Poly(L-lysine)-graft-poly(N-isopropylacrylamide),” *Macromolecules* **36**, 6863-6872 (2003).

Pan, J., W. Hamad and S. K. Straus, “Parameters Affecting the Chiral Nematic Phase of Nanocrystalline Cellulose Films,” *Macromolecules* **43**, 3851-3858 (2010).

Patrickios, C. S., L. R. Sharma, S. P. Armes and N. C. Billingham, “Precipitation of a Water-Soluble ABC Triblock Methacrylic Polyampholyte: Effects of Time, pH, Polymer Concentration, Salt Type and Concentration, and Presence of a Protein,” *Langmuir* **15**, 1613-1620 (1999).

Park, J. H., Y. W. Cho, H. Chung, I. C. Kwon and S. Y. Jeong, "Synthesis and Characterization of Sugar-Bearing Chitosan Derivatives: Aqueous Solubility and Biodegradability," *Biomacromolecules* **4**, 1087-1091 (2003).

Pavinatto, F. J., L. Caseli and O. N. Oliveira Jr., "Chitosan in Nanostructured Thin Films," *Biomacromolecules* **11**, 1897-1908 (2010).

Peng, B. L., N. Dhar, H. L. Liu and K. C. Tam, "Chemistry and Applications of Nanocrystalline Cellulose and its Derivatives: A Nanotechnology Perspective," *Can. J. Chem. Eng.* **89**, 1191-1206 (2011).

Peng, B. L., N. Grishkewich, Z. L. Yao, X. Han, H. L. Liu and K. C. Tam, "Self-Assembly Behavior of Thermoresponsive Oligo(ethylene glycol) Methacrylates Random Copolymer," *ACS Macro Lett.* **1**, 632-635 (2012).

Pepić, I., J. Filipović-Grčić and I. Jalšenjak, "Interactions in a nonionic surfactant and chitosan mixtures," *Colloids Surf. A* **327**, 95-102 (2008).

Phani Kumar, B. V. N., S. U. Priyadharsini, G. K. S. Prameela and A. B. Mandal, "NMR investigations of self-aggregation characteristics of SDS in a model assembled tri-block copolymer solution," *J. Colloid Interface Sci.* **360**, 154-162 (2011).

Pi, Y. Y., Y. Z. Shang, C. J. Peng, H. L. Liu, Y. Hu and J. W. Jiang, "Interactions between Bovine Serum Albumin and Gemini Surfactant Alkanediyl-α,ω-Bis(Dimethyldodecyl Ammonium Bromide)," *Biopolymers* **83**, 243-249 (2006).

Pi, Y. Y., Y. Z. Shang, C. J. Peng, H. L. Liu, Y. Hu and J. W. Jiang, "Interactions between gemini surfactant alkanediyl-*α,ω*-bis(dodecyldimethylammonium bromide) and polyelectrolyte NaPAA," *J. Colloid Interface Sci.* **301**, 631-636 (2006).

Podczeck, F., A. Maghetti and J. M. Newton, “The influence of non-ionic surfactants on the rheological properties of drug/microcrystalline cellulose/water mixtures and their use in the preparation and drug release performance of pellets prepared by extrusion/spheronization,” *Eur. J. Pharm. Sci.* **37**, 334-340 (2009).

Rafati, A. A. and E. Ghasemian, “Thermodynamic and binding study of hemoglobin, oxy-hemoglobin and carbamino-hemoglobin upon interaction with cationic surfactants, using surfactant membrane selective electrodes,” *J. Mol. Liq.* **144**, 131-137 (2009).

Ramkissoon-Ganorkar, C., F. Liu, M. Baudyš and S. W. Kim, “Modulating insulin-release profile from pH/ thermosensitive polymeric beads through polymer molecular weight,” *J. Control. Release* **59**, 287-298 (1999).

Ramkissoon-Ganorkar, C. M. Baudyš and S. W. Kim, “Effect of ionic strength on the loading ef. ciency of model polypeptide/protein drugs in pH-/temperature-sensitive polymers,” *J. Biomater. Sci. Polymer Edn* **11**, 45-54 (2000).

Ramzi, M., C. Rochas and J. -M. Guenet, “Structure-Properties Relation for Agarose Thermoreversible Gels in Binary Solvents,” *Macromolecules* **31**, 6106-6111 (1998).

Ravi Kumar, M. N. V., R. A. A. Muzzarelli, C. Muzzarelli, H. Sashiwa and A. J. Domb, “Chitosan Chemistry and Pharmaceutical Perspectives,” *Chem. Rev.* **104**, 6017-6084 (2004).

Ravi, P., C. Wang, K. C. Tam and L. H. Gan, “Association Behavior of Poly(methacrylic acid)-*block*-poly(methyl methacrylate) in Aqueous Medium: Potentiometric and Laser Light Scattering Studies,” *Macromolecules* **36**, 173-179 (2003).

Ray, J. and G. S. Manning, “Formation of Loose Clusters in Polyelectrolyte Solutions,” *Macromolecules* **33**, 2901-2908 (2000).

Revol, J. -F., H. Bradford, J. Giasson, R. H. Marchessault and D. G. Gray, "Helicoidal self-ordering of cellulose microfibrils in aqueous suspension," *Int. J. Biol. Macromol.* **14**, 170-172 (1992).

Revol, J. -F., L. Godbout, X. M. Dong, D. G. Gray, H. Chanzy and G. Maret, "Chiral Nematic Suspensions of Cellulose Crystallites; Phase-Separation and Magnetic-Field Orientation," *Liquid Crystals* **16**,127-134 (1994).

Ridell, A., H. Evertsson and S. Nilsson, "Influence of Counterion on the Interaction of Dodecyl Sulfates and Cellulose Ethers," *J. Colloid Interface Sci.* **247**, 381-388 (2002).

Rojas, O. J., G. A. Montero and Y. Habibi, "Electrospun nanocomposites from polystyrene loaded with cellulose nanowhiskers," *J. Appl. Polym. Sci.* **113**, 927-935 (2009).

Roman M., S. P. Dong, H. Anjali and Y. W. Lee, "Cellulose Nanocrystals for Drug Delivery," in "Polysaccharide Materials: Performance by Design," Anonymous American Chemical Society (2010), pp. 81-91.

Roy, D., M. Semsarilar, J. T. Guthrie and S. Perrier, "Cellulose modification by polymer grafting: a review," *Chem. Soc. Rev.* **38**, 2046-2064 (2009).

Sabhapondit, A., A. Borthakur and I. Haque, "Water Soluble Acrylamidomethyl Propane Sulfonate (AMPS) Copolymer as an Enhanced Oil Recovery Chemical," *Energy Fuels* **17**, 683-688 (2003).

Saito, T. and A. Isogai, "TEMPO-Mediated Oxidation of Native Cellulose. The Effect of Oxidation Conditions on Chemical and Crystal Structures of the Water-Insoluble Fractions," *Biomacromolecules* **5**, 1983-1989 (2004).

Saito, T., M. Hirota, N. Tamura and A. Isogai, “Oxidation of bleached wood pulp by TEMPO/NaClO/NaClO2 system: effect of the oxidation conditions on carboxylate content and degree of polymerization,” *J. Wood Sci.* **56**, 227-232 (2010).

Samir, M. A. S. A., F. Alloin and A. Dufresne, “Review of Recent Research into Cellulosic Whiskers, Their Properties and Their Application in Nanocomposite Field,” *Biomacromolecules* **6**, 612-626 (2005).

Sashiwa, H., N. Yamamori, Y. Ichinose, J. Sunamoto and S. Aiba, “Chemical Modification of Chitosan, Michael Reaction of Chitosan with Acrylic Acid in Water,” *Macromol. Biosci.* **3**, 231-233 (2003).

Sashiwa, H., N. Yamamori, Y. Ichinose, J. Sunamoto and S. Aiba, “Michael Reaction of Chitosan with Various Acryl Reagents in Water,” *Biomacromolecules* **4**, 1250-1254 (2003).

Sassi, J. and H. Chanzy, “Ultrastructural aspects of the acetylation of cellulose,” *Cellulose* **2**, 111-127 (1995).

Satter, B. and G. C. Thakur, Integrated Petroleum Reservoir Management - A Team Approach, Penn Well Publishing Company, Oklahoma 1994

Schacher, F., M. Müllner, H. Schmalz and A. H. E. Müller, “New Block Copolymers with Poly(N,Ndimethylaminoethyl methacrylate) as a Double Stimuli-Responsive Block,” *Macromol. Chem. Phys.* **210**, 256-262 (2009).

Scherlund, M., A. Brodin and M. Malmsten, “Nonionic Cellulose Ethers as Potential Drug Delivery Systems for Periodontal Anesthesia,” *J. Colloid Interface Sci.* **229**, 365-374 (2000).

Schild, H. G., “Poly(*N*-isopropylacrylamide): Experiment, Theory and Applacation,” *Prog. Polym. Sci.* **17**, 163-249 (1992).

Schmaljohann, D. “Thermo- and pH-responsive polymers in drug delivery,” *Adv. Drug Delivery Rev.* **58**, 1655-1670 (2006).

Schuch, H., J. Klingler, P. Rossmanith, T. Frechen, M. Gerst, J. Feldthusen and A. H. E. Müller, “Characterization of Micelles of Polyisobutylene-block-poly(methacrylic acid) in Aqueous Medium,” *Macromolecules* **33**, 1734-1740 (2000).

Schulz, P. C., M. S. Rodríguez, L. F. Blanco, M. Pistonesi and E. Agulló, “Emulsification properties of chitosan,” *Colloid Polym. Sci.* **276**, 1159-1165 (1998).

Sedlák, M. and Č. Koňák, “A New Approach to Polymer Self-assembly into Stable Nanoparticles: Poly(ethylacrylic acid) Homopolymers,” *Macromolecules* **42**, 7430-7438 (2009).

Serres, A., M. Baudyš and S. W. Kim, “Temperature and Ph-sensitive Polymers for Human Calcitonin Delivery,” *Pharm. Res.* **13**, 196-201 (1996).

Shin, Y., I. Bae, B. W. Arey and G. J. Exarhos, “Facile Stabilization of Gold-silver Alloy Nanoparticles on Cellulose Nanocrystal,” *J. Phys. Chem. C* **112**, 4844-4848 (2008).

Shin, Y., I. Bae, B. W. Arey and G. J. Exarhos, “Simple preparation and stabilization of nickel nanocrystals on cellulose nanocrystal,” *Mater. Lett.* **61**, 3215-3217 (2007).

Shopsowitz, K. E., H. Qi, W. Y. Hamad and M. J. MacLachlan, “Free-standing mesoporous silica films with tunable chiral nematic structures,” *Nature* **468**, 422-426 (2010).

Singh, S. K. and S. Nilsson, “Thermodynamics of Interaction between Some Cellulose Ethers and SDS by Titration Microcalorimetry,” *J. Colloid Interface Sci.* **213**, 133-151 (1999).

Skorik, Y. A., C. A. R. Gomes, M. Vasconcelos, S. D. Teresa and Y. G. Yatluk, “*N*-(2-Carboxyethyl)chitosans: regioselective synthesis, characterisation and protolytic equilibria,” *Carbohydr. Res.* **338**, 271-276 (2003).

Skrabania, K., J. Kristen, A. Laschewsky, Ö. Akdemir, A. Hoth and J. -F. Lutz, "Design, Synthesis, and Aqueous Aggregation Behavior of Nonionic Single and Multiple Thermoresponsive Polymers," *Langmuir* **23**, 84-93 (2007).

Soga, O., C. F. van Nostrum and W. E. Hennink, "Poly(N-(2-hydroxypropyl) Methacrylamide Mono/Di Lactate): A New Class of Biodegradable Polymers with Tuneable Thermosensitivity," *Biomacromolecules* **5**, 818-821 (2004).

Stodghill, S. P., A. E. Smith and J. H. O'Haver, "Thermodynamics of Micellization and Adsorption of Three Alkyltrimethylammonium Bromides Using Isothermal Titration Calorimetry," *Langmuir* **20**, 11387-11392 (2004).

Stuart, M. A. C., W. T. S. Huck, J. Genzer, M. Müller, C. Ober, M. Stamm, G. B. Sukhorukov, I. Szleifer, V. V. Tsukruk, M. Urban, F. Winnik, S. Zauscher, I. Luzinov and S. Minko, "Emerging applications of stimuli-responsive polymer materials," *Nature Materials* **9**, 101-113 (2010).

Sugiyama, J., H. Chanzy and G. Maret, "Orientation of cellulose microcrystals by strong magnetic fields," *Macromolecules* **25**, 4232-4234 (1992).

Suwa, K., K. Yamamoto, M. Akashi, K. Takano, N. Tanaka and S. Kunugi, "Effects of salt on the temperature and pressure responsive properties of poly(N-vinylisobutyramide) aqueous solutions," *Colloid Polym. Sci.* **276**, 529-533 (1998).

Tam, K. C. and E. Wyn-Jones, "Insights on polymer surfactant complex structures during the binding of surfactants to polymers as measured by equilibrium and structural techniques," *Chem. Soc. Rev.* **35**, 693-709 (2006).

Taylor, K. C. and H. A. Nasr-El-Din, "Water-soluble hydrophobically associating polymers for improved oil recovery: A literature review," *J. Petrol. Sci. Eng.* **19**, 265-280 (1998).

Terayama, H., K. Okumura, K. Sakai, K. Torigoe and K. Esumi, "Aqueous dispersion behavior of drug particles by addition of surfactant and polymer," *Colloids Surf. B* **20**, 73-77 (2001).

Thongngam, M. and D. J. McClements, "Influence of pH, Ionic Strength, and Temperature on Self-Association and Interactions of Sodium Dodecyl Sulfate in the Absence and Presence of Chitosan," *Langmuir* **21**, 79-86 (2005).

Thuresson, K., B. Lindman and B. Nyström, "Effect of Hydrophobic Modification of a Nonionic Cellulose Derivative on the Interaction with Surfactants. Rheology," *J. Phys. Chem. B* **101**, 6450-6459 (1997).

Trabelsi, S., E. Raspaud and D. Langevin, "Aggregate Formation in Aqueous Solutions of Carboxymethylcellulose and Cationic Surfactants," *Langmuir* **23**, 10053-10062 (2007).

Trabelsi, S., P. -A. Albouy, M. Impéror-Clerc, S. Guillot and D. Langevin, "X-ray Diffraction Study of the Structure of Carboxymethylcellulose–Cationic Surfactant Complexes," *ChemPhysChem* **8**, 2379-2385 (2007).

VandeVord, P. J., H. W. T. Matthew, S. P. Desilva, L. Mayton, B. Wu and P. H. Wooley, "Evaluation of the biocompatibility of a chitosan scaffold in mice," *J. Biomed. Mater. Res.* **59**, 585-590 (2002).

Walderhaug, H., B. Nystriöm, F. K. Hansen and B. Lindman, "Interactions of Ionic Surfactants with a Nonionic Cellulose Ether in Solution and in the Gel State Studied by Pulsed Field Gradient NMR," *J. Phys. Chem.* **99**, 4672-4678 (1995).

Walter, R., J. Rička, Ch. Quellet, R. Nyffenegger and Th. Binkert, "Coil-Globule Transition of Poly(*N*-isopropylacrylamide): A Study of Polymer-Surfactant Association," *Macromolecules* **29**, 4019-4028 (1996).

Wang, C. and K. C. Tam, "Interaction between Polyelectrolyte and Oppositely Charged Surfactant: Effect of Charge Density," *J. Phys. Chem. B* **108**, 8976-8982 (2004).

Wang, C. and K. C. Tam, "New Insights on the Interaction Mechanism within Oppositely Charged Polymer/Surfactant Systems," *Langmuir* **18**, 6484-6490 (2002).

Wang, C., E. Wyn-Jones, J. Sidhu and K. C. Tam, "Supramolecular Complex Induced by the Binding of Sodium Dodecyl Sulfate to PAMAM Dendrimers," *Langmuir* **23**, 1635-1639 (2007).

Wang, G. and G. Olofsson, "Ethyl(hydroxyethy1)cellulose and Ionic Surfactants in Dilute Solution. Calorimetric and Viscosity Study of the Interaction with SDS and Some Cationic Surfactants," *J. Phys. Chem.* **99**, 5588-5596 (1995).

Wang, G. and G. Olofsson, "Titration Calorimetric Study of the Interaction between Ionic Surfactants and Uncharged Polymers in Aqueous Solution," *J. Phys. Chem. B* **102**, 9276-9283 (1998).

Wang, J. and K. Matyjaszewski, "Controlled/living" radical polymerization. atom transfer radical polymerization in the presence of transition-metal complexes," *J. Am. Chem. Soc.* **117**, 5614-5615 (1995).

Wangsakan, A., P. Chinachoti and D. J. McClements, "Effect of Surfactant Type on Surfactant-Maltodextrin Interactions: Isothermal Titration Calorimetry, Surface Tensiometry, and Ultrasonic Velocimetry Study," *Langmuir* **20**, 3913-3919 (2004).

Wang, X. -S., S. F. Lascelles, R. A. Jackson and S. P. Armes, "Facile synthesis of well-defined water-soluble polymers via atom transfer radical polymerization in aqueous media at ambient temperature," *Chem. Commun.* **18**, 1817-1818 (1999).

Wang, X. -S. and S. P. Armes, “Facile Atom Transfer Radical Polymerization of Methoxy-Capped Oligo(ethylene glycol) Methacrylate in Aqueous Media at Ambient Temperature,” *Macromolecules* **33**, 6640-6647 (2000).

Wang, X., Y. Li, J. Li, J. Wang, Y. Wang, Z. Guo and H. Yan “Salt Effect on the Complex Formation between Polyelectrolyte and Oppositely Charged Surfactant in Aqueous Solution,” *J. Phys. Chem. B* **109**, 10807-10812 (2005).

Weber, C., R. Hoogenboomd and U. S. Schubert, “Temperature responsive bio-compatible polymers based on poly(ethylene oxide) and poly(2-oxazoline)s,” *Prog. Polym. Sci.* **37**, 686-714 (2012).

Weiss, J., C. Böttcher and A. Laschewsky, “Self-assembly of double thermoresponsive block copolymers end-capped with complementary trimethylsilyl groups,” *Soft Matter* **7**, 483-492 (2011).

Wiseman, T., S. Williston, J. F. Brandts and L. -N. Lin, “Rapid measurement of binding constants and heats of binding using a new titration calorimeter,” *Anal. Biochem.* **179**, 131-137 (1989).

Wong, K. K. H., M. Zinke-Allmang, J. L. Hutter, S. Hrapovic, J. H. T. Luong and W. Wan, “The effect of carbon nanotube aspect ratio and loading on the elastic modulus of electrospun poly(vinyl alcohol)-carbon nanotube hybrid fibers,” *Carbon* **47**, 2571-2578 (2009).

Wu, D., G. Y. Xu, Y. H. Sun, H. X. Zhang, H. Z. Mao and Y. J. Feng, “Interaction between Proteins and Cationic Gemini Surfactant,” *Biomacromolecules* **8**, 708-712 (2007).

Wu, Q., Y. Shangguan, M. Du, J. Zhou, Y. Song and Q. Zheng, “Steady and dynamic rheological behaviors of sodium carboxymethyl cellulose entangled semi-dilute solution with opposite

charged surfactant dodecyltrimethylammonium bromide," *J. Colloid Interface Sci.* **339**, 236-242 (2009).

Xie, D. H., X. D. Ye, Y. W. Ding, G. Z. Zhang, N. Zhao, K. Wu, Y. Cao and X. X. Zhu, "Multistep Thermosensitivity of Poly(*N*-*n*-propylacrylamide)-*block*-poly(*N*-isopropylacrylamide)-*block*-poly(*N*,*N*-ethylmethylacrylamide) Triblock Terpolymers in Aqueous Solutions As Studied by Static and Dynamic Light Scattering," *Macromolecules* **42**, 2715-2720 (2009).

Xu, J., X. Z. Jiang and S. Y. Liu, "Synthesis of low-polydispersity poly(Nethylmethylacrylamide) by controlled radical polymerizations and their thermal phase transition behavior," *J. Polym. Sci. Polym. Chem.* **46**, 60-69 (2008).

Yamamoto, S., J. Pietrasik and K. Matyjaszewski, "ATRP Synthesis of Thermally Responsive Molecular Brushes from Oligo(ethylene oxide) Methacrylates," *Macromolecules* **40**, 9348-9353 (2007).

Yancheva, E., D. Paneva, V. Maximova, L. Mespouille, P. Dubois, N. Manolova and I. Rashkov, "Polyelectrolyte Complexes between (Cross-linked) *N*-Carboxyethylchitosan and (Quaternized) Poly[2-(dimethylamino)ethyl methacrylate]: Preparation, Characterization, and Antibacterial Properties," *Biomacromolecules* **8**, 976-984 (2007).

Yao, Z. L. and K. C. Tam, "Self-assembly of thermo-responsive poly(oligo(ethylene glycol) methyl ether methacrylate)-C60 in water-methanol mixtures," *Polymer* **52**, 3769-3775 (2011).

Yao, Z. L. and K. C. Tam, "Temperature induced micellization and aggregation of biocompatible poly(oligo(ethylene glycol)methyl ether methacrylate) block copolymer analogs in aqueous solutions," *Polymer* **53**, 3446-3453 (2012).

Yi, J., Q. Xu, X. Zhang and H. Zhang, "Chiral-nematic self-ordering of rodlike cellulose nanocrystals grafted with poly(styrene) in both thermotropic and lyotropic states," *Polymer* **49**, 4406-4412 (2008).

Yuan, H., Y. Nishiyama, M. Wada and S. Kuga, "Surface Acylation of Cellulose Whiskers by Drying Aqueous Emulsion," *Biomacromolecules* **7**, 696-700 (2006).

Zana, R., M. Benrraou and R. Rueff, "Alkanediyl-α,ω-bis(dimethylalky1ammonium bromide) Surfactants. Effect of the Spacer Chain Length on the Critical Micelle Concentration and Micelle Ionization Degree," *Langmuir* **7**, 1072-1075 (1991).

Zana, R., W. Binana-Limbelé, N. Kamenka and B. Lindman, "Ethyl(hydroxyethyl)cellulose-cationic surfactant interactions: electrical conductivity, self-diffusion and time-resolved fluorescence quenching investigations," *J. Phys. Chem.* **96**, 5461-5465 (1992).

Zhang, Z. X., K. L. Liu and J. Li, "Self-Assembly and Micellization of a Dual Thermoresponsive Supramolecular Pseudo-Block Copolymer," *Macromolecules* **44**, 1182-1193 (2011).

Zhao, J. P., G. Z. Zhang and S. Pispas, "Thermo-Induced Aggregation Behavior of Poly(ethylene oxide)-b-poly(N-isopropylacrylamide) Block Copolymers in the Presence of Cationic Surfactants," *J. Phys. Chem. B* **113**, 10600-10606 (2009).

Zhou, Y., E. Ding and W. Li, "Synthesis of TiO2 nanocubes induced by cellulose nanocrystal (CNC) at low temperature," *Mater. Lett.* **61**, 5050-5052 (2007).

Zhu, A. P., M. B. Chan-Park, S. Dai and L. Li, "The aggregation behavior of O-carboxymethylchitosan in dilute aqueous solution," *Colloids Surf. B* **43**, 143-149 (2005).

Zoppe, J. O., Y. Habibi, O. J. Rojas, R. A. Venditti, L. -S. Johansson, K. Efimenko, M. Österberg and J. Laine, "Poly(*N*-isopropylacrylamide) Brushes Grafted from Cellulose

Nanocrystals via Surface-Initiated Single-Electron Transfer Living Radical Polymerization," *Biomacromolecules* **11**, 2683-2691 (2010).